A New Approach to the Design of Adaptive MIMO Wireless Communication Systems

Mabruk Gheryani

A Thesis

in

The Department

of

Eletrical and Computer Engineering

Presented in Partial Fulfillment of the Requirements
for the Degree of Doctor of Philosophy at
Concordia University
Montreal, Quebec, Canada

April 2009

Your file Votre référence
ISBN: 978-0-494-63366-3
Our file Notre référence
ISBN: 978-0-494-63366-3

Abstract

A New Approach to the Design of Adaptive MIMO Wireless Communication Systems

Mabruk Gheryani, PhD

Concordia University, 2009

Since the capabilities of MIMO systems were discovered, much research effort has been invested in this field. However, in most applications, the channel state information (CSI) is assumed to be known to the receiver only. To further improve the performance, the transmission rate will adapt to the levels of CSI fed back from the receiver.

The capacity and performance of linear dispersion code (LDC) are studied. An analytical expression of the ergodic capacity and a tight upper bound of the pairwise error probability of full-rate LDC are derived. The tight upper bound demonstrates the relationship between the pairwise error probability, the constellation size and the space-time (ST) symbol rate, which will be a guideline for the adaptation.

The probability density function of the signal-to-interference-noise ratio (SINR) of a MIMO transceiver using LDC and linear minimum-mean-square-error (MMSE) receiver is then derived, over a Rayleigh fading channel. With these theoretical results as a guideline, we study the design of adaptive systems with discrete selection modes. An adaptive algorithm for the selection-mode adaptation is proposed. Based on the proposed algorithm, two adaptation techniques are presented, using constellation size and ST symbol rate, respectively. To improve the average transmission rate,

a new adaptation design is developed, which is based on joint constellation size and ST symbol rate adaptation.

Next, we propose a novel scheme called "beam-nulling" for MIMO adaptation. In the beam-nulling scheme, the eigenvector of the weakest subchannel is fed back and then signals are sent over a generated subspace orthogonal to the weakest subchannel. Theoretical analysis and numerical results show that the capacity of beam-nulling is close to the optimal water-filling scheme at medium SNR. Additionally, the SINR of an MMSE receiver is derived for beam-nulling, followed by a presentation of the associated numerical average bit-error rate (BER) of beam-nulling.

Finally, to further improve the performance, beam-nulling is concatenated with LDC. Simulation results show that the concatenated beam-nulling schemes outperform the beamforming scheme at higher rate. Additionally, the existing beamforming and new proposed beam-nulling schemes can be extended if more than one eigenvector is available at the transmitter. Theoretical analysis and simulation results are also provided to evaluate the new extended schemes.

Acknowledgments

It is my great pleasure to thank all people who helped me to complete my PhD thesis. I thank the Libyan Government and Garyounis University for the financial support and Concordia university for the academic support.

My most earnest acknowledgment must go to my supervisor Prof. Yousef R. Shayan. During the four years of my PhD, I have seen in him an excellent supervisor who can bring the best out from his students, an outstanding researcher who can constructively criticize research, and a nice human being who is honest, fair and helpful to others.

I would also like to thank Dr. Xiaofeng Wang for all his help and support as my co-supervisor for the initial period of my graduate studies. My sincere thanks go out to Dr. Zhiyuan Wu for his generous help, constructive feedback, and valuable comments in my research works. I would like to thank the members of my dissertation committee for their invaluable comments and suggestions during my study. I am grateful to Dr. Amir Khandani at Waterloo University for his kind acceptance to be the external examiner of this dissertation.

I would like to thank my parents and parents-in-law for their love, care and dedication. Next to my parents, I thank my brother-in-law Mohamed Feituri for his support and endless concern. The most important person who has been with me in every moment of my PhD study is my wife Rania Feituri. I would like to thank my wife for many sacrifices she has made to support me in undertaking my doctoral studies.

MABRUK GHERYANI

This dissertation is dedicated to
my parents, my parents-in-law
and my wife.

Contents

List of Figures xi

Notations and Abbreviations xiv

Chapter 1 Introduction 1

1.1 Literature Survey and Motivation 2

1.2 Problem Statement and Objectives 6

1.3 Outline of the Thesis Work 7

1.4 Contributions 9

Chapter 2 Preliminaries 11

2.1 MIMO Channel Model 11

2.2 Performance Measures and Their Tradeoffs 14

2.2.1 Tradeoff Between Diversity and Multiplexing Gain 14

2.2.2 Error Performance and Design Criteria for Fixed Data Rate . 15

2.3 Linear Dispersion Code 17

2.3.1 Coding 17

2.3.2 Decoding 18

2.4 Adaptive Modulation and Coding 20

2.5 Power Allocation among Spatial Subchannels 21

2.5.1 Equal Power 21

2.5.2 Water-Filling 22

2.5.3 Eigen-Beamforming 25

Chapter 3 Theoretical Analysis of Full Rate Linear Dispersion Codes 28

3.1 Introduction 28

3.2 System Model 29

3.3 Capacity Analysis 31

3.4 Performance Analysis 37

3.5 Conclusions 42

Chapter 4 New Adaptive MIMO System using Full Rate Linear Dispersion Code with Selection Modes 43

4.1 Introduction 43

4.2 Adaptive System Model using LDC 44

4.3 The Statistics of SINR with the MMSE Receiver 48

4.4 Design of Adaptive Transceiver 57

4.4.1 Adaptation using Variable Constellations 60

4.4.2 Adaptation using Variable ST Symbol Rate 66

4.5 Joint Adaptive Technique 72

4.6 Conclusions 77

Chapter 5 New Power Allocation Strategy among MIMO Spatial Subchannels - Beam-Nulling 78

5.1 Introduction 78

5.2 Beam-Nulling 79

5.3 Capacity Comparisons among Four Strategies 83

5.3.1 Capacity Comparisons at Low SNR 85

5.3.2 Capacity Comparisons at Medium SNR 86

5.3.3 Capacity Comparisons at High SNR 86

5.4 Extended Adaptive Frameworks 90

5.4.1 MD Beamforming 90
5.4.2 MD Beam-nulling 94
5.4.3 Capacity Comparison 95
5.5 Conclusions 98

Chapter 6 Performance of New Power Allocation Scheme Beam-Nulling 99

6.1 Introduction 99
6.2 Performance of 1D Beamforming and 1D Beam-nulling 100
6.2.1 Performance of 1D Beamforming 100
6.2.2 Performance of 1D Beam-nulling 102
6.2.3 Design of Subspaces Orthogonal to the Weakest Subchannel . 106
6.2.4 Performance Comparison between 1D Beamforming and 1D Beam-nulling 107
6.2.5 Concatenation of 1D Beam-nulling and LDC 111
6.2.6 Performance of 1D Beam-nulling with LDC 112
6.3 MD Schemes Concatenated with Linear Space-Time Code 116
6.4 Conclusions 120

Chapter 7 Conclusions and Future Works 122

7.1 Conclusions 122
7.1.1 Theoretical Analysis of LDC 122
7.1.2 New Adaptive MIMO System 122
7.1.3 Capacity of Beam-Nulling and Extended Multi- Dimensional Frameworks 123
7.1.4 Performance of Beam-Nulling and Extended Multi- Dimensional Frameworks 124
7.2 Future Works 125

Bibliography 126

List of Figures

2.1 MIMO channel model. 13

2.2 Adaptive modulation and coding system. 21

2.3 Capacity for equal power allocation. 22

2.4 Water-filling scheme. 23

2.5 Capacity for water-filling. 24

2.6 Eigen-beamforming scheme. 25

2.7 Capacity for eigen-beamforming. 27

3.1 LDC system block diagram. 29

3.2 Numerical result and the associated exact capacity SNR. 36

3.3 Simulation result and the associated upper bound at high SNR. . . . 41

4.1 Selection-mode adaptive system block diagram. 44

4.2 Comparison between the theoretical PDF of SINR and Monte Carlo simulation when $N_r = N_t = 2$ at $P/\sigma_z^2 = 20dB$ 55

4.3 Comparison between the theoretical PDF of SINR and Monte Carlo simulation when $N_r = N_t = 4$ at $P/\sigma_z^2 = 20dB$ 56

4.4 Numerical and simulation results for LDC with MMSE receiver . . . 58

4.5 Adaptive constellation size when ST symbol rate=1 61

4.6 Adaptive constellation size when ST symbol rate=2 62

4.7 Adaptive constellation size when ST symbol rate=3 63

4.8 Adaptive constellation size when ST symbol rate=4 64
4.9 Adaptive ST symbol rate when constellation size is BPSK 67
4.10 Adaptive ST symbol rate when constellation size is QPSK 68
4.11 Adaptive ST symbol rate when constellation size is 8PSK 69
4.12 Adaptive ST symbol rate when constellation size is 16QAM. 70
4.13 Joint adaptation of ST symbol rate and constellation size 73
4.14 Average spectral efficiency comparison for the three adaptive schemes. 76

5.1 Beam-nulling scheme. 80
5.2 Capacity for beam-nulling. 82
5.3 2×2 Rayleigh fading channel. 86
5.4 3×3 Rayleigh fading channel. 87
5.5 4×4 Rayleigh fading channel. 88
5.6 5×5 Rayleigh fading channel. 89
5.7 MD beamforming over 5×5 Rayleigh fading channel. 93
5.8 MD beam-nulling over 5×5 Rayleigh fading channel. 96
5.9 Comparison over 5×5 Rayleigh fading channel. 97

6.1 1D beamforming scheme. 101
6.2 1D beam-nulling scheme. 102
6.3 Numerical and simulation results for beam-nulling scheme. 105
6.4 Different designs of $\mathbf{\Phi}$ 107
6.5 Comparison over 3×3 Rayleigh fading channel. 108
6.6 Comparison over 4×4 Rayleigh fading channel. 109
6.7 1D beam-nulling concatenated with LDC scheme. 111
6.8 Comparison over 3×3 Rayleigh fading channel. 114
6.9 Comparison over 4×4 Rayleigh fading channel. 115
6.10 Concatenated MD beamforming scheme. 116
6.11 Concatenated MD beam-nulling scheme. 117

6.12 BER of concatenated MD beamforming when $R = 2$. 118
6.13 BER of concatenated MD beam-nulling when $R = 3$. 119
6.14 BER comparison of concatenated MD schemes when $R = 6$. 120

Notations and Abbreviations

- $\mathbf{X}$: upper bold letter for matrix
- $\mathbf{x}$: lower bold letter for column vector
- $\mathbf{X}^H$: hermitian of $\mathbf{X}$
- $\mathbf{X}^T$: transpose of $\mathbf{X}$
- $\otimes$: Kronecker product
- diag[x]: a diagonal matrix with x on its main diagonal
- tr($\mathbf{X}$): trace of $\mathbf{X}$
- det($\mathbf{X}$): determinant of $\mathbf{X}$
- vec($\mathbf{X}$): a column vector formed by stacking the column vectors of $\mathbf{X}$ in order
- $\| \ \|$: Euclidean norm
- $\{x\}$: a set of x
- $P(x)$: probability of event x
- $E(x)$: expectation of x
- AWGN: additive white Gaussian noise
- BER: bit error rate

- BF: beamforming
- BLAST: Bell-labs layered space-time
- BN: beam-nulling
- CSI: channel state information
- EQ: equal power
- FDFR: full diversity full rate
- LDC: linear dispersion code
- MD: multi-dimensional
- MIMO: multiple-input-multiple-output
- ML: maximum-likelihood
- MMSE: minimum mean square error
- MRC: maximum ratio combining
- PDF: probability density function
- QoS: quality of service
- SINR: signal-to-interference-noise ratio
- SISO: single-input-single-output
- SNR: signal-to-noise ratio
- ST: space-time
- STBC: space-time block code
- STTC: space-time trellis code

- ST Turbo TC: space-time turbo trellis code
- SVD: singular value decomposition
- TCM: trellis-coded modulation
- T-BLAST: thread BLAST
- V-BLAST: vertical BLAST
- WF: water-filling
- *i.i.d.*: independently identically distributed

Chapter 1

Introduction

Today, wireless systems support not only voice communications but also other types of services, such as facsimile, file transfer, email and video communications. Accordingly, the demand for bandwidth efficiency in wireless communications has experienced unprecedented growth. With this growth, the radio spectrum has been recognized as one of the very precious resources of nature. However, due to battery life and device size, the power available for wireless communications is limited. The radio spectrum deserves to be further explored, along with the power constrains.

Recently, one significant advance in wireless communications is the so-called multiple-input-multiple-output (MIMO) technology [1][2]. It makes use of multiple transmit and receive antennas to improve data rate and performance over fading channels. Since the advent of MIMO technology, tremendous research and development efforts in academia and industry have been undertaken, and this investment is ever increasing. To date, MIMO technology has been widely used in modern wireless communication systems, such as WLAN and 3G cellular systems, and is recognized as the most important enabling technology for future wireless communication systems. Information theory has demonstrated that a significant gain in capacity over fading channels can be obtained in MIMO systems [1][2]. Furthermore, the use of multiple antennas increases the diversity and thus combats fading [3]-[5].

To achieve the promised theoretical capacity and diversity, one of the promising techniques is adaptation. The adaptive technique was first proposed for single-input-single-output (SISO) systems to maximize the average spectral efficiency in an ever-fluctuating channel [6]-[10]. Recently, it was recognized that the adaptive technique can also be applied in MIMO wireless systems [11]-[16].

1.1 Literature Survey and Motivation

Since the capabilities of MIMO systems was discovered, much research effort has been invested in this field [1][2]. To exploit their significant capacity and diversity, space-time (ST) codes are the most promising technique. In most applications, the CSI [11] is assumed to be known or can be estimated at the receiver but unknown to the transmitter.

To combat channel quality variation and thus further improve system performance such as power efficiency, error rate and average data rate, adaptive transmission can be applied. In this method, a feedback channel is utilized to provide CSI from the receiver to the transmitter. According to the CSI feedback, the transmitter will adjust transmission parameters, such as power allocation, modulation, and coding rate. This adjustment is conditioned by the fact that the channel keeps relatively constant until the transmitter receives the CSI and then transmits the next data block accordingly. Adaptation algorithms can be classified into two categories: One approach is designed with a power constraint to optimize the throughput while maintaining a target bit error rate (BER); the other approach focuses on optimizing the performance, i.e., BER, with a constant throughput. The potential of adaptation transmission was recognized much earlier by Cavers [6], but, probably due to hardware constraints, lack of accurate channel estimation and unavailability of feedback, it received little interest at that time. Recently, the advent of high-speed devices and the possibility of transceiver reconfiguration contribute to a renewed interest in adaptive techniques

[17][18].

The concept of adaptation transmission can also be applied to MIMO systems. The ideal scenario is that the transmitter has full knowledge of the channel state information (CSI) fed back from the receiver while the CSI is assumed to be constant before the transmitter sends signals to the receiver. With a perfect CSI feedback [11], the original MIMO channel is converted to multiple uncoupled single-input-single-output (SISO) channels via singular value decomposition (SVD). In other words, the original MIMO channel can be decomposed into several orthogonal "spatial sub-channels" with various propagation gains. To optimize the system throughput, the so-called water-filling (WF) principle is performed on the multiple SISO channels. Numerous schemes have been proposed based on this optimal solution. For example, over time-invariant MIMO channels, it is known that the optimal performance (ergodic capacity) is attained by power water-filling across channel eigenvalues with the total power constraint [1]. Also, for time-varying MIMO channels, the optimal performance is obtained through power water-filling over both space and time domains with the average power constraint [19]. The space-time WF-based scheme and the spatial WF-based scheme for MIMO fading channels were compared in [20]. The comparison shows that for Rayleigh channels without shadowing, the space-time WF-based scheme gains little in capacity over the spatial WF-based scheme. However, for Rayleigh channels with shadowing, space-time WF-based schemes achieve higher spectral efficiency per antenna over spatial WF-based schemes. A WF-based scheme using imperfect CSI in MIMO systems was studied in [21]. In [22], a so-called QoS-based WF was proposed to solve the power allocation problem for a given fixed bit error rate threshold. However, these approaches often suffer from the following disadvantages: the feedback bandwidth for the full CSI grows with respect to the number of transmit and receive antennas, and the performance is often very sensitive to channel estimation errors.

To mitigate these disadvantages, various beamforming techniques for MIMO

channels are also investigated intensively. Beamforming is a linear signal processing technique that controls the complex weights of the transmit and receive antennas jointly, in order to optimize the signal-to-noise ratio (SNR) in one direction [16][23]. In other words, beamforming can increase the sensitivity in the direction of desired signals but decrease the sensitivity in the direction of interfering signals. In an adaptive beamforming scheme, complex weights of the transmit antennas are fed back from the receiver. For example, an optimal eigen-beamforming STBC scheme based on channel mean feedback was proposed in [16]. The eigen-beamforming scheme only allocates power to the strongest spatial subchannel but can achieve full diversity and high SNR. In practice, the eigen-beamforming scheme has to cooperate with the other adaptive parameters to improve performance or/and data rate, such as constellation and coding rate. A MIMO system based on transmit beamforming and adaptive modulation was proposed in [24], where the transmit power, the signal constellation, the beamforming direction, and the feedback strategy were considered jointly. The analysis of MIMO beamforming systems with quantized CSI for uncorrelated Rayleigh fading channels was provided in [25]. The conventional beamforming is optimal in terms of maximizing the SNR at the receiver. However, it is sub-optimal from a MIMO capacity point of view, since only one data stream, instead of parallel streams, is transmitted through the MIMO channel [26]. The above schemes often require near-perfect CSI feedback for optimal adaptation.

In practice, the channel estimation may exhibit some inaccuracy depending on the estimation method. The receiver requires time to process the channel estimate. The feedback is subject to some transmission delay. The transmitter needs some time to choose the best code. And there are also possible errors in the feedback channel. All these factors make the CSI at the transmitter inaccurate. In these cases, adaptive schemes with a set of discrete transmission modes are often more preferable. We can call these "selection-mode" adaptations. At the receiver, the channel is measured and then one transmission mode with the highest transmission rate is chosen, which

also meets the BER requirement. The optimal mode is fed back to the transmitter. Hence, the selection-mode scheme can save more feedback bandwidth.

For the MIMO communication system, the structures of most existing ST coding designs mainly fall into two categories, either trellis structure or linear structure. ST codes with trellis structure, such as space-time trellis codes (STTCs) [4] and space-time turbo trellis codes (ST Turbo TCs) [27]-[29], can achieve full diversity and large coding gain. However, their computational complexity grows exponentially with respect to the numbers of states and transmit antennas. They are often designed by hand and the trellis structure is not flexible for rate adaptation. ST codes with linear structure can also be referred to as linear dispersion codes (LDCs), such as space-time block codes (STBCs)[5][30], various Bell-labs layered space-time (BLAST) architectures [31]-[33] and other high-rate LDCs such as [34]-[37]. The LDC breaks the data stream into sub-streams, each sub-stream is dispersed over space and time and then the sub-streams are combined linearly at the transmit antennas. STBCs and BLAST schemes are geared to error performance and high rate, respectively. A common drawback is that they are not flexible in a rate-versus-performance tradeoff [38]. For high-rate LDCs, the mutual information between transmitted and received signals is optimized. Although any structure of ST codes can be a potential candidate for the inner ST modulation, a particularly desirable choice is linear dispersion codes (LDCs) instead of ST codes with trellis structure. Because LDCs are linear, many existing block codes are subsumed as its special cases, and they are flexible with relatively low complexity.

In this section, we have reviewed various adaptive techniques for different levels of CSI, such as WF-based, beamforming and selection-mode schemes. Also, we have reviewed current ST coding designs, such as STTCs, ST Turbo TCs, STBCs, BLAST schemes, and LDCs. The literature survey indicates that studying the design of adaptive space-time schemes over the MIMO wireless channel for various levels of CSI would be the most productive effort.

In this thesis, we are motivated to develop new adaptive space-time schemes over the MIMO wireless channel for various levels of channel state information (CSI) at the transmitter. In this context, the CSI consists of estimating of MIMO channel matrix coefficients and the signal-to-noise ratio (SNR). The level of CSI at the transmitter will depend on the bandwidth of error-free feedback channel. For example, if the bandwidth is very limited, only the SNR can be fed back. If the bandwidth is sufficiently large, perfect CSI can be obtained at the transmitter.

1.2 Problem Statement and Objectives

First, we consider the imperfect CSI scenario, i.e., the selection-mode adaptation. In this case, several discrete parameters are available for linear ST adaptation, such as active transmit antennas and constellation size (i.e., bit-loading). For example, adaptive modulation with antenna selection combined with STBC was discussed in [39]- [41]. The advantage of this scheme using STBC is to simplify the design of an adaptive modulation system. The disadvantage of this scheme is that it is not flexible for different rates, which is the key requirement in the future wireless communications. For these conventional schemes with STBC, the most convenient adaptive parameter is constellation size. However, the gaps between the available transmission rates are often very large due to the use of discrete constellations [24]. Since the high-rate LDC is applied as linear ST modulation, it makes the ST symbol rate available for adaptation, together with the constellation size. this means there are more available transmission modes and hence the average transmission rate is improved. There is no literature available to predict the relationship between the ST symbol rate, the constellation size, and the error probability. The development of this relationship is essential, as it will be a guideline for our design.

Note that the selection-mode adaptation only requires the selected mode to be fed back. In reality, if more information can be fed back, one or more spatial

subchannels can be available at the transmitter. In this case, various beamforming schemes can be considered for adaptation. The conventional beamforming scheme is optimal in terms of maximizing the SNR at the receiver. However, it is sub-optimal from a MIMO capacity point of view, since only one data stream, instead of parallel streams, is transmitted through the MIMO channel [26]. Therefore, schemes possessing higher capacity and better error performance but with limited feedback bandwidth should be investigated.

1.3 Outline of the Thesis Work

This thesis consists of seven chapters.

Chapter 2 introduces the research backgrounds and concepts on adaptive MIMO system, including MIMO channel models, performance measures and tradeoffs, linear dispersion codes (LDCs), adaptive modulation and coding, and power allocation among spatial subchannels.

The capacity and the error performance of linear dispersion codes are studied in chapter 3. First, an analytical formula of the ergodic capacity is derived for the full-rate linear dispersion code. Next, an exact tight upper bound of the pairwise error probability at high SNR is studied for the linear dispersion code. Further, a tight bound for high signal-to-noise ratio is derived to show the relationships between the error probability and the constellation size and the space-time symbol rate. The theoretical results are verified by comparison with simulation results. The study provides a guideline for adaptation.

In chapter 4, we study the probability density function of the signal-to-interference-noise ratio for a MIMO transceiver using a linear dispersion code and linear minimum-mean-square-error receiver over a Rayleigh fading channel. With the statistics as a guideline, we study the design of an adaptive selection-mode transceiver. Two adaptation techniques are studied, using constellation size and the space-time symbol rate,

respectively. To improve the average transmission rate, a new adaptation design is proposed, in which the constellation and the space-time symbol rate are considered jointly. As a result, more transmission rates are available, and the gaps between the transmission rates are reduced and hence the average transmission rate is improved. Theoretical analysis and simulation results are provided to verify the new design.

In chapter 5, we propose a novel scheme called "beam-nulling" using the same feedback bandwidth as beamforming. The capacity of beam-nulling is compared with the equal power, beamforming and optimal water-filling techniques, using theoretical analysis and numerical results. In the case when there is enough bandwidth to feed back more than one eigenvector to the transmitter, extended schemes called multi-dimensional beamforming and multi-dimensional beam-nulling are proposed and evaluated. The results show that the capacity of beam-nulling is close to that of optimal water-filling at medium SNR.

In chapter 6, the average bit-error rates of 1D beamforming and 1D beam-nulling with MMSE receivers are evaluated numerically and verified by simulation results. At the same data rate, 1D beamforming and 1D beam-nulling are compared in terms of bit-error rate. To achieve better performance, 1D beam-nulling can be concatenated with a linear dispersion code. Similarly, both MD beamforming and MD beam-nulling can be concatenated with LDC and STBC. Simulation results are provided for the evaluation of concatenated schemes. The results show that if the data rate is low, beam-nulling with linear dispersion code can approach beamforming at high SNR. If the data rate is high, beam-nulling outperforms beamforming, even with a suboptimal MMSE receiver.

Finally, in chapter 7, we summarize the conclusions of this thesis and identify some future work areas.

1.4 Contributions

The main contribution of chapter 3 is the study of the error performance and capacity of linear dispersion codes. First, the ergodic capacity of full-rate linear dispersion code in frequency-flat Rayleigh fading environments is derived in terms of signal-to-noise ratio and multiple antenna dimensions. Next, an upper bound of average error probability for full-rate linear dispersion code is derived. Based on the bound, a tight upper bound of average error probability at high signal-to-noise ratio is further derived to show the diversity advantage of linear dispersion codes and demonstrate the relationship of error probability to constellation size and space-time symbol rate. This study will be useful in the design and study of linear dispersion codes. The relevant contributions of this study are published in [58], and [59].

The main contribution of chapter 4 is the proposal of a new adaptation scheme for MIMO systems using linear dispersion codes. The statistics of signal-to-interference-noise for a MIMO transceiver using linear dispersion code and a linear minimum-mean-square-error (MMSE) receiver over a Rayleigh fading channel are studied. The associated probability density function of the signal-to-interference-noise is derived and verified. The average BER over MIMO fading channel for a given constellation using the MMSE receiver is calculated numerically. The numerical and simulation results match very well. With the statistics as a guideline, we study a new aspect of selection-mode adaptation using a linear dispersion code. A new adaptive parameter, called the space-time symbol rate, can be applied thanks to the use of linear dispersion code. An adaptive algorithm for the selection-mode adaptation is proposed. Based on the proposed algorithm, two adaptive techniques are studied, which use constellation size and space-time symbol rate, respectively. If constellation size and the space-time symbol rate are considered jointly, more selection modes can be available, and theoretical analysis demonstrates that the average transmission rate of selection-mode adaptation can be improved. Simulation results are provided to show

the benefits of our new design. The relevant contributions of this study are published in [60], [61], and [62].

The main contribution of Chapter 5 is the proposal of a novel scheme called "beam-nulling". Unlike the eigen-beamforming scheme in which only the best spatial subchannel is considered, only the worst spatial subchannel is discarded in beam-nulling. Hence, the loss of channel capacity can be reduced compared to the optimal water-filling scheme. The existing beamforming and new proposed beam-nulling can be extended if more than one eigenvector is available at the transmitter. The new extended schemes are called MD beamforming and MD beam-nulling. Additionally, the capacities of water-filling, equal power, beamforming and beam-nulling are compared through theoretical analysis and numerical results. It is shown that at medium signal-to-noise ratio, beam-nulling comes close to the optimal water-filling capacity. The relevant contributions of this study are published in [63], [64], [65], and [67].

The main contribution of Chapter 6 is the study of the performance of the beam-nulling and the extended MD beamforming and MD beam-nulling. Based on the derived signal-to-interference-plus-noise ratio of a minimum-mean-square-error receiver, an average bit-error rate for beam-nulling is given and verified by numerical and simulation results. Simulation results are provided to compare beam-nulling with beamforming at the same data rate. To further improve performance and keep within reasonable complexity, beam-nulling is concatenated with linear dispersion code. Simulation results are also provided to evaluate the concatenated scheme. Similarly, both multi-dimensional schemes can be concatenated with a linear dispersion code or a space-time block code. It is shown that the multi-dimensional scheme with linear dispersion code can significantly outperform the multi-dimensional scheme with space-time block code when the data rate is high. The relevant contributions of this study are published in [63], [66], and [67].

Chapter 2

Preliminaries

Certain background concepts and terminologies pertaining to adaptive MIMO systems are presented. The content in this chapter provides the foundation for the development of subsequent chapters.

2.1 MIMO Channel Model

In wireless communications, the surrounding static and moving objects such as buildings, trees and vehicles act as reflectors so that multiple reflected waves of the transmitted signals arrive at the receive antennas from different directions and with different propagation delays. When these signals are collected at the receiver, they may add constructively or destructively depending on the random phases of the signals arriving at the receiver. The amplitudes and phases of the combined multiple signals vary with the relative movement of the surrounding objects in the wireless channel. The resultant fluctuation is known as fading [57].

Fading, can be categorized as flat fading, also known as frequency non-selective fading, and frequency selective fading. In a flat fading channel, the transmitted signal bandwidth is smaller than the coherence bandwidth of the channel. Hence, all frequency components in the transmitted signal are subjected to the same fading at-

tenuation. In a frequency selective fading channel, the transmitted signal bandwidth is larger than the coherence bandwidth of the channel, and so different frequency components in the transmitted signal experience different fading attenuation. As a result, the spectrum of the received signal differs from that of the transmitted signal. This process is called distortion.

Fading can also be classified as fast fading or slow fading, depending on how rapidly the channel changes compared to the symbol duration. If the channel can be deemed constant over a large number of symbols, the channel is said to be a slow fading channel; otherwise it is a fast fading channel [52].

In wireless communications, the envelope of the received signal can be described by *Rayleigh* or *Ricean* distributions. In no line-of-sight propagation, Rayleigh distribution is applied and the fading is called Rayleigh fading. Since there is a dominant non-fading component in line-of-sight propagation, Ricean distribution is often used to model the envelope of the received signal, which is known as Ricean fading.

In this study, the channel is assumed to be a Rayleigh flat fading channel with N_t transmit and N_r ($N_r \geq N_t$) receive antennas. Let's denote the complex gain from transmit antenna n to receiver antenna m by h_{mn} and collect them to form an $N_r \times N_t$ channel matrix $\mathbf{H} = [h_{mn}]$. The channel is known perfectly at the receiver but is partially informed to the transmitter. The entries in $\mathbf{H}$ are assumed to be independently identically distributed ($i.i.d.$) symmetrical complex Gaussian random variables with zero mean and unit variance. The MIMO channel is shown in Figure 2.1.

The singular-value decomposition of $\mathbf{H}$ can be written as

$$\mathbf{H} = \mathbf{U}\mathbf{\Lambda}\mathbf{V}^H \tag{2.1}$$

where $\mathbf{U}$ is an $N_r \times N_r$ unitary matrix, $\mathbf{\Lambda}$ is an $N_r \times N_t$ matrix with singular values $\{\lambda_i\}$ on the diagonal and zeros off the diagonal, and $\mathbf{V}$ is an $N_t \times N_t$ unitary matrix. For

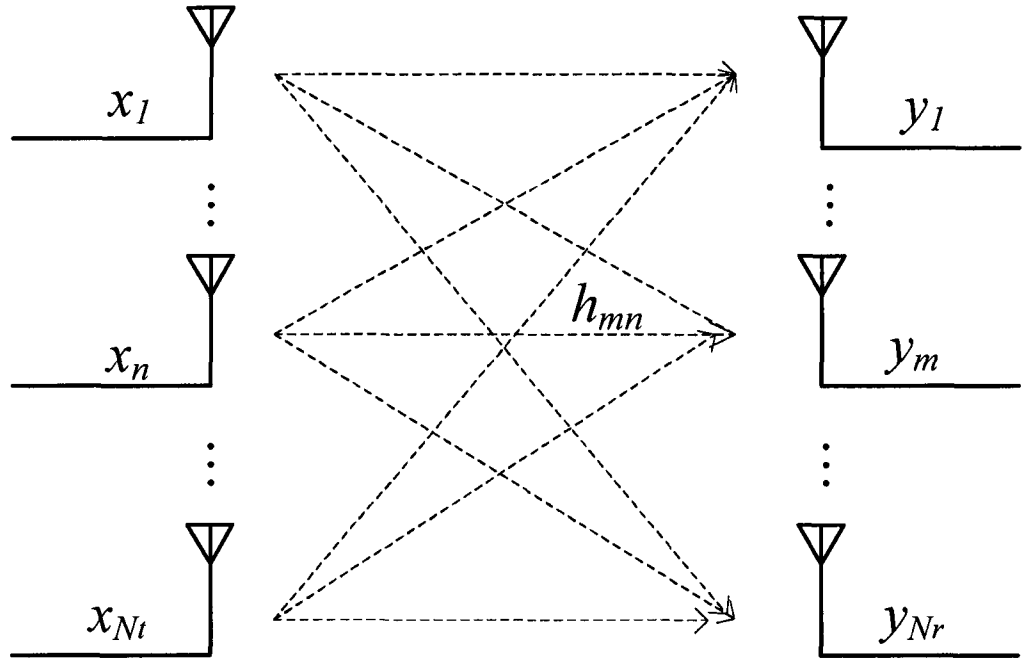

Figure 2.1: MIMO channel model.

convenience, we assume $\lambda_1 \geq \lambda_2 \ldots \geq \lambda_{N_t}$, $\mathbf{U} = [\mathbf{u}_1 \mathbf{u}_2 \ldots \mathbf{u}_{N_r}]$ and $\mathbf{V} = [\mathbf{v}_1 \mathbf{v}_2 \ldots \mathbf{v}_{N_t}]$. $\{\mathbf{u}_i\}$ and $\{\mathbf{v}_i\}$ are column vectors. We assume that the rank of $\mathbf{H}$ is r ($r \leq N_t$). That is, the number of non-zero singular values is r.

From (2.1), the original channel can be considered as consisting of r uncoupled parallel subchannels. Each subchannel corresponds to a singular value of $\mathbf{H}$. In the following context, the subchannel is also referred to as a "spatial subchannel". For instance, one spatial subchannel corresponds to λ_i, $\mathbf{u}_i$ and $\mathbf{v}_i$.

When the MIMO channel $\mathbf{H} = [h_{mn}]$ is known perfectly to the receiver but unknown to the transmitter, the ergodic capacity of such a MIMO channel is given by [1][2]

$$C\left(\frac{P}{\sigma_z^2}\right) = E\left[\log\det(\mathbf{I}_{N_t} + \frac{P}{N_t\sigma_z^2}\mathbf{H}\mathbf{H}^H)\right] \tag{2.2}$$

2.2 Performance Measures and Their Tradeoffs

From (2.2), at high signal-to-noise ratio (SNR), the ergodic capacity becomes [38]

$$C\left(\frac{P}{\sigma_z^2}\right) = \min(N_t, N_r)\log\left(\frac{P}{N_t\sigma_z^2}\right) + \sum_{i=|N_t-N_r|+1}^{\max(N_t,N_r)} E(\log\chi_{2i}^2) + o(1) \qquad (2.3)$$

where χ_{2i}^2 is chi-square distributed with $2i$ degrees of freedom. From (2.3), we observe that at high SNR, a MIMO channel can offer $\min(N_t, N_r)$ times of capacity compared to a single-antenna channel. In addition, multiple antennas can also be used to improve communication reliability. A "good" MIMO transmission scheme must exploit the available temporal and spatial resources as much as possible and provide a flexible tradeoff between the reliability and the data rate.

2.2.1 Tradeoff Between Diversity and Multiplexing Gain

The increase of the data rate in a MIMO transmission scheme can be characterized by multiplexing gain. A MIMO transmission scheme is said to achieve a multiplexing gain r if, at high SNR ρ, its transmission rate is $R \approx r\log\rho$, which is r times the capacity of a single-input single-output channel with the same SNR ρ.

The improvement in reliability of a MIMO transmission scheme is often characterized by diversity gain. There are two definitions for diversity gain.

Zheng's spatial diversity is defined as the exponent of the error performance of a scheme when the data rate is fixed against the channel capacity [38]. Denote $P_e(\rho)$ as the error probability with respect to the SNR ρ of a scheme whose data rate is $R = r\log\rho$. Then Zheng's spatial diversity can be found in the asymptotic behavior, i.e.,

$$\lim_{\rho\to\infty}\frac{\log P_e(\rho)}{\log\rho} = -d(r) \qquad (2.4)$$

where $d(r)$ is the diversity order.

Tarokh's diversity is the more widely used definition, it is the exponent of

the error performance of a scheme when the data rate is constant [4].

The first definition is useful when discussing the tradeoff between data rate and reliability; whereas the second definition is useful when discussing the error performance of a scheme with a fixed data rate.

It was shown in [38] that there is a fundamental tradeoff between how much of the multiplexing gain and Zheng's diversity gain can be achieved simultaneously. Specifically, a MIMO system with N_t transmit and N_r receive antennas can provide the maximum diversity gain $d_{max} = N_t N_r$ or the maximum spatial multiplexing gain $r_{max} = \min(N_t, N_r)$ but not both at the same time. Therefore, in designing a MIMO transmission scheme, flexible tradeoff is particularly important for multi-rate wireless communications.

2.2.2 Error Performance and Design Criteria for Fixed Data Rate

Pairwise error probability is often used to analyze the error performance of a MIMO transmission scheme with a given data rate. The pairwise error probability between a codeword pair $(\mathbf{X}, \hat{\mathbf{X}})$ is the probability that a decoder decides in favor of $\hat{\mathbf{X}}$ when in fact $\mathbf{X}$ is transmitted [4].

Let $x_i(n)$ be the symbol to be transmitted at time n over transmit antenna i, and collect a block of transmitted symbols (a codeword) as

$$\mathbf{X} = \begin{pmatrix} x_1(1) & x_1(2) & \dots & x_1(L) \\ x_2(1) & x_2(2) & \dots & x_2(L) \\ \vdots & \vdots & \ddots & \vdots \\ x_{N_t}(1) & x_{N_t}(2) & \dots & x_{N_t}(L) \end{pmatrix} \tag{2.5}$$

Then with ML decoding, the upper bound of the pairwise error probability of $(\mathbf{X}, \hat{\mathbf{X}})$

in the case of Rayleigh fading, is given by [4]

$$P_r(\mathbf{X}, \hat{\mathbf{X}}) \leq \left(\prod_{i=1}^{N_t} \frac{1}{1 + \frac{E_s}{4N_0}\lambda_i} \right)^{N_r} \tag{2.6}$$

where E_s is the average symbol energy, N_0 is the noise power spectral density, and λ_i is the i-th non-zero eigenvalue of matrix $\mathbf{A} = (\mathbf{X} - \hat{\mathbf{X}})(\mathbf{X} - \hat{\mathbf{X}})^H$. At high SNR, the above upper bound can be simplified as

$$P_r(\mathbf{X}, \hat{\mathbf{X}}) \leq \left(\prod_{i=1}^{r} \lambda_i \right)^{-N_r} \left(\frac{E_s}{4N_0} \right)^{-rN_r} \tag{2.7}$$

where r is the rank of matrix $\mathbf{A}$. The pairwise error probability decreases exponentially as SNR increases as shown in (2.7). The exponent rN_r in the error probability of (2.7) determines the slope of the error probability curve as SNR increases and is called Tarokh's diversity gain. It can also be observed that a coding gain of $\left(\prod_{i=1}^{r} \lambda_i \right)^{\frac{1}{r}}$ is achieved.

Based on the above observations, two design criteria were obtained by Tarokh *et al.* in [4]:

The Rank Criterion: In order to achieve the maximum diversity $N_t N_r$, the difference matrix $(\mathbf{X} - \hat{\mathbf{X}})$ has to be full rank for all pairs of $\mathbf{X}$ and $\hat{\mathbf{X}}$. If $(\mathbf{X} - \hat{\mathbf{X}})$ has minimum rank r over the set of two pairs of distinct codewords, then a diversity of rN_r is achieved.

The Determinant Criterion: Suppose that a diversity gain of rN_r is our target, then the design goal is making the minimum product $\left(\prod_{i=1}^{r} \lambda_i \right)$ as large as possible over all pairs of distinct codewords $\mathbf{X}$ and $\hat{\mathbf{X}}$. If a diversity gain of $N_t N_r$ is the design target, then the minimum product $\prod_{i=1}^{r} \lambda_i$ must be maximized over all pairs of distinct codewords. Note that the coding gain $\prod_{i=1}^{r} \lambda_i$ is the absolute value of the sum of the determinants of all $r \times r$ principal co-factors of $\mathbf{A}$ taken over all pairs of codewords $\mathbf{X}$ and $\hat{\mathbf{X}}$.

2.3 Linear Dispersion Code

Since the discovery of the significant gain in capacity of MIMO channels [1][2], tremendous research and development efforts have been invested in MIMO technology. and numerous MIMO transmission schemes have been developed. Early examples include space-time trellis codes (STTC) [4] and space-time block codes (STBC) [5][30] designed to improve error performance, and spatial multiplexing schemes such as Bell-labs layered space-time (BLAST) schemes [31]-[33] aiming at achieving higher data rates.

At very high data rates and with a large number of antennas, many of the current space-time codes, such as STTCs [4] and STBCs [5][30] suffer from complexity or performance difficulties. For instance, the number of states in the trellis codes of [4] grows exponentially with either the rate or the number of transmit antennas. The block codes of [5][30] suffer from rate and error performance loss as the number of antennas grows. The BLAST schemes only consider the high data rate and thus the performance is unsatisfactory. A common drawback of early MIMO transmission schemes is that they are not flexible as far as the rate-performance tradeoff. As such, many linear dispersion (LD) codes are proposed [34]-[36], which have many of the coding and diversity advantages associated with simple decoding and flexible linear structure. We briefly describe the general structure of the LDC introduced by the pioneering paper of Hassibi et al.[34].

2.3.1 Coding

We assume that the LDC breaks the data stream into L sub-streams and $x_1, x_2, \ldots, x_L$ are the complex symbols taken from a finite alphabet, such as 2^η-PSK or 2^η-QAM. with no loss of generality, $x_1, x_2, \ldots, x_L$ are assumed to be uncorrelated and to have zero mean and unit variance. Suppose that there are N_t transmit and N_r receive antennas, and an interval of T symbols are available while the channel is constant

and known to the receiver. The transmitted signal can be written as [34]

$$\mathbf{X} = \sum_{i=1}^{L} \mathbf{M}_i x_i + \sum_{i=1}^{L} \mathbf{N}_i x_i^* \tag{2.8}$$

where $\mathbf{M}_i$, $\mathbf{N}_i$ are fixed $N_t \times T$ dispersion matrices for the i-th symbol. The LDC is defined by the set of dispersion matrices $\{\mathbf{M}_i, \mathbf{N}_i\}$, whereas each individual codeword is determined by the choice of complex symbols $x_1, x_2, \ldots, x_L$.

The choices for the dispersion matrices $\mathbf{M}_i$, $\mathbf{N}_i$, T and L are critical factors in designing LDCs. To choose the $\{\mathbf{M}_i, \mathbf{N}_i\}$ we propose to optimize a nonlinear information-theoretic criterion. The mutual information between the transmitted signals $\{x_i, x_i^*\}$ and the received signal is maximized.

We decompose x_i into its real and imaginary parts,

$$x_i = \alpha_i + j\beta_i, \qquad i = 1, \quad , L$$

and write

$$\mathbf{X} = \sum_{i=1}^{L} (\alpha_i \mathbf{A}_i + j\beta_i \mathbf{B}_i) \tag{2.9}$$

where $\mathbf{A}_i = \mathbf{M}_i + \mathbf{N}_i$ and $\mathbf{B}_i = \mathbf{M}_i - \mathbf{N}_i$. The dispersion matrices $\mathbf{A}_i, \mathbf{B}_i$ also specify the code.

2.3.2 Decoding

The received data block can generally be expressed with

$$\mathbf{Y} = \sqrt{\frac{P}{N_t}}\mathbf{H}\mathbf{X} + \mathbf{Z} = \sqrt{\frac{P}{N_t}}\mathbf{H}\sum_{i=1}^{L}(\alpha_i \mathbf{A}_i + j\beta_i \mathbf{B}_i) + \mathbf{Z} \tag{2.10}$$

We decompose the the matrices in (2.10) into their real and imaginary parts to obtain

$$\mathbf{Y}_R + \mathbf{j}\mathbf{Y}_I = \sqrt{\frac{P}{N_t}} \sum_{i=1}^{L} [\alpha_i(\mathbf{A}_{R,i} + \mathbf{j}\mathbf{A}_{I,i}) + \mathbf{j}\beta_i(\mathbf{B}_{R,i} + \mathbf{j}\mathbf{B}_{I,i})] * (\mathbf{H}_R + \mathbf{j}\mathbf{H}_I) + \mathbf{Z}_R + \mathbf{j}\mathbf{Z}_I$$

where $\mathbf{H}_R = \Re(\mathbf{H})$ and $\mathbf{H}_I = \Im(\mathbf{H})$. We denote the columns of $\mathbf{Y}_R, \mathbf{Y}_I, \mathbf{H}_R, \mathbf{H}_I, \mathbf{Z}_R$, and $\mathbf{Z}_I$ by $y_{R,n}, y_{I,n}, b_{R,n}, b_{I,n}, v_{R,n}$, and $v_{I,n}$, respectively, and define

$$\mathring{A}_L = \begin{bmatrix} \mathbf{A}_{R,i} & -\mathbf{A}_{I,i} \\ \mathbf{A}_{I,i} & \mathbf{A}_{R,i} \end{bmatrix}, \quad ß_L = \begin{bmatrix} -\mathbf{B}_{R,i} & -\mathbf{B}_{I,i} \\ \mathbf{B}_{I,i} & -\mathbf{B}_{R,i} \end{bmatrix}, \quad \bar{\mathbf{b}}_n = \begin{bmatrix} b_{R,n} \\ b_{I,n} \end{bmatrix}$$

where $n = 1, ..., N_r$. We then gather the equations in $\mathbf{Y}_R$ and $\mathbf{Y}_I$ to form the single real system of equations

$$\begin{bmatrix} \Re\{y_1\} \\ \Im\{y_1\} \\ \vdots \\ \Re\{y_{N_r}\} \\ \Im\{y_{N_r}\} \end{bmatrix} = \sqrt{\frac{P}{N_t}} \widetilde{\mathbf{H}} \cdot \begin{bmatrix} \alpha_1 \\ \beta_1 \\ \vdots \\ \alpha_L \\ \beta_L \end{bmatrix} + \begin{bmatrix} \Re\{v_1\} \\ \Im\{v_1\} \\ \vdots \\ \Re\{v_{N_r}\} \\ \Im\{v_{N_r}\} \end{bmatrix} \tag{2.11}$$

where the equivalent $2N_rT \times 2L$ real channel matrix is given by

$$\widetilde{\mathbf{H}} = \begin{bmatrix} \mathring{A}_1\bar{\mathbf{b}}_1 & ß_1\bar{\mathbf{b}}_1 & \dots & \mathring{A}_L\bar{\mathbf{b}}_1 & ß_L\bar{\mathbf{b}}_1 \\ \vdots & \vdots & \ddots & \vdots & \vdots \\ \mathring{A}_1\bar{\mathbf{b}}_{N_r} & ß_1\bar{\mathbf{b}}_{N_r} & \dots & \mathring{A}_{1L}\bar{\mathbf{b}}_{N_r} & ß_L\bar{\mathbf{b}}_{N_r} \end{bmatrix}$$

We now have a linear relation between the input and output vectors $\mathbf{x}$ and $\mathbf{y}$ given by

$$\mathbf{y} = \sqrt{\frac{P}{N_t}} \widetilde{\mathbf{H}}\mathbf{x} + \mathbf{z}$$

where the equivalent channel $\widetilde{\mathbf{H}}$ is known to the receiver because the original channel $\mathbf{H}$ and the dispersion matrices $\mathbf{A}_i$ and $\mathbf{B}_i$ are also known to the receiver.

The key to the LDC design is that the basis matrices are chosen such that the resulting codes maximize the ergodic capacity of the equivalent MIMO system [35]. However, the LDCs proposed in [34] only optimize the ergodic capacity; thus, corresponding good error probability performance is not explicitly guaranteed [1].

More recent research [33] [36] [42] in the design of linear dispersion codes based on number theory has shown that it is possible to provide full rate and full diversity without information loss, that is, the ergodic capacity of a linear dispersion coded MIMO channel can be equal to that of its original MIMO channel.

2.4 Adaptive Modulation and Coding

To combat channel quality variation and thus further improve system performance, such as the power consumption, error rate and average throughput, adaptive constellation and coding can be applied. Adaptive transmission was first investigated in the late sixties and early seventies [6]. The basic tactic is to estimate the channel at the receiver and feed it back to the transmitter, and then a suitable modulation and coding will be selected to adapt relatively to the channel characteristics as shown in Figure 2.2. Transmission schemes that do not adapt to fading conditions require a fixed link margin to maintain acceptable performance when the channel quality is poor. For example, Rayleigh fading can cause a signal power loss of up to 30dB, and so to maintain reasonable performance, a 30 dB margin has to be satisfied. Adapting to the channel fading can increase average throughput, reduce the required transmit power, or reduce the average probability of bit error by taking advantage of favorable channel conditions to send at higher transmission rates or lower power and by reducing the data rate or increasing power as the channel degrades.

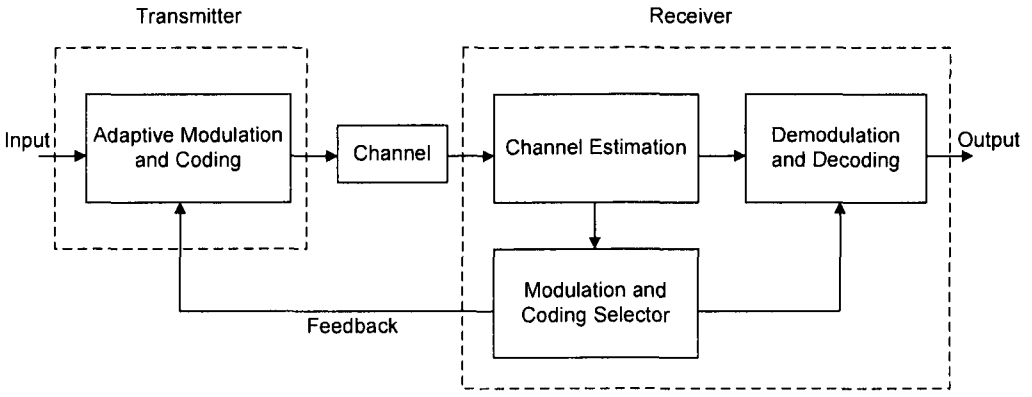

Figure 2.2: Adaptive modulation and coding system.

2.5 Power Allocation among Spatial Subchannels

We assume that the total transmitted power is constrained to P. Given this power constraint, different power allocation among spatial subchannels can affect the channel capacity tremendously. In the following context, depending on the power allocation among spatial subchannels, several popular schemes are presented.

2.5.1 Equal Power

If the transmitter has no knowledge about the channel, the most judicious strategy is to allocate the power to each transmit antenna equally. In this case, the received signals can be written as

$$\mathbf{y} = \sqrt{\frac{P}{N_t}}\mathbf{H}\mathbf{x} + \mathbf{z} \tag{2.12}$$

The associated instantaneous channel capacity with respect to $\mathbf{H}$ can be written as [1]

$$C_{eq} = \sum_{i=1}^{N_t} \log\left(1 + \frac{P}{N_t\sigma_z^2}\lambda_i^2\right) \tag{2.13}$$

The numerical results of ergodic (average) channel capacity for 2×2, 3×3 and 4×4 Rayleigh flat fading channels are shown in Figure 2.3.

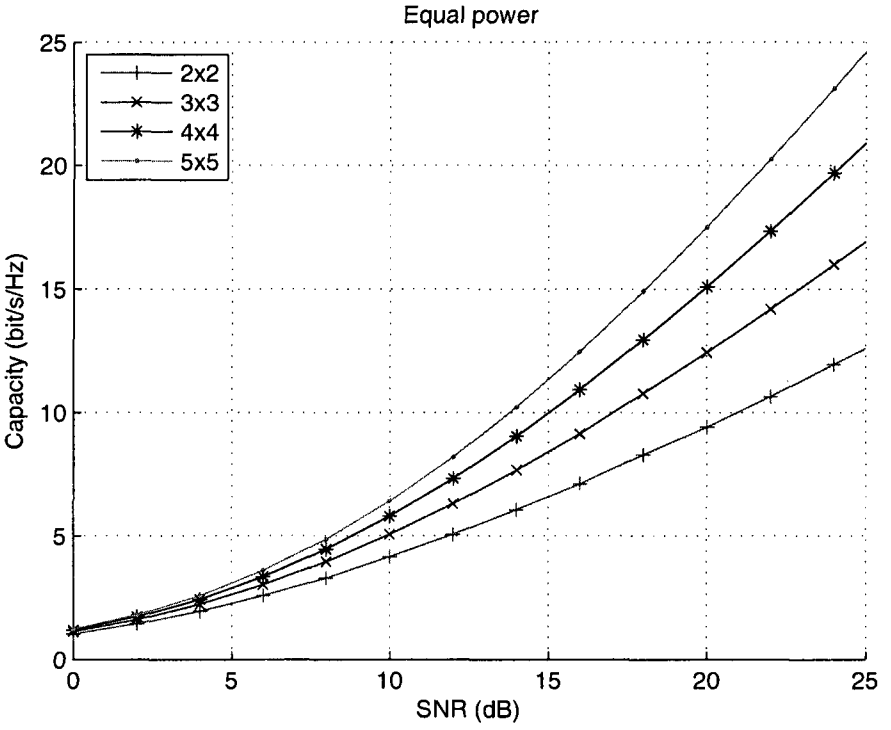

Figure 2.3: Capacity for equal power allocation.

2.5.2 Water-Filling

If the transmitter has full knowledge about the channel, the most judicious strategy is to allocate the power to each spatial subchannel by the water-filling principle [1]. This allocates more power when a spatial subchannel has larger gain (i.e. $\{\lambda_i\}$) and less when a subchannel gets worse. With $\mathbf{V}$ at the transmitter and $\mathbf{U}$ at the receiver, the original MIMO channel is converted to r uncoupled parallel SISO channels. The WF scheme is shown in Figure 2.4.

For spatial subchannel $i, \forall i = 1, 2, \ldots, r$, the received signal is

$$\tilde{y}_i = \sqrt{P_i}\lambda_i x_i + \tilde{z}_i \tag{2.14}$$

where $\sum_{i=1}^{r} P_i = P$ and $\tilde{z}_i$ the is AWGN variable with zero mean and σ_z^2 variance.

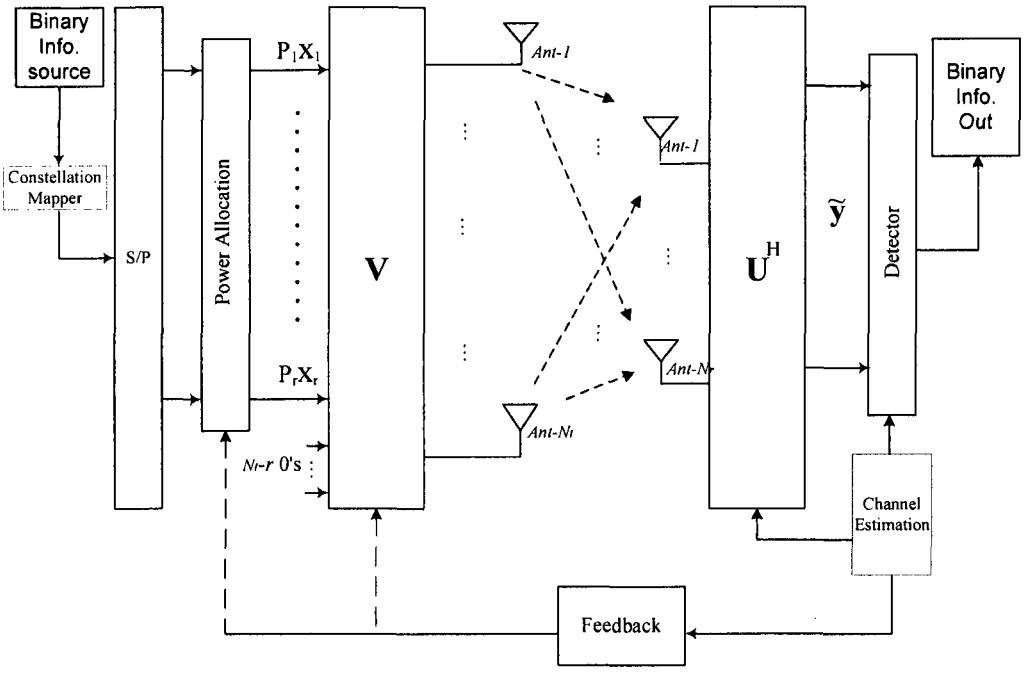

Figure 2.4: Water-filling scheme.

Following the method of Lagrange multipliers, the optimal P_i can be found as [1]

$$P_i = \max\left(\frac{1}{L\ln 2} - \frac{\sigma_z^2}{\lambda_i}, 0\right), \forall i = 1, 2, \ldots, r \tag{2.15}$$

where L is the Lagrange multiplier. The instantaneous channel capacity for this spatial subchannel is

$$C_{wf,i} = \log\left(1 + \frac{P_i}{\sigma_z^2}\lambda_i^2\right) \tag{2.16}$$

The total channel capacity with respect to $\mathbf{H}$ is then

$$C_{wf} = \sum_{i=1}^{r} C_{wf,i} \tag{2.17}$$

The WF scheme maximizes the channel capacity by controlling the power allocation over spatial subchannels. Since $\lambda_1 \geq \lambda_2 \ldots \geq \lambda_r$, we have $P_1 \geq P_2 \ldots \geq P_r$ and $C_{wf,1} \geq C_{wf,2} \ldots \geq C_{wf,r}$. In practice, if each spatial subchannel requires the same error rate performance, the spatial subchannel with a larger gain (i.e. $\sqrt{P_i}\lambda_i$)

can have a higher rate; while if each spatial subchannel has the same rate, the one with the larger gain will have better performance. The application of these two approaches will depend on the type of service. For example, important data mandate high quality but the voice transmission can tolerate low quality.

The numerical results of ergodic (average) channel capacity for 2×2, 3×3 and 4×4 Rayleigh flat fading channels are shown in Figure 2.5.

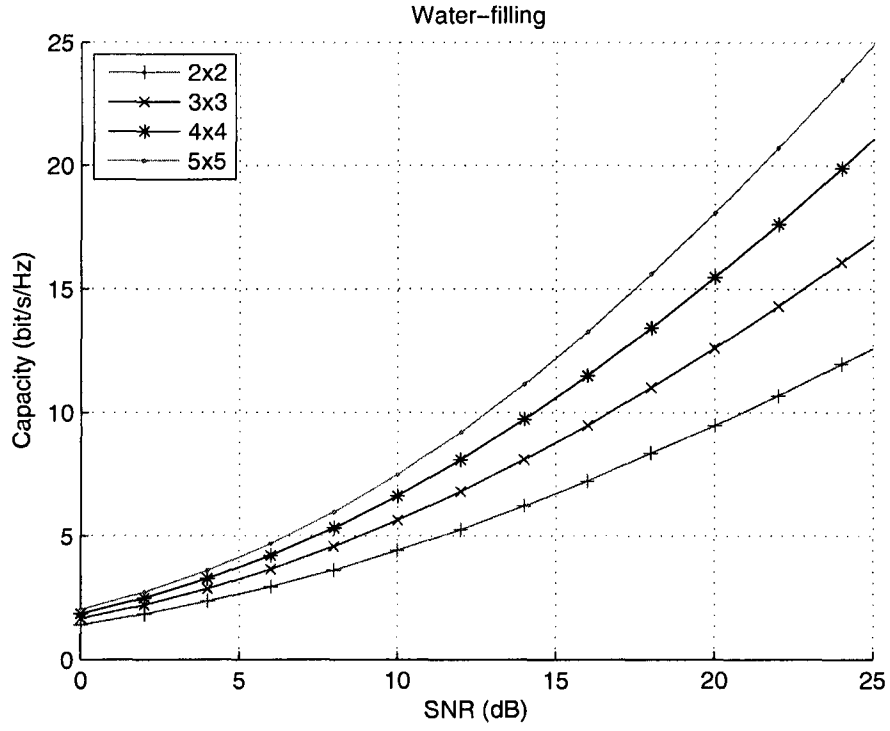

Figure 2.5: Capacity for water-filling.

In the WF scheme, the feedback bandwidth for the perfect CSI grows with respect to the number of transmit and receive antennas. In practice, the bandwidth for CSI feedback is often very limited. A large feedback bandwidth also affects the transmission efficiency.

2.5.3 Eigen-Beamforming

To save feedback bandwidth, beamforming can be considered. Beamforming is a linear signal processing technique that jointly controls the complex weights of the transmit and receive antennas to optimize the signal-to-noise ratio (SNR) in one direction [16][23]. For the MIMO model, optimal beamforming is called "eigen-beamforming". In the following context, this optimal solution is referred to as beamforming.

In this scheme, the eigenvector associated with the maximum singular value λ_1 from the transmitter side, i.e., $\mathbf{v}_1$, is fed back to the transmitter as the transmission beamformer. The Eigen-beamforming scheme is shown in Figure 2.6.

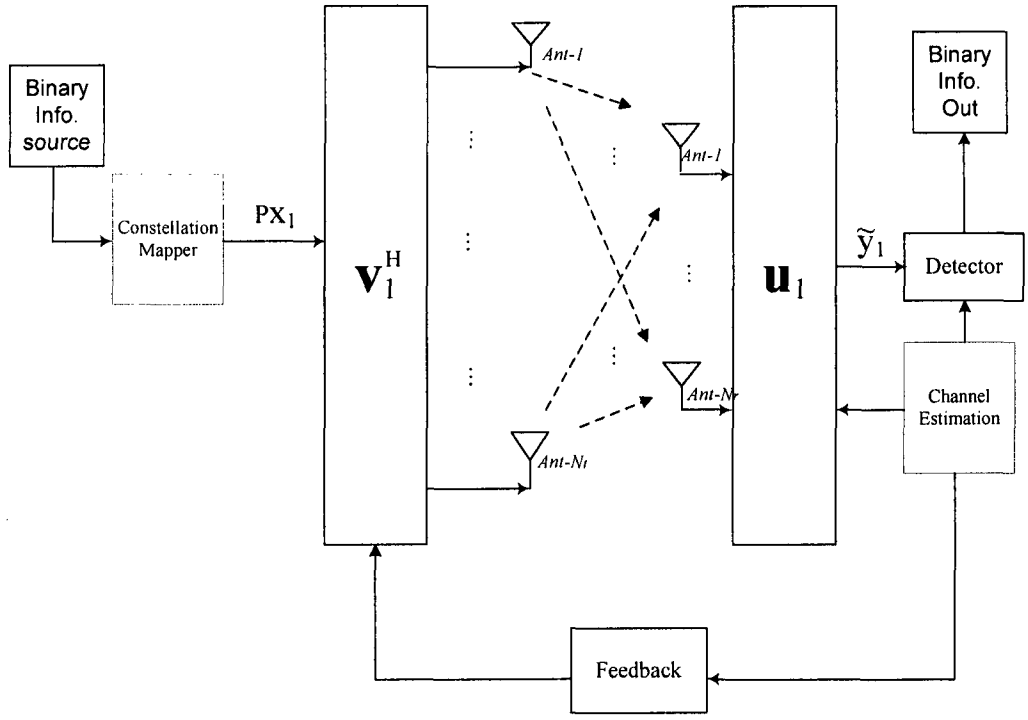

Figure 2.6: Eigen-beamforming scheme.

We assume that one symbol, say x_1, is transmitted. At the receiver, the received vector can be written as

$$\mathbf{y}_1 = \sqrt{P}\mathbf{H}\mathbf{v}_1 x_1 + \mathbf{z}_1 \tag{2.18}$$

where $\mathbf{z}_1$ is the additive white Gaussian noise vector with *i.i.d.* symmetrical complex Gaussian elements of zero mean and variance σ_z^2.

The eigenvector associated with the maximum singular value from the receiver side, i.e., $\mathbf{u}_1$, is applied as the receiver beamformer. Then we have

$$\tilde{y}_1 = \mathbf{u}_1^H \mathbf{y}_1 = \sqrt{P}\lambda_1 x_1 + \tilde{z}_1 \tag{2.19}$$

where $\tilde{z}_1$ is the Gaussian noise vector with zero mean and variance σ_z^2. As can be seen from (2.19), only the spatial subchannel associated with the maximum singular value λ_1 is applied.

The associated instantaneous channel capacity with respect to $\mathbf{H}$ can be written as

$$C_{bf} = \log\left(1 + \frac{P}{\sigma_z^2}\lambda_1^2\right) \tag{2.20}$$

The numerical results of the ergodic (average) channel capacity for 2×2, 3×3 and 4×4 Rayleigh flat fading channels are shown in Figure 2.7.

The eigen-beamforming scheme can save feedback bandwidth and is optimized in terms of SNR [23]. However, since only one spatial subchannel is considered, this scheme suffers from loss of channel capacity [26], especially when the number of antennas grows. Also, as can be seen from Figure 2.7, the capacity gap between different numbers of antennas is nearly the same for all of the SNR region.

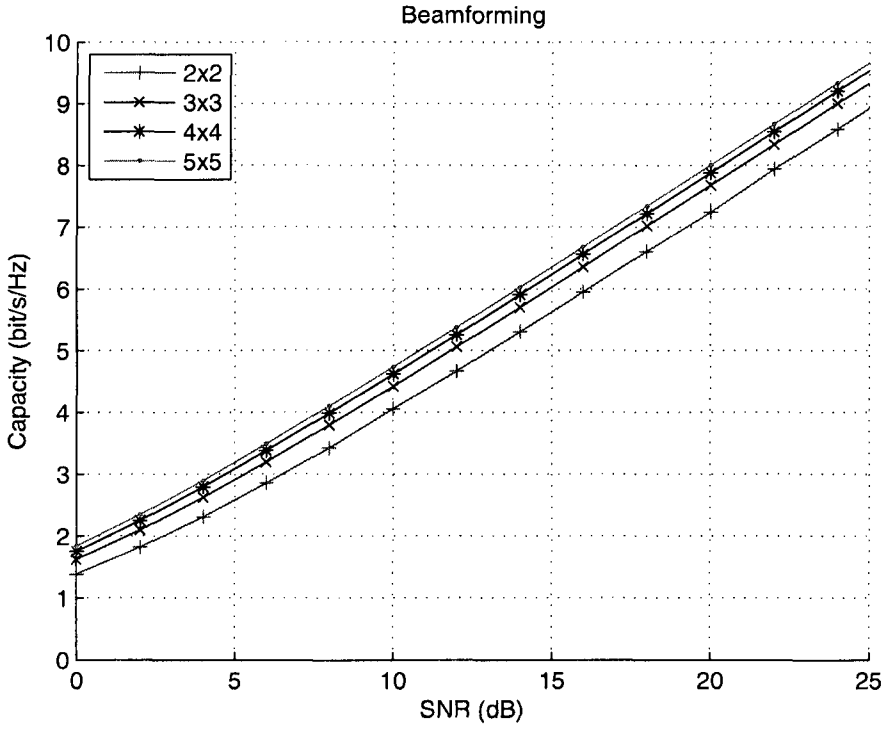

Figure 2.7: Capacity for eigen-beamforming.

Chapter 3

Theoretical Analysis of Full Rate Linear Dispersion Codes

3.1 Introduction

Although any space-time code can be a potential candidate for adaptation, the LDC is a particular desirable choice. This is because it subsumes many existing block codes [5][30] and layered schemes [31]-[33] as its special cases, allows the inclusion of suboptimal linear receivers with greatly reduced complexity, and provides a flexible rate-versus-performance tradeoff [34]. Hence, we focus on adaptive design of the LDC in our research. However, error probability analysis of LDCs, which is important for adaptation design, is scarce in the current literatures. For example, in [34], an upper bound of average pairwise error probability is derived but it is still a function of random matrices. The capacity and pairwise error probability of LDCs have been derived, but only in terms of random eigenvalues, such as in [35][37]. Based on these results, we pursue the analysis of the capacity and error performance of LDCs further.

We present our system model below. Based on the system mode, an analytical formula of the capacity and a tight upper bound at high signal-to-noise ratio (SNR) will be derived in terms of constellation size and space-time (ST) symbol rate.

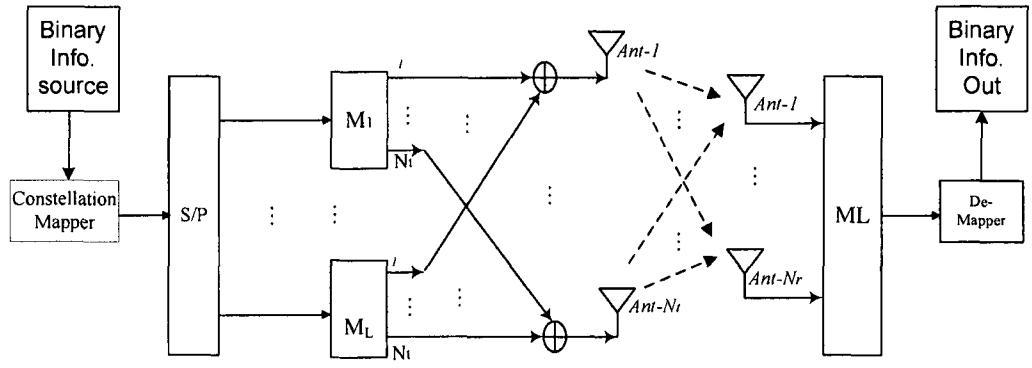

Figure 3.1: LDC system block diagram.

Simulation results are provided to verify the theoretical analysis.

3.2 System Model

In this study, a block fading channel model is assumed, whereby the channel stays constant throughout one modulation block but may change from block to block. Furthermore, the channel is assumed to be a Rayleigh flat fading channel with N_t transmit and N_r receive antennas. Let's denote the complex gain from transmit antenna j to receiver antenna i by h_{ij} and collect the gains to form an $N_r \times N_t$ channel matrix $\mathbf{H} = [h_{ij}]$, known perfectly to the receiver but unknown to the transmitter. The entries in $\mathbf{H}$ are assumed to be independently identically distributed $(i.i.d.)$ symmetrical complex Gaussian random variables with zero mean and unit variance. The LDC system is shown in Fig. 3.1.

In this system, information bits are first mapped into symbols. The symbol stream is then parsed into blocks of length L. The symbol vector associated with one modulation block is denoted by $\mathbf{x} = [x_1, x_2, \ldots, x_L]^T$ with $x_i \in \Omega \equiv \{\Omega_m | m = 0, 1, \ldots, 2^Q - 1, Q \geq 1\}$, which indicates a complex constellation of size 2^Q, such as 2^Q-QAM. The average symbol energy is assumed to be 1, i.e., $\frac{1}{2^Q} \sum_{m=0}^{2^Q-1} |\Omega_m|^2 = 1$. Each symbol in the block will be mapped by the ST modulator to a dispersion matrix of size $N_t \times T$. The dispersion matrices are then combined linearly and transmitted

over the N_t transmit antennas over T channel uses. An $N_t \times T$ codeword matrix is constructed as [34]

$$\mathbf{X} = \sum_{i=1}^{L} \mathbf{M}_i x_i + \sum_{i=1}^{L} \mathbf{N}_i x_i^* \tag{3.1}$$

where $\mathbf{M}_i$ and $\mathbf{N}_i$ are the dispersion matrices for the i-th symbol. For simplicity, the following model will be considered in this study

$$\mathbf{X} = \sum_{i=1}^{L} \mathbf{M}_i x_i \tag{3.2}$$

The ST modulator is defined by its L $N_t \times T$ dispersion matrices, i.e., $\mathbf{M}_i = [\mathbf{q}_{i1}, \mathbf{q}_{i2}, \ldots, \mathbf{q}_{iT}], \forall i = 1, 2, \ldots, L$. $\mathbf{q}_{ij}$ is the j-th column vector of $\mathbf{M}_i$. The results thus obtained can be extended to the model in (3.1). With a 2^Q-ary constellation, the data rate of the space-time modulator per channel use in bits is

$$R = Q \cdot L/T \tag{3.3}$$

The ST symbol rate L/T and constellation size Q can be adjusted to meet different requirements on data rate and error performance. The space-time mapping schemes used in existing layered space-time architectures, e.g., in [31] and [33], are also linear dispersion modulations. The linear dispersion modulation subsumes existing layered space-time schemes as special cases. At the receiver, the received signals associated with one modulation block can be written as

$$\mathbf{Y} = \sqrt{\frac{P}{N_t}}\mathbf{H}\mathbf{X} + \mathbf{Z} = \sqrt{\frac{P}{N_t}}\mathbf{H}\sum_{i=1}^{L} \mathbf{M}_i x_i + \mathbf{Z} \tag{3.4}$$

where $\mathbf{Y}$ is a complex matrix of size $Nr \times T$ whose (m, n)-th entry is the received signal at a receive antenna m, time instant n, $\mathbf{Z}$ is the additive white Gaussian noise (AWGN) matrix with *i.i.d.* symmetrical complex Gaussian elements of zero mean and variance σ_z^2, and P is the average energy per channel use at each receive antenna. It is

often desirable to write the matrix input-output relationship in (3.4) in an equivalent vector notation. Let vec() be the operator that forms a column vector by stacking the columns of a matrix, and define $\mathbf{y} = \text{vec}(\mathbf{Y})$, $\mathbf{z} = \text{vec}(\mathbf{Z})$, and $\mathbf{m}_i = \text{vec}(\mathbf{M}_i)$, then (3.4) can be rewritten as

$$\mathbf{y} = \sqrt{\frac{P}{N_t}}\overline{\mathbf{H}}\mathbf{G}\mathbf{x} + \mathbf{z} = \sqrt{\frac{P}{N_t}}\widetilde{\mathbf{H}}\mathbf{x} + \mathbf{z} \tag{3.5}$$

where $\overline{\mathbf{H}} = \mathbf{I}_T \otimes \mathbf{H}$ with $\otimes$ as the Kronecker product operator, $\mathbf{I}_T$ is $T \times T$ identity matrix and $\mathbf{G} = [\mathbf{m}_1, \mathbf{m}_2, \ldots, \mathbf{m}_L]$. In the following context, $\mathbf{G}$ will be referred to as the modulation matrix. Since the average energy of the signal per channel used at a receive antenna is assumed to be P, we have $\text{tr}(\mathbf{G}\mathbf{G}^H) = N_t T$.

3.3 Capacity Analysis

Under the assumption of *i.i.d.* Gaussian inputs, the associated ergodic channel capacity with respect to $\mathbf{H}$ is given in [1] as follows:

$$\begin{aligned} C &= \max_{tr(\mathbf{G}\mathbf{G}^H) \le N_t T} \frac{1}{T} E_{\mathbf{H}} \left\{ \log\det\left(\mathbf{I}_{N_r T} + \frac{P}{N_t \sigma_z^2} \overline{\mathbf{H}}\mathbf{G}\mathbf{G}^H\overline{\mathbf{H}}^H \right) \right\} \\ &= \max_{tr(\mathbf{G}\mathbf{G}^H) \le N_t T} \frac{1}{T} E_{\mathbf{H}} \left\{ \log\det\left(\mathbf{I}_L + \frac{P}{N_t \sigma_z^2} \overline{\mathbf{H}}^H\mathbf{G}^H\mathbf{G}\overline{\mathbf{H}} \right) \right\} \end{aligned} \tag{3.6}$$

Let $\mathbf{R}_t$ is the matrix consisting of rows and columns $(t-1)N_t + 1$ to tN_t of $\mathbf{G}\mathbf{G}^H$, i.e., $\mathbf{R}_t$ is the t-th diagonal block of size $N_t \times N_t$ of $\mathbf{G}\mathbf{G}^H$, then we have

$$\tilde{C} \le \frac{1}{T} E_{\mathbf{H}} \left\{ \log \left[\prod_{t=1}^{T} \det\left(\mathbf{I}_{N_r} + \frac{P}{N_t \sigma_z^2} \mathbf{H}\mathbf{R}_t\mathbf{H}^H \right) \right] \right\} \tag{3.7}$$

The equality in (3.7) holds on when $\mathbf{G}\mathbf{G}^H = \text{diag}[\mathbf{R}_1, \mathbf{R}_2, \ldots, \mathbf{R}_T]$, i.e., $\mathbf{G}\mathbf{G}^H$ is block

diagonal. In this case, we can further write

$$\tilde{C} \leq \frac{1}{T} E_{\mathbf{H}} \left\{ \log \left[\prod_{t=1}^{T} \det \left(\mathbf{I}_{N_r} + \frac{P}{N_t \sigma_z^2} F_t^2 \mathbf{H}\mathbf{H}^H \right) \right] \right\} \tag{3.8}$$

where $F_t^2 = \mathrm{tr}(\mathbf{R}_t)/N_t$. Note that to ensure that P is the average energy per channel use at each receive antenna, one needs to have $\mathrm{tr}(\mathbf{G}\mathbf{G}^H) = L$. Hence, $\sum_{t=1}^{T} F_t^2 = \sum_{t=1}^{T} \mathrm{tr}(\mathbf{R}_t)/N_t = L/N_t$. From (3.8), it can be checked that $\tilde{F}$ is maximized only when $F_t^2 = \frac{L}{N_t T}$ and $L = N_t T$ for any $t = 1, 2, \ldots, T$. Apparently, this is possible only if

$$\mathbf{G}\mathbf{G}^H = \mathbf{I}_{N_t T} \tag{3.9}$$

is satisfied.

We consider only a full-rate LDC that is $L = N_t T$. Then, we have

$$C = \frac{1}{T} E_{\mathbf{H}} \left\{ \log \det \left(\mathbf{I}_{N_t T} + \bar{\gamma} \overline{\mathbf{H}}\, \overline{\mathbf{H}}^H \right) \right\} \tag{3.10}$$

where $E\{\quad\}$ is the expectation over the channel matrix $\mathbf{H}$ and $\bar{\gamma} = \frac{P}{N_t \sigma_z^2}$, with

$$\begin{aligned} \det \left(\mathbf{I}_{N_t T} + \bar{\gamma} \widetilde{\mathbf{H}} \widetilde{\mathbf{H}}^H \right) &= \det \left(\mathbf{I}_T \otimes \mathbf{I}_{N_t} + \mathbf{I}_T \otimes \bar{\gamma} \mathbf{H}\mathbf{H}^H \right) \\ &= \left[\det \left(\mathbf{I}_{N_r} + \bar{\gamma} \mathbf{H}\mathbf{H}^H \right) \right]^T \\ &= \left[\det \left(\mathbf{I}_{N_t} + \bar{\gamma} \mathbf{H}^H \mathbf{H} \right) \right]^T . \end{aligned} \tag{3.11}$$

Equation (3.10) can be written as

$$C = \frac{1}{T} E_{\mathbf{H}} \left\{ \log \left[\det \left(\mathbf{I}_{N_t} + \bar{\gamma} \mathbf{H}\mathbf{H}^H \right) \right]^T \right\} . \tag{3.12}$$

We can define

$$\mathbf{W} = \begin{cases} \mathbf{H}\mathbf{H}^H & N_r \leq N_t \\ \mathbf{H}^H \mathbf{H} & N_r \geq N_t \end{cases} \tag{3.13}$$

where $n = \max(N_r, N_t)$, and $m = \min(N_r, N_t)$. $\mathbf{W}$ is a $m \times m$ random non-negative definite matrix and thus has non-negative eigenvalues. The distribution law of $\mathbf{W}$ is called the Wishart distribution with parameters m and n [1][44]. Let $\{\lambda_i, \forall i = 0, \ldots, m-1\}$ be eigenvalues of $\mathbf{W}$ and define $\mathbf{\Lambda} := [\lambda_0, \ldots, \lambda_{m-1}]^T$. Equation (3.12) can then be written as

$$C = \frac{1}{T} E_\lambda \left\{ \log \left[\prod_{i=0}^{m-1} (1 + \bar{\gamma}\lambda_i) \right]^T \right\}, \tag{3.14}$$

and

$$C = E_\lambda \left\{ \sum_{i=0}^{m-1} \log (1 + \bar{\gamma}\lambda_i) \right\}. \tag{3.15}$$

The i^{th} unordered eigenvalues have probability density function(PDF) $f_\lambda(\lambda)$, given in [1][43][45] as

$$f_\lambda(\lambda) = \frac{1}{m} \sum_{i=1}^{m} \Phi_i(\lambda)^2 \lambda^{n-m} \exp(-\lambda) \tag{3.16}$$

where

$$\Phi_{k+1}(\lambda) = \left(\frac{k!}{(k+n-m)!} \right)^{\frac{1}{2}} L_k^{n-m}(\lambda) \quad k = 0, \ldots m-1$$

and $L_k^{n-m}(\lambda)$ is the associated Laguere polynomial of order k, defined as [46]

$$L_k^{n-m}(\lambda) = \sum_{c=0}^{k} (-1)^c \begin{pmatrix} k+n-m \\ k-c \end{pmatrix} \frac{\lambda^c}{c!}$$

Equation (3.16) can be written as

$$f_\lambda(\lambda) = \frac{1}{m} \sum_{k=0}^{m-1} \frac{k!}{(k+n-m)!} [L_k^{n-m}(\lambda)]^2. \tag{3.17}$$

Substituting (3.17) into (3.15), we have

$$C = \int_0^{\infty} \log\left(1 + \bar{\gamma}\lambda\right)] \sum_{k=0}^{m-1} \frac{k!}{(k+n-m)!} [L_k^{n-m}(\lambda)]^2 d\lambda. \tag{3.18}$$

Next, we define

$$K1(k) = \frac{k!}{(k+n-m)!} \frac{\Gamma(k+n')}{2^{2k}k!}$$

$$K2(i) = \frac{(2i)!(2k-2i)!}{i![(k-i)!]^2\Gamma(k+n')}$$

$$K3(d) = \frac{(-2)^d}{d!} \begin{pmatrix} 2k+2n-2m \\ 2k-d \end{pmatrix} \tag{3.19}$$

where $n' = n - m + 1$.

Next, we can write (3.18) as

$$C = \sum_{k=0}^{m-1} K1(k) \sum_{i=0}^{k} K2(i) \sum_{d=0}^{2k} K3(d) \times I \tag{3.20}$$

where I is the integration part, defined as

$$I = \frac{1}{\ln 2} \int_0^{\infty} \ln\left(1 + \bar{\gamma}\lambda\right) \exp(-\lambda) \lambda^{n-m+d} d\lambda \tag{3.21}$$

Using the integration by parts, equation (3.21) can be written as

$$I = \frac{(m'-1)!}{\ln 2} \times \left(\sum_{i'=0}^{m'-1} \bar{\gamma}^{i'} \int_0^{\infty} \frac{\lambda^{m'-i'}}{1+\lambda} e^{\frac{-\lambda}{\bar{\gamma}}} \, d\lambda \right) +$$

$$\frac{(m'-1)!}{\ln 2} \times \left(\gamma^{m'-1} \int_0^{\infty} e^{\frac{-\lambda}{\bar{\gamma}}} \ln\left(1+\lambda\right) d\lambda \right) \tag{3.22}$$

where $m' = n - m + d + 1$. We compute the above integration using [46].

$$\int_0^{\infty} \frac{x^{\nu} e^{-\mu x}}{x+\beta} dx =$$

$$(-1)^{\nu-1} \beta^{\nu} e^{\beta\mu} E_i(-\beta\mu) + \sum_{k'=1}^{\nu} (k'-1)!(-\beta)^{\nu-k'} \mu^{-k'}$$

and

$$\int_0^{\infty} e^{-\mu x} \ln(x+\beta) dx = \frac{1}{\mu}[\ln(\beta) - e^{\mu\beta} E_i(-\mu\beta)]$$

where $E_i(.)$ is the exponential-integral function, $\nu = m' - i'$, $\mu = \frac{1}{\bar{\gamma}}$, and $\beta = 1$.

Then (3.22) can be written as

$$I = \frac{(m'-1)!\ \bar{\gamma}\ e^{\bar{\gamma}^{-1}} E_i\left(-\bar{\gamma}^{-1}\right)}{\ln 2} \times$$

$$\left(\sum_{i'=0}^{m'-1} (-1)^{(m'-i'-1)}\ \bar{\gamma}^{(i'-1)}\ - 1 \right)$$

$$+ \quad \frac{(m'-1)!}{\ln 2} \times \left(\sum_{k'=1}^{m'-i'} (-1)^{m'-k'-i'}\ (k'-1)! \bar{\gamma}^{k'} \right) \tag{3.23}$$

Substituting (3.23) into (3.20), we have

$$C = \sum_{k=0}^{m-1} K1(k) \sum_{i=0}^{k} K2(i) \sum_{d=0}^{2k} K3(d) \times \frac{(m'-1)!\ \bar{\gamma}\ e^{\bar{\gamma}^{-1}} E_i\left(-\bar{\gamma}^{-1}\right)}{\ln 2} \times$$

$$\left(\sum_{i'=0}^{m'-1} (-1)^{(m'-i'-1)}\ \bar{\gamma}^{(i'-1)}\ - 1 \right)$$

$$+ \quad \frac{(m'-1)!}{\ln 2} \times \left(\sum_{k'=1}^{m'-i'} (-1)^{m'-k'-i'}\ (k'-1)! \bar{\gamma}^{k'} \right). \tag{3.24}$$

We compare the derived exact ergodic capacity with Monte Carlo results for various numbers of transmit and receive antennas, as a function of the average SNR. In

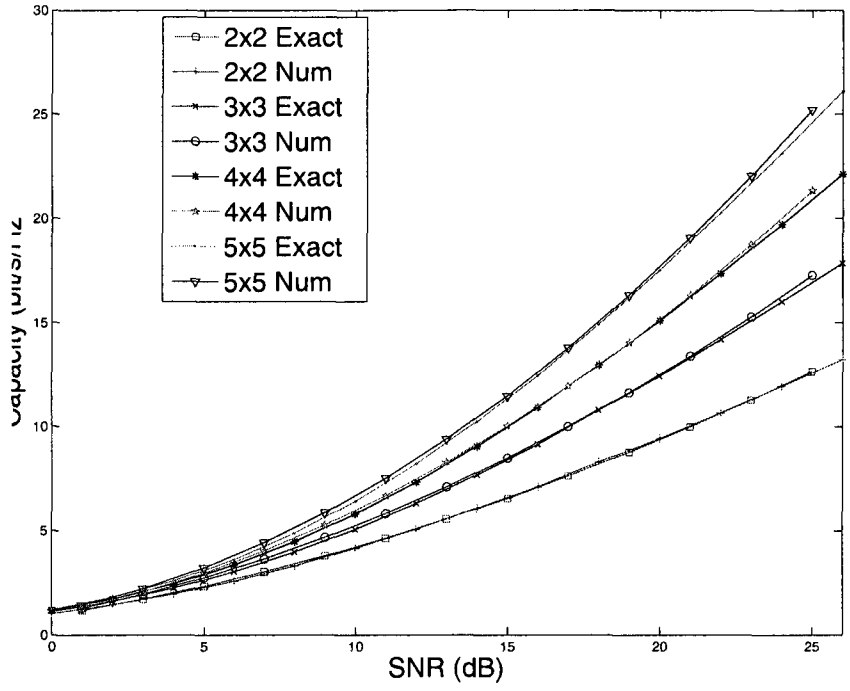

Figure 3.2: Numerical result and the associated exact capacity SNR.

Fig. 3.2, the numerical results and the associated theoretical exact ergodic capacity are compared. "Num" denotes the numerical results and "Exact" indicates a theoretical result. As can be seen from the figure, the exact analytical expression fits well with the numerical results.

3.4 Performance Analysis

We study the performance of LDCs based on the system model given in (3.5). Using maximum likelihood (ML) detection, the pairwise error probability conditioned on $\widetilde{\mathbf{H}}$ is given by

$$\begin{aligned} & P_e(\mathbf{x} \rightarrow \mathbf{x}'|\widetilde{\mathbf{H}}) \\ &= P(\| \mathbf{y} - \sqrt{\tfrac{P}{N_t}}\widetilde{\mathbf{H}}\mathbf{x}' \| < \| \mathbf{y} - \sqrt{\tfrac{P}{N_t}}\widetilde{\mathbf{H}}\mathbf{x} \| \ | \mathbf{x} \text{ sent}) \end{aligned} \tag{3.25}$$

To find the upper bound of the above error probability we can start from the result in [34]. Hassibi *et al*[34] first derived an upper bound of the average pairwise error probability conditioned on $\widetilde{\mathbf{H}}$. Applying a union bound to this average pairwise probability error yields an upper bound on the error probability of a signal constellation conditional on $\widetilde{\mathbf{H}}$. The upper bound of the average error probability in (3.25) was found in [34] as

$$P_e \leq 2^{RT-1} E\left\{\left[\det\left(\mathbf{I}_{2N_tT} + \bar{\gamma}\widetilde{\mathbf{H}}\widetilde{\mathbf{H}}^H\right)\right]^{-1/2}\right\} \tag{3.26}$$

Following a procedure similar to that in Section 3.3, equation (3.26) can be written as

$$P_e \leq 2^{RT-1} E\left\{\left[\det\left(\mathbf{I}_{N_t} + \bar{\gamma}\mathbf{H}\mathbf{H}^H\right)\right]^{-T}\right\} \tag{3.27}$$

With the definition of the (3.13) in Section 3.3, equation (3.27) can be written as

$$P_e \leq 2^{RT-1} E\left\{\left[\prod_{i=0}^{m-1}(1 + \bar{\gamma}\lambda_i)\right]^{-T}\right\} \tag{3.28}$$

We can write (3.28) in terms of the eigenvalues of $\mathbf{W}$ as

$$P_e \leq 2^{RT-1} \int^{(m)} \prod_{i=0}^{m-1} (1 + \bar{\gamma}\lambda_i)^{-T} P_\lambda(\mathbf{\Lambda})\, d^{(m)}\lambda \tag{3.29}$$

where $\int^{(m)} := \underbrace{\int_0^\infty \dots \int_0^\infty}_{m}$, $d^{(m)}x := dx_0 \dots dx_{m-1}$ and

$$\begin{aligned} P_\lambda(\mathbf{\Lambda}) &= (m!K_{m,n})^{-1} \prod_i e^{-\lambda_i} \lambda_i^{n-m} \prod_{i<j} (\lambda_i - \lambda_j)^2 \\ &= \frac{1}{m!} \det{}^2 \left[\tilde{\phi}_i(\lambda_j)\right]_{ij=0}^{m-1} \end{aligned} \tag{3.30}$$

is the joint density function of the unordered eigenvalues [1][43][45], where

$$K_{m,n} := \left[m! \prod_{i=0}^{m-1} \Gamma(m-i+1)\Gamma(n-i+1) \right]^{-1}$$

is a normalizing factor and

$$\tilde{\phi}_i(\lambda) := \left[\frac{i!}{(i+n-m)!} \right]^{\frac{1}{2}} L_i^{n-m}(\lambda) \lambda^{\frac{n-m}{2}} e^{-\frac{\lambda}{2}}$$

in which $i = 0, \dots, m-1$, and $L_i^{n-m}(\lambda)$ is the associated Laguere polynomial of order i, defined as [46]

$$L_i^{n-m} = \frac{1}{i!} e^\lambda \lambda^{-(n-m)} \frac{d^i}{d\lambda^i} e^{-\lambda} \lambda^{n-m+i}$$

We can define

$$f(\mathbf{\Lambda}) = \prod_{i=0}^{m-1} (1 + \bar{\gamma}\lambda_i)^{-T} P_\lambda(\mathbf{\Lambda}) \tag{3.31}$$

so that, substituting (3.30) into (3.31), we have

$$f(\mathbf{\Lambda}) = \tilde{K} \prod_{i<j} (\lambda_i - \lambda_j)^2 \prod_{i=0}^{m-1} e^{-\lambda_i} \lambda_i^{n-m} (1 + \bar{\gamma}\lambda_i)^{-T}$$

$$= \tilde{K} \left\{ \det \begin{bmatrix} 1 & \dots & 1 \\ \lambda_0 & \dots & \lambda_{m-1} \\ \vdots & \vdots & \vdots \\ \lambda_0^{m-1} & \dots & \lambda_{m-1}^{m-1} \end{bmatrix} \right\}^2$$

$$
\begin{aligned}
&\times \quad \left[\prod_{i=0}^{m-1} e^{-\lambda_i}\lambda_i^{n-m}(1+\bar{\gamma}\lambda_i)^{-T}\right] \\
&= \quad \tilde{K}\left\{\det\begin{bmatrix} g_0(\lambda_0) & \cdots & g_0(\lambda_{m-1}) \\ \vdots & \vdots & \vdots \\ g_{m-1}(\lambda_0) & \cdots & g_{m-1}(\lambda_{m-1}) \end{bmatrix}\right\}^2 \\
&= \quad \tilde{K}\det{}^2[g_i(\lambda_j)]_{ij=0}^{m-1} \qquad (3.32)
\end{aligned}
$$

where $\tilde{K} = (m!K_{m,n})^{-1}$ and

$$g_i(\lambda) = \left[e^{-\lambda}\lambda^{n-m}(1+\bar{\gamma}\lambda)^{-T}\right]^{\frac{1}{2}}\lambda^i.$$

Lemma 1: Let $\{g_i(x), \forall i = 0, \ldots, m-1\}$ be m functions for which the following integrals exist. That is, these integrals decay sufficiently fast at infinity. It holds that

$$\int^{(m)} \det{}^2[g_i(x_j)]_{ij=0}^{m-1} d^{(m)}x = m!\det[D_{ij}]_{ij=0}^{m-1} \qquad (3.33)$$

where $D_{ij} = \int_0^\infty g_i(x)g_j(x)dx$.

Proof: See Gram's result stated in Chapter 5 and Appendix A.12 of [47]. ■

Substituting (3.32) into (3.29), we have

$$P_e \leq 2^{RT-1}\tilde{K}\int^{(m)} \det{}^2[g_i(\lambda_j)]_{ij=0}^{m-1} d^{(m)}\lambda \qquad (3.34)$$

Using Lemma 1, we have

$$P_e \leq 2^{RT-1}\tilde{K}m!\det[d_{ij}]_{ij=0}^{m-1} \qquad (3.35)$$

where

$$d_{ij} = \int_0^\infty (1+\bar{\gamma}\lambda)^{-T}\lambda^{n-m+i+j}e^{-\lambda}d\lambda. \qquad (3.36)$$

which can be written as

$$d_{ij} = \bar{\gamma}^{-T} \int_0^{\infty} (u+\lambda)^{-T} \lambda^{n-m+i+j} e^{-\lambda} d\lambda \tag{3.37}$$

where $u = \bar{\gamma}^{-1}$. To compute the above integration, we make use of the result in [46].

$$\int_0^{\infty} x^{\nu}(x+u)^{-\mu} \exp(-\beta x)\, dx$$

$$= \beta^{\frac{\mu-\nu}{2}-1} u^{\frac{-\mu+\nu}{2}} \Gamma(\nu+1) \exp\left(\frac{-1}{2\beta u}\right) W_{p,s}\left(\bar{\gamma}^{-1}\right)$$

where $W_{p,s}(\quad)$ is the Whittaker function defined by Gradshteyn and Ryzhik in [46] as follows.

$$W_{p,s}(z) = \frac{e^{-z/2} z^p}{\Gamma(\frac{1}{2}-p+s)} \cdot \int_0^{\infty} t^{-p-1/2+s}(1+\frac{t}{z})^{p-1/2+s} e^{-t} dt \tag{3.38}$$

Then (3.37) can be written as

$$d_{ij} = (\bar{\gamma})^{\frac{m-n-i-j-T}{2}} e^{-\frac{\bar{\gamma}}{2}} \Gamma(i+j+n') W_{p,s}\left(\bar{\gamma}^{-1}\right) \tag{3.39}$$

where $p = -\frac{i+j+n}{2}$, $s = \frac{i+j+n-2m+1}{2}$ and $n' = n-m+1$. The above upper bound probability of error does not show the diversity advantage that is an important measure of code performance. We examine the performance at high SNR instead. The equation(3.36) can be approximated as

$$\begin{aligned} d_{ij} &\approx \bar{\gamma}^{-T} \int_0^{\infty} \lambda^{n-m+i+j-T} e^{-\lambda} d\lambda \\ &= \bar{\gamma}^{-T} \Gamma(n-m+i+j-T) \end{aligned} \tag{3.40}$$

Substituting (3.40) into (3.35), we get the upper bound at high SNR as

$$P_e \leq 2^{RT-1} \tilde{K} m! \bar{\gamma}^{-mT} \det[\Gamma(n-m+i+j-T)]_{ij=0}^{m-1}$$

$$\leq C \cdot 2^{QL-1} \left(\frac{\rho}{2N_t}\right)^{-mT} \tag{3.41}$$

where $\rho = \frac{P}{\sigma_z^2}$ is the SNR and

$$C = \tilde{K} m! \prod_{i=0}^{m-1} \Gamma(n - m + i - T).$$

We compare the derived upper bound at high SNR with the error probability for symbols drawn from a finite alphabet, such as PSK and QAM constellations. The simulation results match well with the theoretical results. A full-rate full-diversity scheme [42] was considered in the simulation. $N_t = N_r = T = 2$, where QPSK and 16QAM constellations were assumed. At the receiver, the optimal maximum-likelihood (ML) detector was applied.

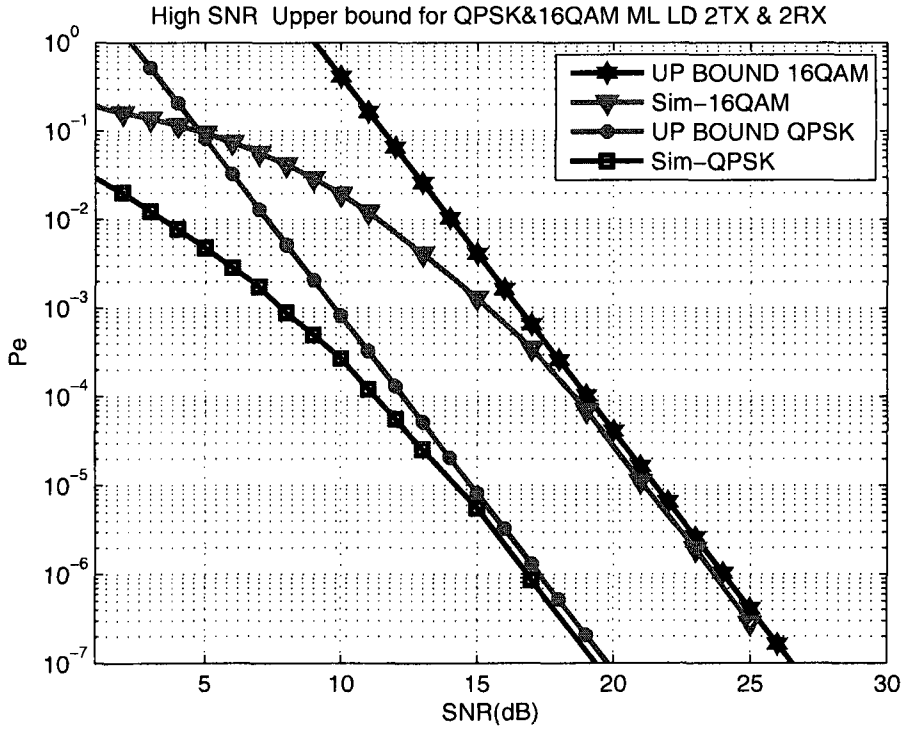

Figure 3.3: Simulation result and the associated upper bound at high SNR.

In Fig. 3.3, the simulation results and the associated theoretical upper bounds

derived at high SNR are compared. "Sim" denotes the simulation results and "UP BOUND" denotes theoretical results. As can be seen from the figure, the upper bound fits well with the simulation results using the optimal receiver. Note that the simulation results and the associated theoretical upper bound have the same slopes at high SNR.

3.5 Conclusions

In this study, first an analytical formula of the ergodic capacity was derived for the full-rate linear dispersion code. The ergodic capacity was given in terms of signal-to-noise ratio and multiple antenna dimension. An exact upper bound of pairwise error probability was derived next. Based on this bound, a tight upper bound of error probability at high signal-to-noise ratio is further derived to show the diversity advantage of linear dispersion codes. The tight bound demonstrates the relationship of error probability to constellation size and to the space-time symbol rate. All of the theoretical results have been verified by simulation results.

Chapter 4

New Adaptive MIMO System using Full Rate Linear Dispersion Code with Selection Modes

4.1 Introduction

The error probability of a full-rate full-diversity(FDFR) LDC is a function of its ST symbol rate and constellation size, as stated earlier. With this information, we can maximize the transmission rate by adjusting the ST symbol rate and constellation size jointly while maintaining the target QoS as described in this chapter.

For the aforementioned reasons, we study the selection-mode adaptive system in this chapter. With the upper bound of pairwise error probability obtained in the previous chapter as a guideline, we design an adaptive MIMO system with discrete selection modes. The associated MIMO transceiver uses an LDC as the ST modulator and the minimum mean square error (MMSE) detector at the receiver, for simplicity. As mentioned before, the new design adds an adaptive parameter to the existing adaptive system, referred to as the ST symbol rate. Since the FRFD LDC takes into account both rate and performance, this modification is appropriate to our study. As

can be seen from the following discussions, by adding the ST symbol rate together with constellation size, the overall throughput of the system is increased.

4.2 Adaptive System Model using LDC

In this study, during one ST modulation block, the channel is assumed to be the same as it was estimated at the receiver. Furthermore, the channel is assumed to be a Rayleigh flat fading channel with N_t transmit and N_r receive antennas. We denote the complex gain from transmit antenna n to receiver antenna m by h_{mn}, and collect them to form an $N_r \times N_t$ channel matrix $\mathbf{H} = [h_{mn}]$, known perfectly to the receiver. The entries in $\mathbf{H}$ are assumed to be independently identically distributed (*i.i.d.*) symmetrical complex Gaussian random variables with zero mean and unit variance.

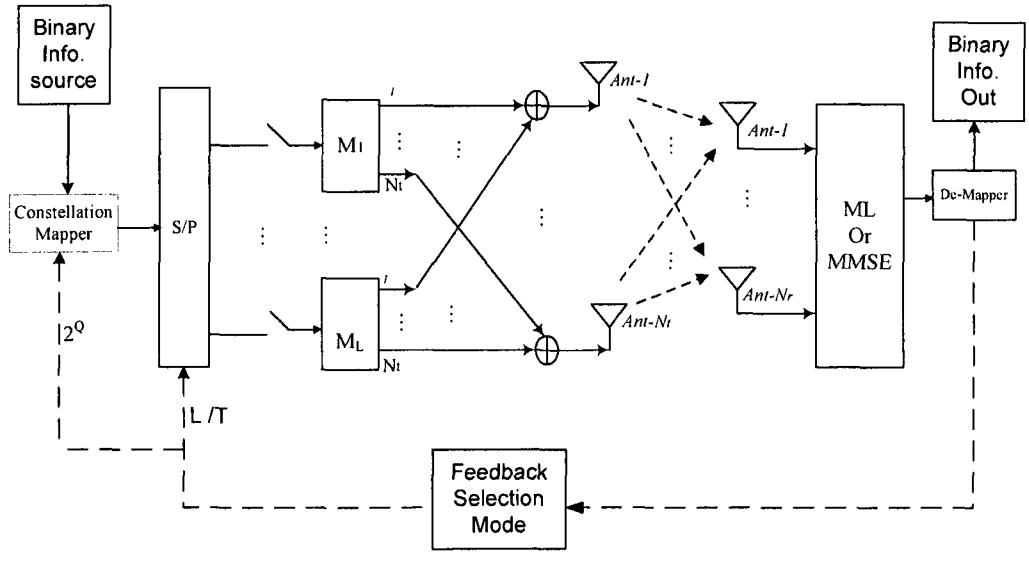

Figure 4.1: Selection-mode adaptive system block diagram.

The selection-mode adaptive system is depicted in Fig. 4.1. In this system, the information bits are first mapped into symbols. The symbol stream is then parsed into blocks of length L. The symbol vector associated with one modulation block is denoted by $\mathbf{x} = [x_1, x_2, \ldots, x_L]^T$ with $x_i \in \Omega \equiv \{\Omega_m | m = 0, 1, \ldots, 2^\eta - 1, \eta \geq 1\}$, i.e.,

a complex constellation of size 2^η, such as 2^η-QAM. The average symbol energy is assumed to be 1, or, $\frac{1}{2^\eta}\sum_{m=0}^{2^\eta-1}|\Omega_m|^2 = 1$. Each block of symbols will be mapped by the ST modulator to a dispersion matrix of size $N_t \times T$ and then transmitted from the N_t transmit antennas over T channel uses. The following model will be considered in this study:

$$\mathbf{X} = \sum_{i=1}^{L} \mathbf{M}_i x_i \tag{4.1}$$

where $\mathbf{M}_i$ is defined by its L $N_t \times T$ dispersion matrices $\mathbf{M}_i = [\mathbf{m}_{i1}, \mathbf{m}_{i2}, \ldots, \mathbf{m}_{iT}]$. The results thus obtained can be extended to the model in [34]. With a constellation of size 2^η, the data rate of the space-time modulator in bits per channel used is

$$R_m = \eta \cdot L/T \tag{4.2}$$

Hence, one can adjust ST symbol rate L/T and constellation size η according to the feedback from the receiver.

At the receiver, the received signals associated with one modulation block can be written as

$$\mathbf{Y} = \mathbf{H}\mathbf{X} + \mathbf{Z} = \mathbf{H}\sum_{i=1}^{L} \mathbf{M}_i x_i + \mathbf{Z} \tag{4.3}$$

where $\mathbf{Y}$ is a complex matrix of size $N_r \times T$ whose (m,n)-th entry is the received signal at receive antenna m and time instant n, $\mathbf{Z}$ is the additive white Gaussian noise matrix with *i.i.d.* symmetrical complex Gaussian elements of zero mean and variance σ_z^2. It is often desirable to write the matrix input-output relationship in (4.3) in an equivalent vector notation. Let vec() be the operator that forms a column vector by stacking the columns of a matrix and define $\mathbf{y} = \text{vec}(\mathbf{Y})$, $\mathbf{z} = \text{vec}(\mathbf{Z})$, and $\mathbf{m}_i = \text{vec}(\mathbf{M}_i)$. Then (3.4) can be rewritten as

$$\mathbf{y} = \overline{\mathbf{H}}\mathbf{G}\mathbf{x} + \mathbf{z} = \widetilde{\mathbf{H}}\mathbf{x} + \mathbf{z} = \sum_{i=1}^{L} \tilde{\mathbf{h}}_i x_i + \mathbf{z} \tag{4.4}$$

where $\overline{\mathbf{H}} = \mathbf{I}_T \otimes \mathbf{H}$ with $\otimes$ as the Kronecker product operator, $\mathbf{G} = [\mathbf{m}_1, \mathbf{m}_2, \ldots, \mathbf{m}_L]$ will be referred to as the modulation matrix, and $\tilde{\mathbf{h}}_i$ is the i-th column of $\widetilde{\mathbf{H}}$. In our design, a full-rate full-diversity (FRFD) LDC is applied. However, the ST symbol rate L/T and constellation size η will adapt to the channel.

To achieve a full rate, the following conditions should be satisfied:

$$L = N_t T \tag{4.5}$$

$$\mathbf{G}\mathbf{G}^H = \mathbf{I} \tag{4.6}$$

that is,

$$\text{trace}(\mathbf{M}_i^H \mathbf{M}_j) = \begin{cases} 1 & \forall i = j \\ 0 & \text{otherwise} \end{cases} \tag{4.7}$$

Furthermore, to achieve full diversity, we shall maximize the outage probability $P_r(\|\tilde{\mathbf{h}}_i\|^2 \geq \epsilon)$, and so the following lemma is introduced [40].

Lemma 1: Consider v_i, $,\forall 1 \leq i \leq n$, *i.i.d.* Gamma random variables with density $p(x) = e^{-\beta x} x^{\alpha-1} \beta^\alpha / \Gamma(\alpha)$. Let $\xi = [\xi_1, \xi_2, \ldots, \xi_n]$ with ξ_i for all i. $b = \sum_{i=1}^n \xi_i v_i$. $P_r(b \geq t)$ is Schur-convex in ξ for

$$t \geq \frac{(n\alpha + 1)(\xi_1 + \xi_2 + \ldots + \xi_n)}{\beta} \tag{4.8}$$

Noting that $\tilde{\mathbf{h}}_i = \overline{\mathbf{H}}\mathbf{m}_i$, we have

$$\|\tilde{\mathbf{h}}_i\|^2 = \sum_{m=1}^{N_r} \mathbf{h}_m^H \mathbf{M}_i \mathbf{M}_i^H \mathbf{h}_m \tag{4.9}$$

where $\mathbf{h}_m$ is the m-th column vector of $\mathbf{H}^H$. The following decomposition is assumed

$$\mathbf{M}_i \mathbf{M}_i^H = \mathbf{U}\mathbf{D}\mathbf{U}^H. \tag{4.10}$$

where $\mathbf{D} = \text{diag}[d_n], \forall n = 1, 2, ..., N_t$. According to Lemma 5 in [1], since $\mathbf{U}^H \mathbf{h}_m$ has

the same distribution as $\mathbf{h}_m$, we need only consider $\mathbf{M}_i\mathbf{M}_i^H = \mathbf{D}$. Then we can have

$$\|\tilde{\mathbf{h}}_i\|^2 = \sum_{n=1}^{N_t} d_n \sum_{m=1}^{N_r} |h_{mn}|^2. \tag{4.11}$$

For the power constraint, we have $\sum_{n=1}^{N_t} d_n = 1$. With no loss of generality, we can assume $d_1 \geq d_2 \geq \ldots \geq d_{N_t} \geq 0$.

Using Lemma 1, since the random variable $\sum_{m=1}^{N_r} |h_{mn}|^2$ in (4.11) is identically chi-square distributed with $2N_r$ degrees of freedom, we know that the outage probability $P_r(\|\tilde{\mathbf{h}}_i\|^2 \geq \epsilon)$ is maximized if all the eigenvalues of $\mathbf{M}_i\mathbf{M}_i^H$ are equal. Since $\mathrm{tr}(\mathbf{M}_i\mathbf{M}_i^H) = 1$, it is implied that $d_i = 1/N_t, \forall 1 \leq i \leq N_t$. As a result, for each i, $\|\tilde{\mathbf{h}}_i\|^2$ has the same value.

In our design, the dispersion matrices are given by

$$\mathbf{M}_{(k-1)N_t+i} = \mathrm{diag}[\mathbf{f}_k]\mathbf{P}^{-(i-1)} \tag{4.12}$$

for $k = 1, 2, \ldots, N_t$ and $i = 1, 2, \ldots, N_t$. $\mathbf{P}$ is the permutation matrix of size N_t and is given by

$$\mathbf{P} = \begin{pmatrix} \mathbf{0}_{1\times(N_t-1)} & 1 \\ \mathbf{I}_{N_t-1} & \mathbf{0}_{(N_t-1)\times 1} \end{pmatrix} \tag{4.13}$$

where $\mathbf{f}_k$ denotes the k-th column vector of $\mathbf{F}$. $\mathbf{F} = [f_{mn}]$ is a Fast Fourier Transform (FFT) matrix and f_{mn} is calculated by

$$f_{mn} = \frac{1}{\sqrt{N_t}} \exp(-2\pi j(m-1)(n-1)/N_t) \tag{4.14}$$

4.3 The Statistics of SINR with the MMSE Receiver

Since the LDC is linear, an MMSE detector can be applied as a suboptimal receiver thanks to its simplicity and good performance [48]. The main goal of this section is to study the error-rate probability and the SINR statistics for LDCs [34]-[42] using a linear MMSE receiver over a Rayleigh fading channel.

We consider a general system model as shown in Section 3.2. In our study, $N_r \geq N_t$ is assumed. Without loss of generality, we can consider the detection of one symbol x_i. Equation (4.4) can also be written as

$$\mathbf{y} = \tilde{\mathbf{h}}_i x_i + \widetilde{\mathbf{H}}_I \mathbf{x}_I + \mathbf{z} \tag{4.15}$$

where $\mathbf{x}_I$ represents the rest of the symbols and $\widetilde{\mathbf{H}}_I = [\tilde{\mathbf{h}}_1, .., \tilde{\mathbf{h}}_{i-1}, \tilde{\mathbf{h}}_{i+1}, ..., \tilde{\mathbf{h}}_L]$ is the matrix obtained by removing the i-th column from $\widetilde{\mathbf{H}}$.

A linear MMSE receiver is applied and the corresponding normalized output is given by

$$\hat{x}_i = \mathbf{w}_i^H \mathbf{y} = x_i + \hat{z}_i. \tag{4.16}$$

where $\hat{z}_i$ is the zero-mean noise term, which is approximated to be Gaussian [49]. The corresponding $\mathbf{w}_i$ can be found as[50]

$$\mathbf{w}_i = \frac{\left(\tilde{\mathbf{h}}_i \tilde{\mathbf{h}}_i^H + \mathbf{R}_I\right)^{-1} \tilde{\mathbf{h}}_i}{\tilde{\mathbf{h}}_i^H \left(\tilde{\mathbf{h}}_i \tilde{\mathbf{h}}_i^H + \mathbf{R}_I\right)^{-1} \tilde{\mathbf{h}}_i} \tag{4.17}$$

where $\mathbf{R}_I = \widetilde{\mathbf{H}}_I \widetilde{\mathbf{H}}_I^H + \sigma_z^2 \mathbf{I}$. Note that the scaling factor $\frac{1}{\tilde{\mathbf{h}}_i^H \left(\tilde{\mathbf{h}}_i \tilde{\mathbf{h}}_i^H + \mathbf{R}_I\right)^{-1} \tilde{\mathbf{h}}_i}$ in the coefficient vector of the MMSE receiver $\mathbf{w}_i$ is added to ensure an unbiased detection, as indicated by (4.16). The variance of the noise term $\hat{z}_i$ can be found from (4.16) and

(4.17), which is

$$\hat{\sigma}_i^2 = \mathbf{w}_i^H \mathbf{R}_I \mathbf{w}_i \tag{4.18}$$

Substituting the coefficient vector for the MMSE receiver in (4.17) into (4.18), the variance can be written as

$$\hat{\sigma}_i^2 = \frac{1}{\tilde{\mathbf{h}}_i^H \mathbf{R}_I^{-1} \tilde{\mathbf{h}}_i} \tag{4.19}$$

Then, the SINR of the MMSE associated with x_i is $1/\hat{\sigma}_i^2$.

$$\gamma_i = \frac{1}{\hat{\sigma}_i^2} = \tilde{\mathbf{h}}_i^H \mathbf{R}_I^{-1} \tilde{\mathbf{h}}_i \tag{4.20}$$

the closed-form BER for a channel model with Gaussian noise as (4.16) can be found in [52]. The average BER over a MIMO fading channel for a given constellation can be found as follows.

$$BER_{av} = E_{\gamma_i}\left[\frac{1}{L}\sum_i BER(\gamma_i)\right] \tag{4.21}$$

In our LDC design, we have

$$\tilde{\mathbf{h}}_i^H \tilde{\mathbf{h}}_j = \sum_{m=1}^{N_r} \mathbf{h}_m^H \mathbf{M}_i \mathbf{M}_j^H \mathbf{h}_m \tag{4.22}$$

Since $\mathbf{M}_i$ is symmetric in our LDC design and $\|\tilde{\mathbf{h}}_i\|^2$ has the same value for each i, as shown in the previous section, all of the symbols have the same SINR, and thus $\gamma_1 = \gamma_2 = \cdots = \gamma_L = \gamma$. Equation (4.21) can be written as

$$BER_{av} = \int BER(\gamma) P_\Gamma(\gamma) d\gamma \tag{4.23}$$

By using singular value decomposition (SVD), we have $\widetilde{\mathbf{H}}_I \widetilde{\mathbf{H}}_I^H = \sum_{j=1}^{L-1} \lambda_j \mathbf{u}_j \mathbf{u}_j^H$ where $\mathbf{u}_1, \ldots, \mathbf{u}_{L-1}$ are orthogonal vectors and $\{\lambda_i, \forall i = 1, \ldots, L-1\}$ are eigenvalues of $\widetilde{\mathbf{H}}_I \widetilde{\mathbf{H}}_I^H$. We assume $\lambda_1 \geq \ldots \geq \lambda_r > \lambda_{r+1} = \ldots = \lambda_{L-1} = 0$ and that r has the

rank of $\widetilde{\mathbf{H}}_I \widetilde{\mathbf{H}}_I^H$. Equation (4.20) can be written as

$$\begin{aligned}\gamma &= \tilde{\mathbf{h}}_i^H \left(\sum_{j=1}^{L-1} \lambda_j \mathbf{u}_j \mathbf{u}_j^H + \sigma_z^2 \mathbf{I} \right)^{-1} \tilde{\mathbf{h}}_i \\ &= \sum_{j=1}^{L-1} \frac{|\tilde{\mathbf{h}}_i^H \mathbf{u}_j|^2}{\lambda_j + \sigma_z^2} \\ &= \sum_{j=1}^{r} \frac{|\tilde{\mathbf{h}}_i^H \mathbf{u}_j|^2}{\lambda_j + \sigma_z^2} + \sum_{j=r+1}^{L-1} \frac{|\tilde{\mathbf{h}}_i^H \mathbf{u}_j|^2}{\sigma_z^2} \end{aligned} \tag{4.24}$$

Since the elements in $\tilde{\mathbf{h}}_i$ are *i.i.d.* Gaussian distributed, the complex random variables $\tilde{\mathbf{h}}_i^H \mathbf{u}_1, \ldots, \tilde{\mathbf{h}}_i^H \mathbf{u}_{L-1}$, conditioned on $\mathbf{u}_1, \ldots, \mathbf{u}_{L-1}$, are also *i.i.d.* Gaussian distributed. Therefore, from (4.24) the probability density function (PDF) of γ can be found using the moment generating function (MGF), following the procedure in Chapter 11 of [53]. First, we find the conditional (on the eigenvalues) MGF of γ as

$$M_{\gamma/\lambda}(s) = [M_\gamma(\bar{\gamma}s)]^{L-1-r} \prod_{l=1}^{r} M_\gamma \left(\frac{\bar{\gamma}s}{(\bar{\gamma}\lambda_l + 1)} \right) \tag{4.25}$$

where $\bar{\gamma} = 1/\sigma_z^2$. Following the procedure in [1], we can write (4.25) as

$$M_{\gamma/\lambda}(s) = [M_\gamma(\bar{\gamma}s)]^{L-1-r} \left[M_\gamma \left(\frac{\bar{\gamma}s}{(\bar{\gamma}\lambda + 1)} \right) \right]^r \tag{4.26}$$

Further,

$$M_{\gamma/\lambda}(s) = \frac{1}{(1-\bar{\gamma}s)^{L-1-r}} \times \frac{1}{\left(1 - \frac{\bar{\gamma}s}{(1+\bar{\gamma}\lambda)}\right)^r} \tag{4.27}$$

and so we can find the probability density function (PDF) of γ conditionally on λ by using the inverse Laplace transform for (4.27) as [51]

$$\begin{aligned} P_{\Gamma/\lambda}(\gamma) = \frac{(\bar{\gamma})^{-L+1}}{\Gamma(L-1)} (\gamma)^{L-2} \exp(-\frac{\gamma}{\bar{\gamma}}) \times \\ (1+\bar{\gamma}\lambda)_1^r \, F_1(L-1-r, L-1, \lambda\gamma) \exp(-\lambda\gamma) \end{aligned} \tag{4.28}$$

where ${}_1F_1(.,.,.)$ is Kummer's confluent hypergeometric function [46] defined as

$$ {}_1F_1(a,b,x) = \sum_n^{\infty} \frac{(a)_n}{(c)_n} \frac{x^n}{n!} $$

where $(*)_n = \frac{\Gamma(*+n)}{\Gamma(*)}$.

We can define

$$ K_\gamma = \frac{(\bar{\gamma})^{-L+1}}{\Gamma(L-1)} (\gamma)^{L-2} \exp(-\frac{\gamma}{\bar{\gamma}}) $$

Then, equation (4.28) can be written as

$$ P_{\Gamma/\lambda}(\gamma) = K_\gamma \sum_n^{\infty} \frac{(L-1-r)_n}{(r)_n} \times $$

$$ \frac{\gamma^n}{n!} \lambda^n \left(1+\bar{\gamma}\lambda\right)^r \exp(-\lambda\gamma) \tag{4.29} $$

Now, we find the PDF of γ as follows:

$$ P_\Gamma(\gamma) = \int_0^{\infty} P_{\gamma/\lambda}(\gamma) f_\lambda(\lambda) \quad d\lambda \tag{4.30} $$

where $f_\lambda(\lambda)$ is the PDF of unordered λ_i, which is given in [1] as

$$ f_\lambda(\lambda) = \frac{1}{r} \sum_{i=1}^{r} \Phi_i(\lambda)^2 \lambda^{L-1-r} \exp(-\lambda), \tag{4.31} $$

where

$$ \Phi_{k+1}(\lambda) = \left(\frac{k!}{(k+L-1-r)!} \right)^{\frac{1}{2}} L_k^{L-1-r}(\lambda) $$

$$ k = 0, \ldots r-1, $$

and in which $L_k^{L-1-r}(\lambda)$ is the associated Laguere polynomial of order k [46]. Equation (4.31) can be written as

$$ f_\lambda(\lambda) = \frac{1}{r} \sum_{k=0}^{r-1} \frac{k!}{(k+L-1-r)!} [L_k^{L-1-r}(\lambda)]^2 \tag{4.32} $$

We define

$$
\begin{aligned}
K1(k) &= \frac{k!}{(k+L-1-r)!}\frac{\Gamma(k+n')}{2^{2k}k!} \\
K2(i) &= \frac{(2i)!(2k-2i)!}{i![(k-i)!]^2\Gamma(k+n')} \\
K3(d) &= \frac{(-2)^d}{d!}\begin{pmatrix} 2k+2(L-1)-2r \\ 2k-d \end{pmatrix}
\end{aligned}
$$

where $n' = L - r$. Then, we can write (4.30) as

$$
P_\Gamma(\gamma) = \frac{K_\gamma}{r}\sum_{k=0}^{r-1} K1(k)\sum_{i=0}^{k} K2(i)\sum_{d=0}^{2k} K3(d)\int_0^\infty
$$

$$
(1+\bar{\gamma}\lambda)^r \lambda^{L-1-r+d}
$$

$$
{}_1F_1(L-1-r, L-1, \lambda\gamma)\exp(-\gamma\lambda)d\lambda \tag{4.33}
$$

The term $(1+\bar{\gamma}\lambda)^r$ can be written as

$$
(1+\bar{\gamma}\lambda)^r = \bar{\gamma}^r\sum_{v=0}^{r}\begin{pmatrix} r \\ v \end{pmatrix}\bar{\gamma}^{v-r}\lambda^v.
$$

Then, equation (4.33) can be written as

$$
P_\Gamma(\gamma) = \frac{K_\gamma\bar{\gamma}^r}{r}\times
$$

$$
\sum_{n}^{\infty}\gamma^n K(n)\sum_{v=0}^{r} K(v)K1(k)\sum_{i=0}^{k} K2(i)\sum_{d=0}^{2k} K3(d)\times
$$

$$
\sum_{k=0}^{r-1}\int_0^\infty \lambda^{L-1-r+d+v+n}\exp(-\gamma\lambda)\quad d\lambda \tag{4.34}
$$

with

$$
K(n) = \frac{(L-1-r)_n}{(r)_n n!}
$$

and

$$K(v) = \begin{pmatrix} r \\ v \end{pmatrix} \bar{\gamma}^{v-r}.$$

The general form of the integration of equation (4.34) can be found in [46]

$$\int_0^\infty x^\Theta \exp(-\mu x) dx = \Theta! \mu^{-\Theta-1}$$

where

$$\Theta = L - 1 - r + d + v + n.$$

Then, equation (4.34) can be written as

$$P_\Gamma(\gamma) = \frac{K_\gamma \bar{\gamma}^r}{r} \sum_n^\infty$$

$$\gamma^n K(n) \sum_{v=0}^{r} K(v) \sum_{k=0}^{r-1} K1(k) \sum_{i=0}^{k} K2(i) \times$$

$$\sum_{d=0}^{2k} K3(d) \gamma^{-L+r-d-v-n} (L - 1 - r + d + v + n)! \quad , \tag{4.35}$$

and further,

$$P_\Gamma(\gamma) = \frac{K_\gamma \bar{\gamma}^r \gamma^r}{r\gamma^L} \sum_{k=0}^{r-1} K1(k) \sum_{i=0}^{k} K2(i) \sum_{d=0}^{2k} K3(d) \times$$

$$\gamma^{-d} \sum_{v=0}^{r} K(v) \gamma^{-v} \sum_n^\infty K(n)(L - 1 - r + d + v + n)!. \tag{4.36}$$

Let's define

$$K(v,d) = (L - 1 - r + d + v)! \times$$

$$\frac{\Gamma(L - r + d + v)\Gamma(d + v - r + 1)}{\Gamma(d + v + 1)\Gamma(L + d + v)} \grave{K}(v)$$

and

$$\grave{K}(v) = \begin{pmatrix} r \\ v \end{pmatrix}.$$

Then, equation (4.36) can be written as

$$P_{\Gamma}(\gamma) = \frac{K_{\gamma}\gamma^{r-L}}{r} \sum_{k=0}^{r-1} K1(k) \sum_{i=0}^{k} K2(i) \times$$

$$\sum_{d=0}^{2k} K3(d)\gamma^{-d} \sum_{v=0}^{r} K(v,d) \tag{4.37}$$

This is the PDF of the SINR for our system over Rayleigh fading channels.

We verify our derivation by simulation. In the simulation, values of $N_t = N_r = T = 2$ and $N_t = N_r = T = 4$ were assumed. In Fig. 4.2 and 4.3, the theoretical PDFs of the SINR in (4.37) and results by Monte Carlo simulation were compared for 2×2 and 4×4 channels, respectively, at $P/\sigma_z^2 = 20dB$. Simulation results match the analytical results.

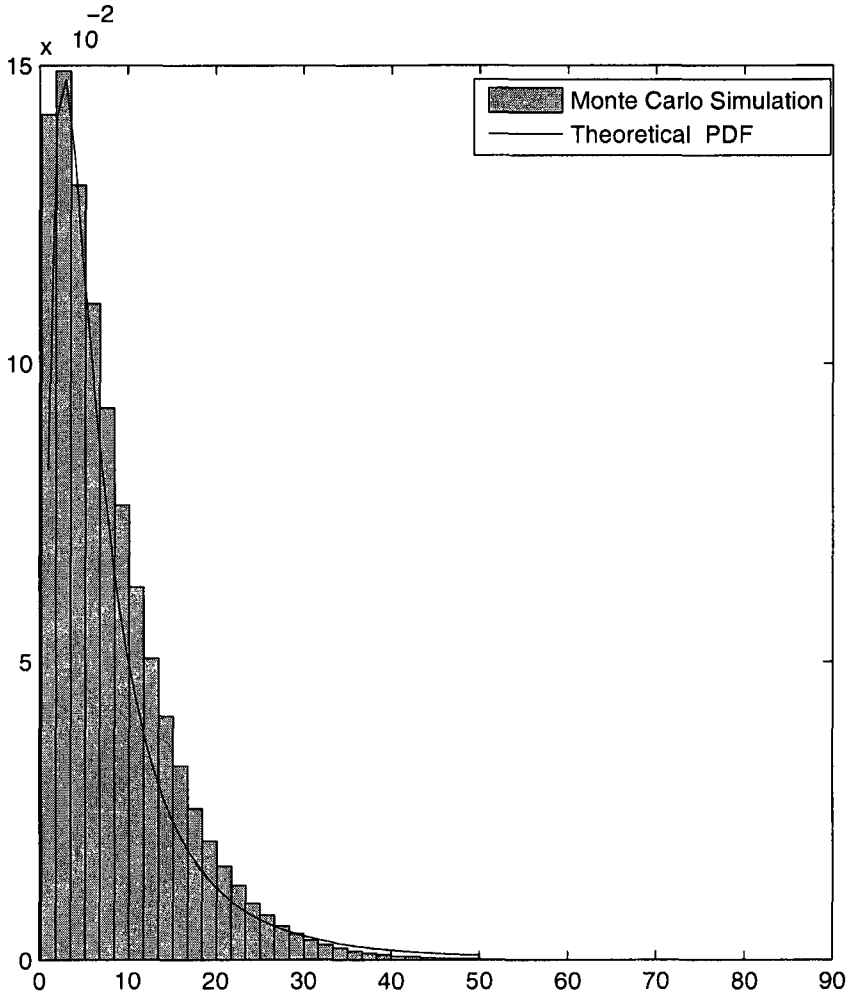

Figure 4.2: Comparison between the theoretical PDF of SINR and Monte Carlo simulation when $N_r = N_t = 2$ at $P/\sigma_z^2 = 20dB$

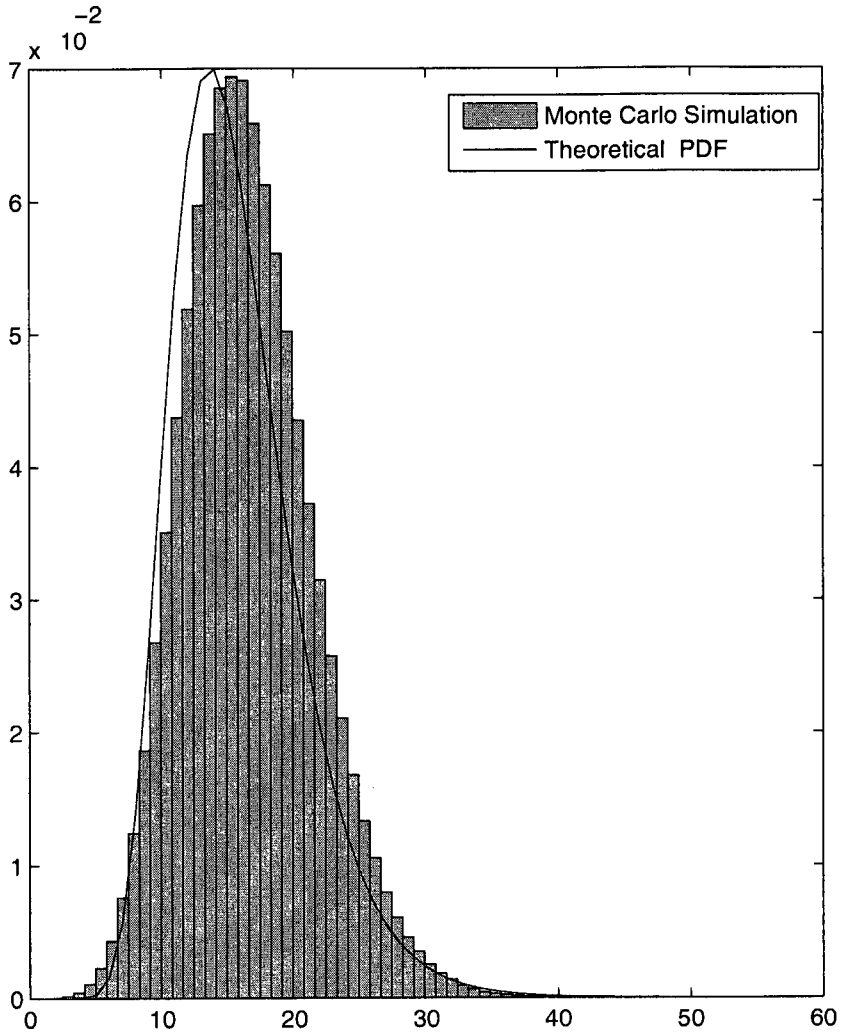

Figure 4.3: Comparison between the theoretical PDF of SINR and Monte Carlo simulation when $N_r = N_t = 4$ at $P/\sigma_z^2 = 20dB$

The closed-form formula for the average BER in (4.23) is difficult to determine. For example, the BER_{av} for 2^{η}-PSK can be written as

$$BER_{av} = \frac{2}{\eta} \int Q\left(\sqrt{2\eta\ \gamma}\ \sin(\frac{\pi}{2^{\eta}})\right) P_{\Gamma}(\gamma)\ d\gamma \tag{4.38}$$

and for rectangular 2^{η}-QAM can be written as

$$BER_{av} = \frac{4}{\eta} \int Q\left(\sqrt{\frac{3\eta\ \gamma}{2^{\eta}-1}}\right) P_{\Gamma}(\gamma)\ d\gamma, \tag{4.39}$$

where $Q(\cdot)$ denotes the Gaussian-Q function. Here, the above average BER is calculated numerically. In Fig. 4.4, numerical and simulation results are compared for 8PSK over 3×3, and for 4PSK over 4×4 fading channels, respectively. As can be seen, the numerical and simulation results match very well. Additionally, these results can be used to evaluate the adaptive system as long as the ST symbol rate does not change and the constellation size is adaptive only. In fact, we will use these performance results in Section 4.4 and 4.5 to confirm the simulation results.

4.4 Design of Adaptive Transceiver

The general idea of selection-mode adaptation is to maximize the average transmission rate by choosing a proper transmission mode from a set of available modes. Based on the particular strategy, the transmitter is informed by the receiver to increase or decrease the transmission rate depending on the channel condition, i.e., CSI. For selection-mode adaptation, the signal-to-noise ratio (SNR) will be considered as a proper metric. In summary, if the SNR at the receiver improves due to a "good" channel condition, the transmitter can increase the rate using the same power and the target BER can be satisfied. Otherwise, if the SNR worsens due to a "bad" channel, the transmitter should reduce the rate to satisfy the target BER.

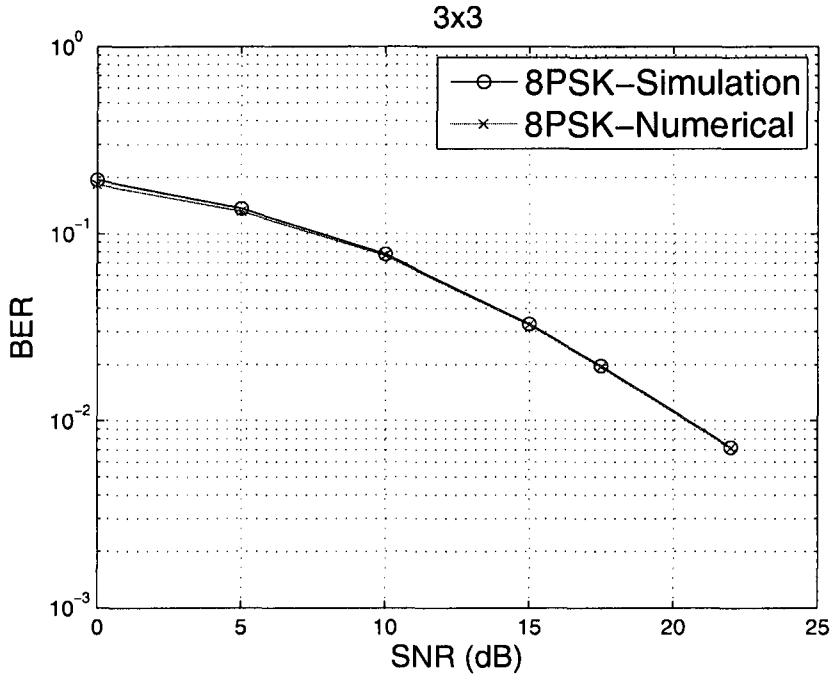

(a) 3×3, 8PSK

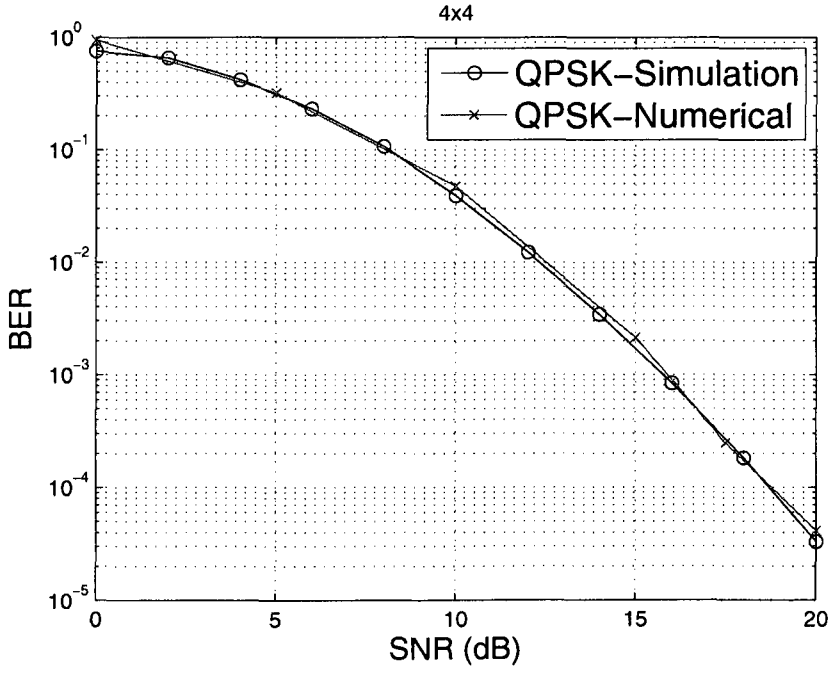

(b) 4×4, 4PSK

Figure 4.4: Numerical and simulation results for LDC with MMSE receiver

The corresponding adaptive algorithm is proposed as follows.

1. Find the SNR, say γ_o, at the receiver;
2. Find the BERs of each mode at the obtained SNR γ_o from BER curves, determined by experimentation;
3. Select a proper transmission mode with the maximum rate while satisfying the target BER; and
4. Feed back the selected mode to the transmitter.

We can formulate the selection of transmission modes as follows.

$$\Theta_{opt} = \arg \max_{\{\Theta_n, \forall n=1,2,\ldots,N\}} R_{\Theta_n}, \tag{4.40}$$

subject to

$$BER_{\Theta_n}(\gamma_o) \leq BER_{target}, \tag{4.41}$$

where $\{\Theta_n, \forall n = 1, 2, \ldots, N\}$ is the set of transmission modes, R_{Θ_n} is the rate of transmission mode Θ_n, $BER_{\Theta_n}(\gamma_o)$ is the BER of transmission mode Θ_n at SNR γ_o and BER_{target} is the target BER. Without loss of generality, we can assume $R_{\Theta_1} < R_{\Theta_2} < \ldots < R_{\Theta_N}$. Θ_{opt} is the optimal transmission mode at SNR γ_o.

Below, we consider the average transmission rate using the proposed adaptive algorithm. Let γ_{Θ_n} denote the minimum SNR satisfying the following condition:

$$\gamma_{\Theta_n} = \arg \min_{\gamma} [BER_{\Theta_n}(\gamma) \leq BER_{target})]. \tag{4.42}$$

That is, for the SNR region $\gamma_{\Theta_n} \leq \gamma \leq \gamma_{\Theta_{n+1}}$, the transmission rate R_{Θ_n} (i.e., the transmission mode Θ_n) should be selected while the target BER is satisfied.

Then, the average transmission rate is

$$\bar{R} = \sum_{n=1}^{N} R_{\Theta_n} \int_{\gamma_{\Theta_n}}^{\gamma_{\Theta_{n+1}}} p_\Gamma(\gamma) d\gamma \tag{4.43}$$

where $p_\Gamma(\gamma)$ is the probability density function (PDF) of the SNR γ and $\gamma_{\Theta_{N+1}} = \infty$. Maximization of the average transmission rate $\bar{R}$ can be solved using Lagrange multipliers. However, due to the structure of both the objective function and the inequality constraint, an analytical solution is extremely difficult to find. Therefore, we will find the SNR region corresponding to each transmission mode by measurement.

In our simulations, we assume that $N_t = N_r = 4$, using the dispersion matrices defined in (4.12), and the MMSE receiver is applied. First, we perform constellation adaptation along with a fixed ST symbol rate. Next, we perform the ST symbol rate adaptation along with a fixed constellation. Finally, we will consider these two parameters jointly, to maximize the average transmission rate while maintaining the target BER, which is equal to 10^{-3} in our design examples. Even if the BER curves intersect with each other, the tables thus obtained will tell the system to use the optimal transmission mode, which should satisfy the target BER.

4.4.1 Adaptation using Variable Constellations

Although the system design for continuous-rate scenarios provides intuitive and useful guidelines[24], the associated constellation-mapper requires high implementation complexity. In practice, discrete constellations are preferable. That is, η only takes an integer number, such as $\eta = 1, 2, 3, ...$ For a given adaptive system, we can adjust the constellation to maximize the transmission rate while keeping the target BER satisfied. The proposed adaptive algorithm is applied to the case. Here, we only consider BPSK ($\eta = 1$), QPSK ($\eta = 2$), 8PSK ($\eta = 3$) and 16QAM ($\eta = 4$) as examples. which can be written as, $\Theta_n \in \{BPSK, QPSK, 8PSK, 16QAM\}$, with a fixed ST symbol rate. The optimal transmission mode is selected by the proposed

adaptive algorithm, i.e., by equation (4.40) and (4.41). Simulation results are shown in Figure 4.5 - 4.8, where each figure has its own ST symbol rate. We summarize our simulation results in Table 4.1. In the following context, $\gamma_{\eta}^{\frac{L}{T}}$ denotes the SNR associated with the transmission mode with 2^{η} constellations and a $\frac{L}{T}$ ST symbol rate.

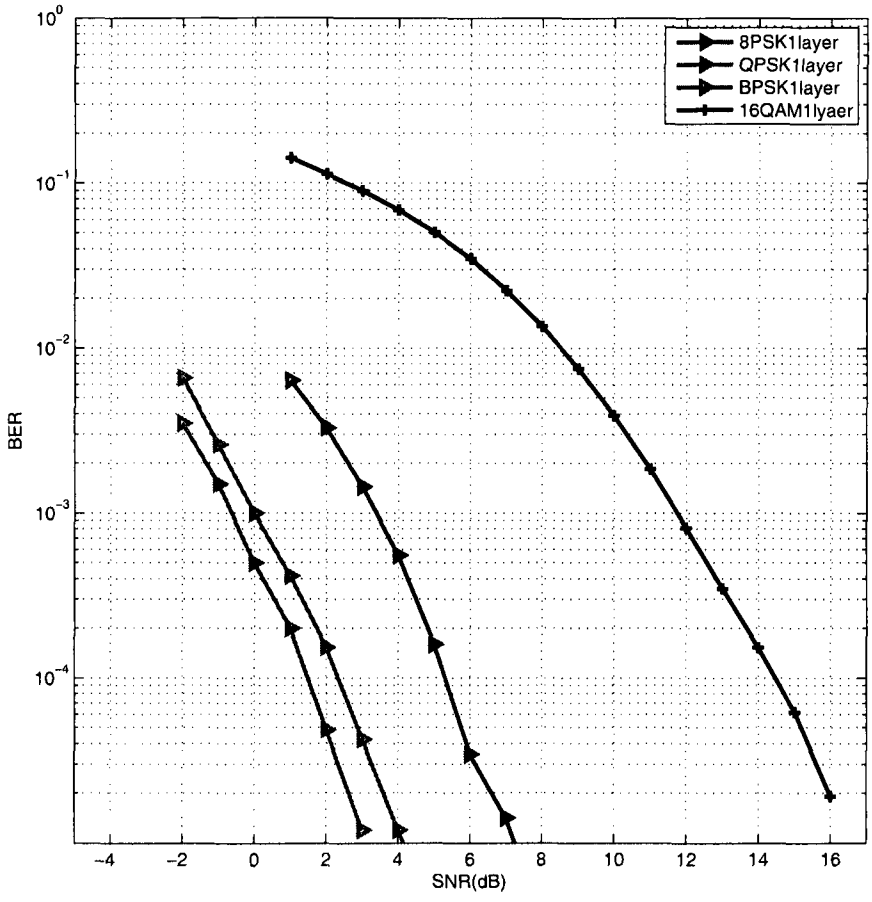

Figure 4.5: Adaptive constellation size when ST symbol rate=1

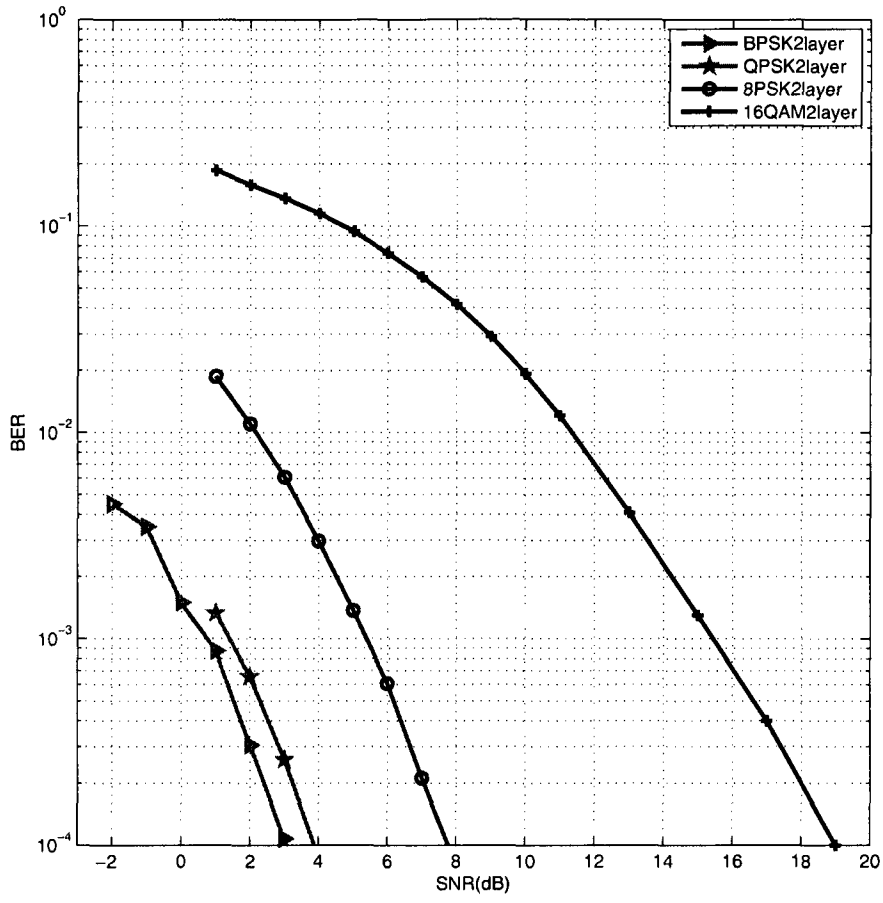

Figure 4.6: Adaptive constellation size when ST symbol rate=2

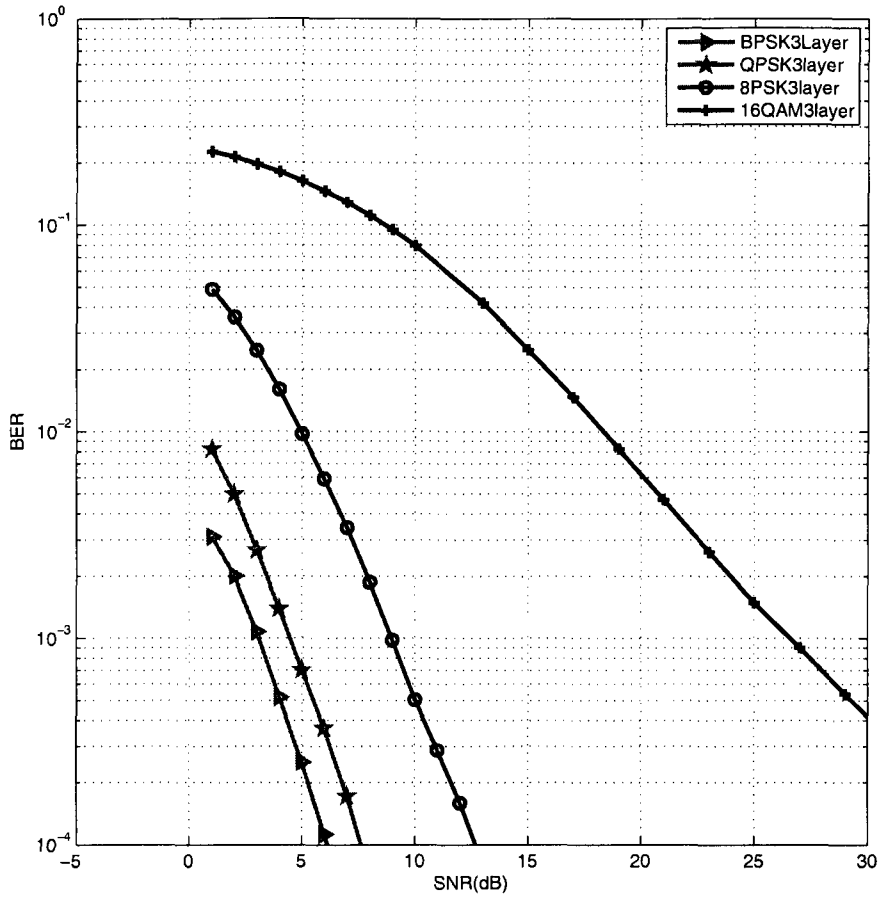

Figure 4.7: Adaptive constellation size when ST symbol rate=3

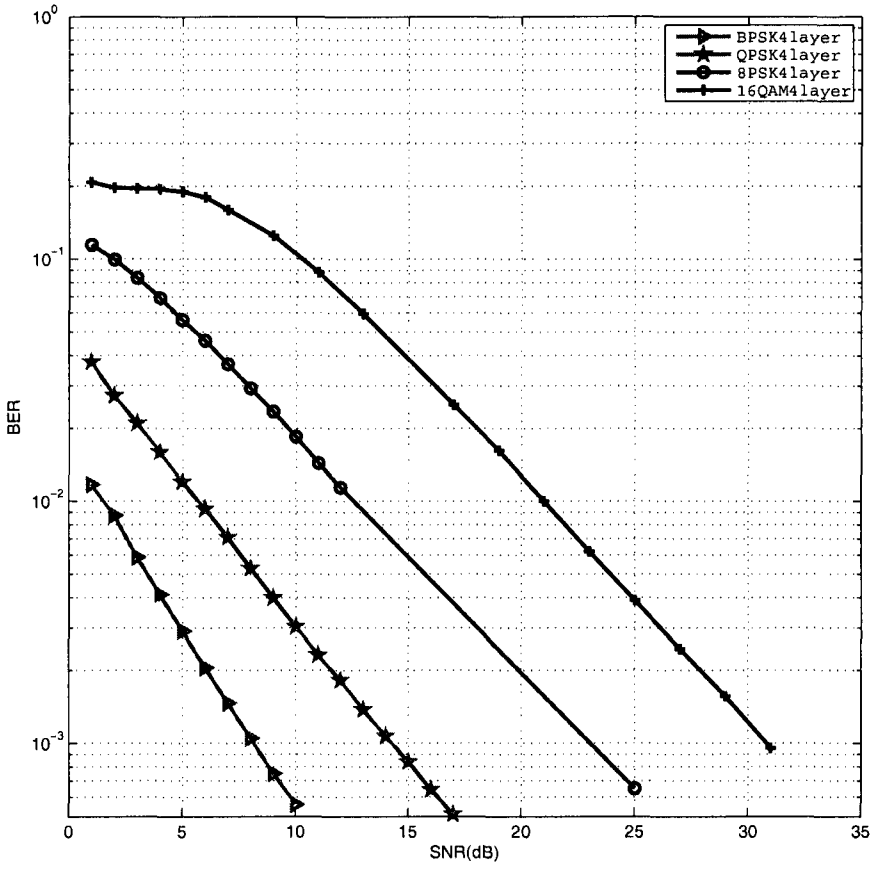

Figure 4.8: Adaptive constellation size when ST symbol rate=4

We can find the SNR region for each constellation by a curve-fitting technique or simply by reading the SNR points corresponding to a target BER. The BER versus SNR relationship can be approximated by the following expression:

$$BER = a_{R_m,\eta} \exp(-b_{R_m,\eta} SNR), \tag{4.44}$$

where R_m and η are the ST symbol rate and the constellation size, respectively, and $a_{R_m,\eta}$ and $b_{R_m,\eta}$ are constants which can be found by a curve-fitting technique.We summarize our simulation results in Table 4.1. In the following context, $\gamma_\eta^{\frac{L}{R}}$ denotes the SNR associated with the transmission mode with a 2^η constellation and an ST

symbol rate of $\frac{L}{T}$.

Table 4.1: Adaptive constellation with ST symbol rate $L/T = 1, 2, 3, 4$

MODE	Constellation	L/T	R	$\gamma_\eta^{\frac{L}{T}}$
0	-	-	-	$\gamma < -0.6309$
1	BPSK	1	1	$-0.6309 \leq \gamma_1^1 < -0.1893$
2	QPSK	1	2	$-0.1893 \leq \gamma_2^1 < 3.384$
3	8PSK	1	3	$3.384 \leq \gamma_3^1 < 11.7479$
4	16QAM	1	4	$\gamma_4^1 \geq 11.7479$
MODE	Constellation	L/T	R	γ_η^2
0	-	-	-	$\gamma < 0.8385$
1	BPSK	2	2	$0.8385 \leq \gamma_1^2 < 1.4058$
2	QPSK	2	4	$1.4058 \leq \gamma_2^2 < 5.3886$
3	8PSK	2	6	$5.3886 \leq \gamma_3^2 < 15.4452$
4	16QAM	2	8	$\gamma_4^2 \geq 15.4452$
MODE	Constellation	L/T	R	γ_η^3
0	-	-	-	$\gamma < 3.1014$
1	BPSK	3	3	$3.1014 \leq \gamma_1^3 < 4.4833$
2	QPSK	3	6	$4.4833 \leq \gamma_2^3 < 8.9696$
3	8PSK	3	9	$8.9696 \leq \gamma_3^3 < 26.5898$
4	16QAM	3	12	$\gamma_4^3 \geq 26.5898$
MODE	Constellation	L/T	R	γ_η^4
0	-	-	-	$\gamma < 8.1509$
1	BPSK	4	4	$8.1509 \leq \gamma_1^4 < 14.2812$
2	QPSK	4	8	$14.2812 \leq \gamma_2^4 < 24.2533$
3	8PSK	4	12	$24.2533 \leq \gamma_3^4 < 30.8208$
4	16QAM	4	16	$\gamma_4^4 \geq 30.8208$

4.4.2 Adaptation using Variable ST Symbol Rate

In other existing schemes, only the orthogonal designs, such as Alamouti scheme, are applied as the ST modulation. In this case, the most convenient adaptive parameter is the constellation size. For our adaptive scheme, the application of LDC makes another adaptive parameter available, i.e., ST symbol rate. In this subsection, we fix the constellation size but adjust the ST symbol rate for adaptation. One advantage of using ST symbol rate is that it is easier to change ST symbol rate than constellation size for adaptation purpose, as can be seen in Figure 4.1. The proposed adaptive algorithm described by (4.40) and (4.41) can be applied to ST symbol rate adaptation.

Observe that this system, with 4 transmit antennas, can have 16 choices of ST symbol rates, i.e., $(\frac{1}{4} \leftarrow \cdots \rightarrow \frac{16}{4})$. For convenience and less complexity, we use 4 choices, i.e., $\frac{L}{T} = 1, 2, 3, 4$, or $\Theta_n \in \{\frac{L}{T} = 1, \frac{L}{T} = 2, \frac{L}{T} = 3, \frac{L}{T} = 4\}$, with a fixed constellation. In the following context, the integer of $\frac{L}{T}$ is referred as "layer".The simulation results are shown in Figure 4.9 - Figure 4.12, where each figure has its own constellation. We summarize these results in Table 4.2.

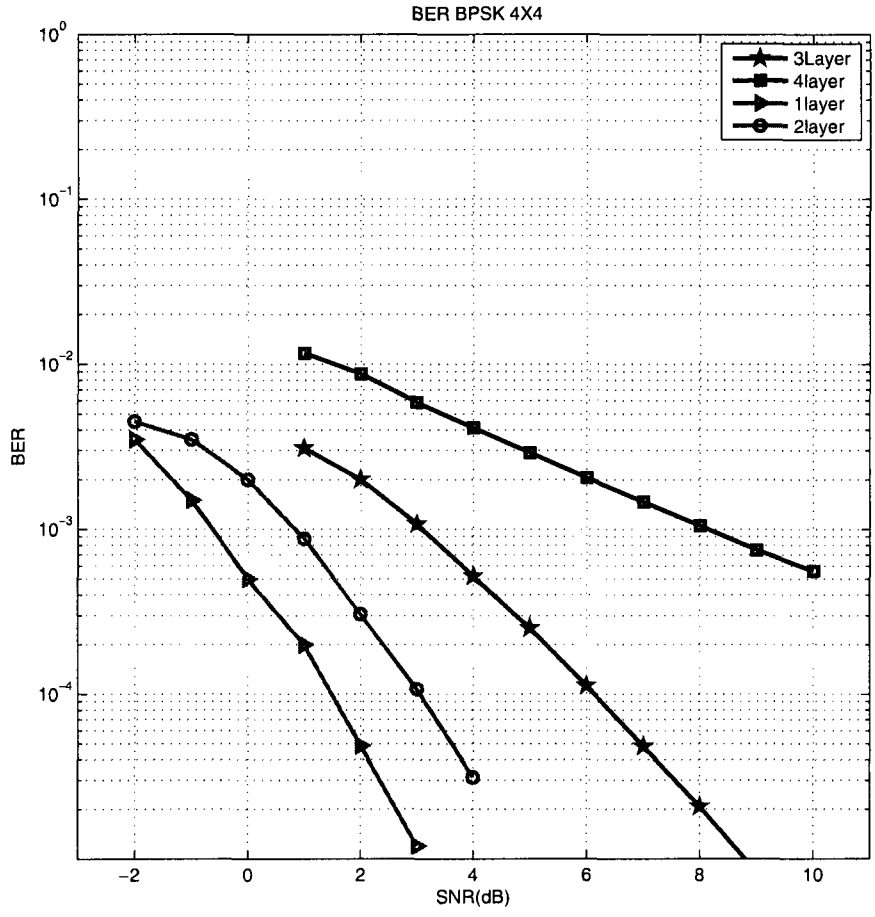

Figure 4.9: Adaptive ST symbol rate when constellation size is BPSK

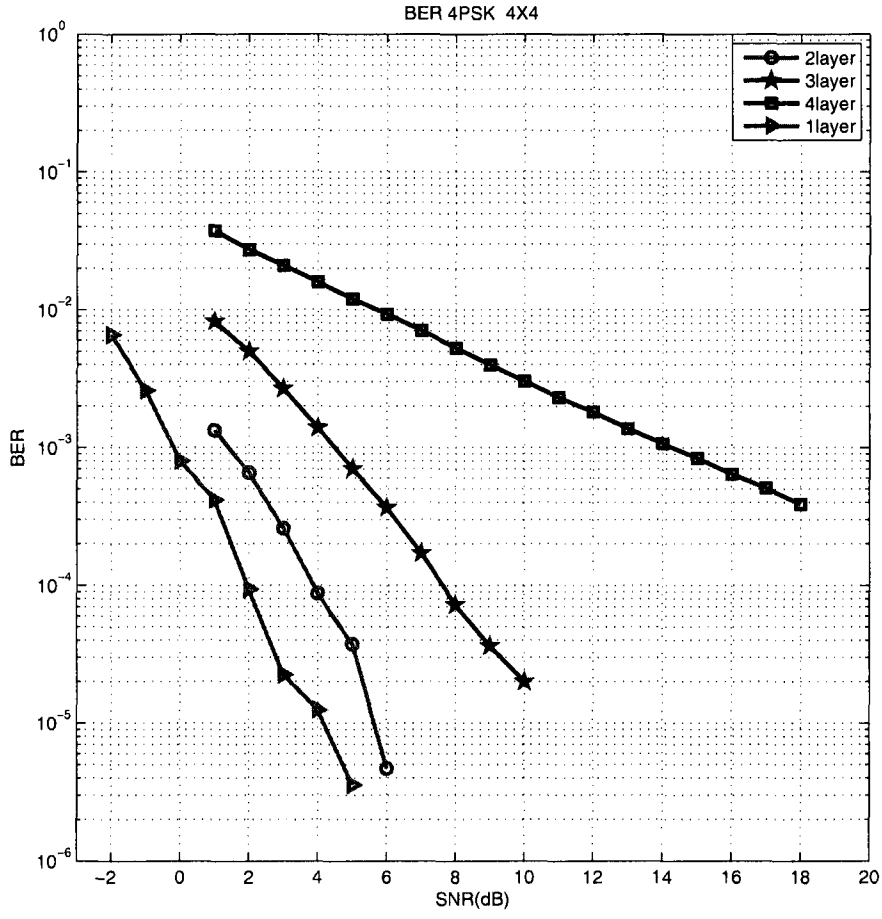

Figure 4.10: Adaptive ST symbol rate when constellation size is QPSK

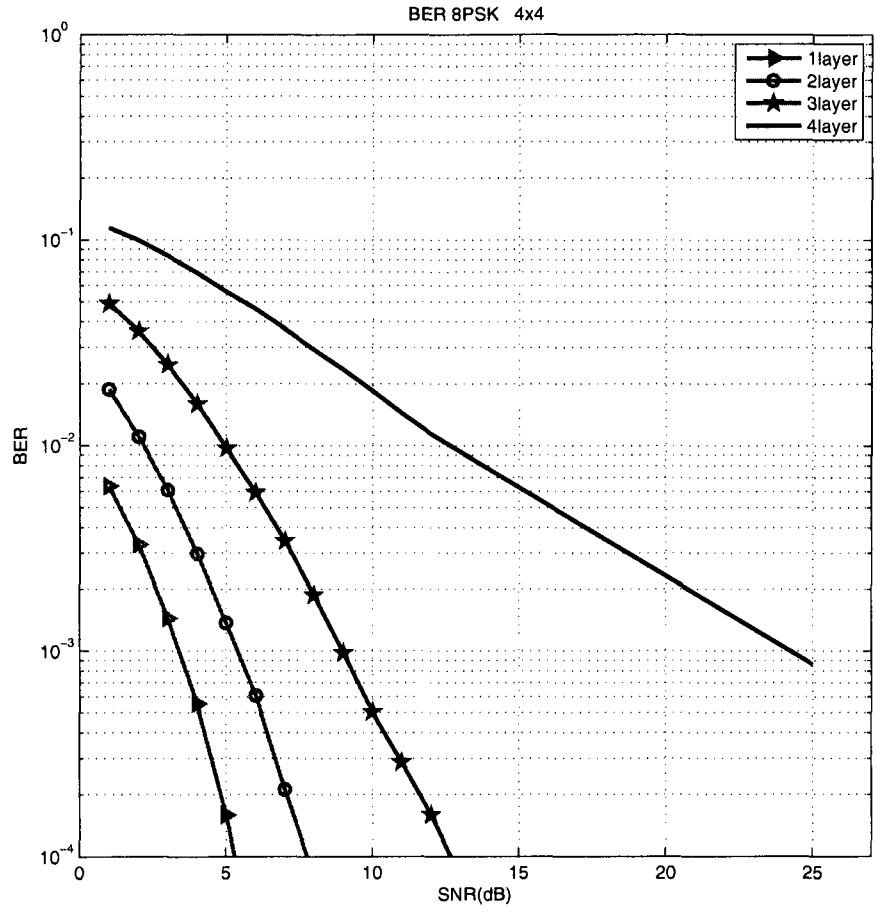

Figure 4.11: Adaptive ST symbol rate when constellation size is 8PSK

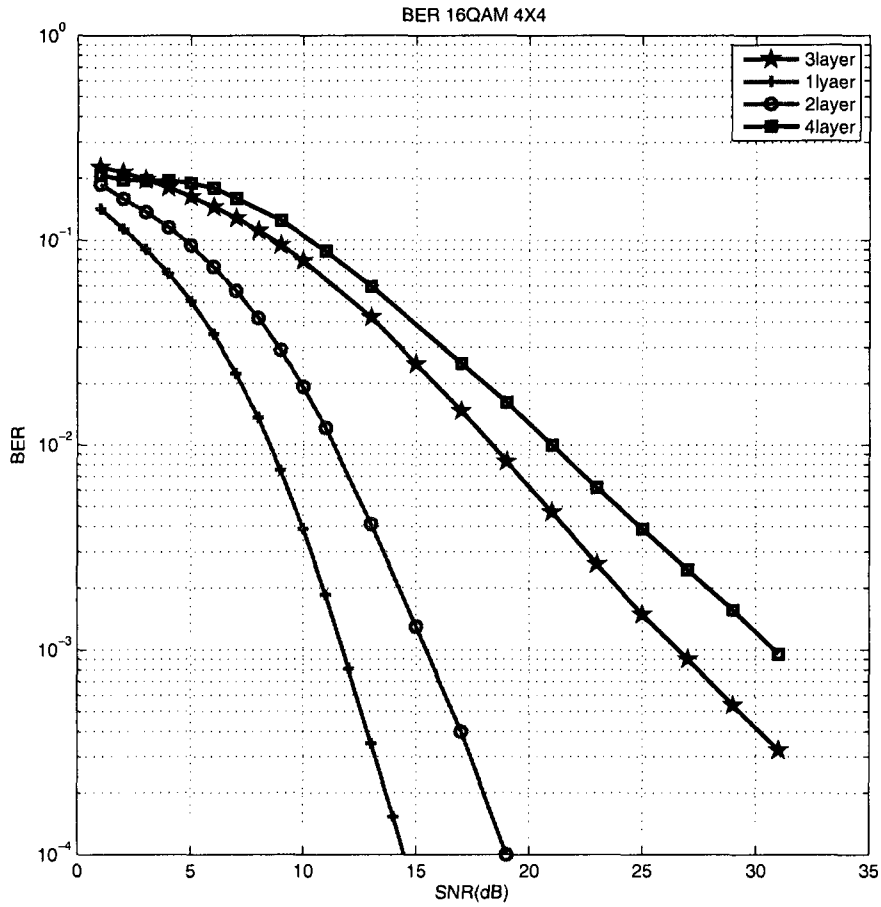

Figure 4.12: Adaptive ST symbol rate when constellation size is 16QAM.

We summarize these results in Table 4.2.

Table 4.2: Adaptive ST symbol rate when constellation is BPSK, QPSK, 8PSK and 16QAM, respectively.

MODE	Constellation	L/T	R	$\gamma_\eta^{\frac{L}{T}}$
0	-	-	-	$\gamma < -0.6309$
1	BPSK	1	1	$-0.6309 \leq \gamma_1^1 < 0.8385$
2	BPSK	2	2	$0.8385 \leq \gamma_1^2 < 3.1014$
3	BPSK	3	3	$3.1014 \leq \gamma_1^3 < 8.1509$
4	BPSK	4	4	$\gamma_1^4 \geq 8.1509$
MODE	Constellation	L/T	R	γ_2^i
0	-	-	-	$\gamma < -0.1893$
1	QPSK	1	2	$-0.1893 \leq \gamma_2^1 < 1.4058$
2	QPSK	2	4	$1.4058 \leq \gamma_2^2 < 4.4833$
3	QPSK	3	6	$4.4833 \leq \gamma_2^3 < 14.2812$
4	QPSK	4	8	$\gamma_2^4 \geq 14.2812$
MODE	Constellation	L/T	R	γ_3^i
0	-	-	-	$\gamma < 3.384$
1	8PSK	1	3	$3.384 \leq \gamma_3^1 < 5.3886$
2	8PSK	2	6	$5.3886 \leq \gamma_3^2 < 8.9696$
3	8PSK	3	9	$8.9696 \leq \gamma_3^3 < 24.2533$
4	8PSK	4	12	$\gamma_3^4 \geq 24.2533$
MODE	Constellation	L/T	R	γ_4^i
0	-	-	-	$\gamma < 11.7479$
1	16QAM	1	4	$11.7479 \leq \gamma_4^1 < 15.4452$
2	16QAM	2	8	$15.4452 \leq \gamma_4^2 < 26.5898$
3	16QAM	3	12	$26.5898 \leq \gamma_4^3 < 30.8208$
4	16QAM	4	16	$\gamma_4^4 \geq 30.8208$

4.5 Joint Adaptive Technique

As shown in the previous two subsections, either constellation adaptation or ST symbol rate adaptation can increase the average transmission rate while the given BER is satisfied compared to non-adaptive schemes. However, we can further improve the average transmission rate by applying a joint adaptation. The joint adaptation is performed by choosing the best match of constellation size and ST symbol rate. The available transmission modes are increased. That is,

$$\begin{aligned}\Theta_n \in \{&(BPSK, \tfrac{L}{T} = 1), \quad \ldots, \quad (BPSK, \tfrac{L}{T} = 4),\\ &(QPSK, \tfrac{L}{T} = 1), \quad \ldots, \quad (QPSK, \tfrac{L}{T} = 4),\\ &(8PSK, \tfrac{L}{T} = 1), \quad \ldots, \quad (8PSK, \tfrac{L}{T} = 4),\\ &(16QAM, \tfrac{L}{T} = 1), \quad \ldots, \quad (16QAM, \tfrac{L}{T} = 4)\}\end{aligned}$$

We can further reduce the gap between the selection modes by adding more choices of transmission rates. For the target BER, a scheme with the joint adaptation can improve the average transmission rate significantly, compared to the two techniques in the previous subsections. The simulation results are shown in Figure 4.13.

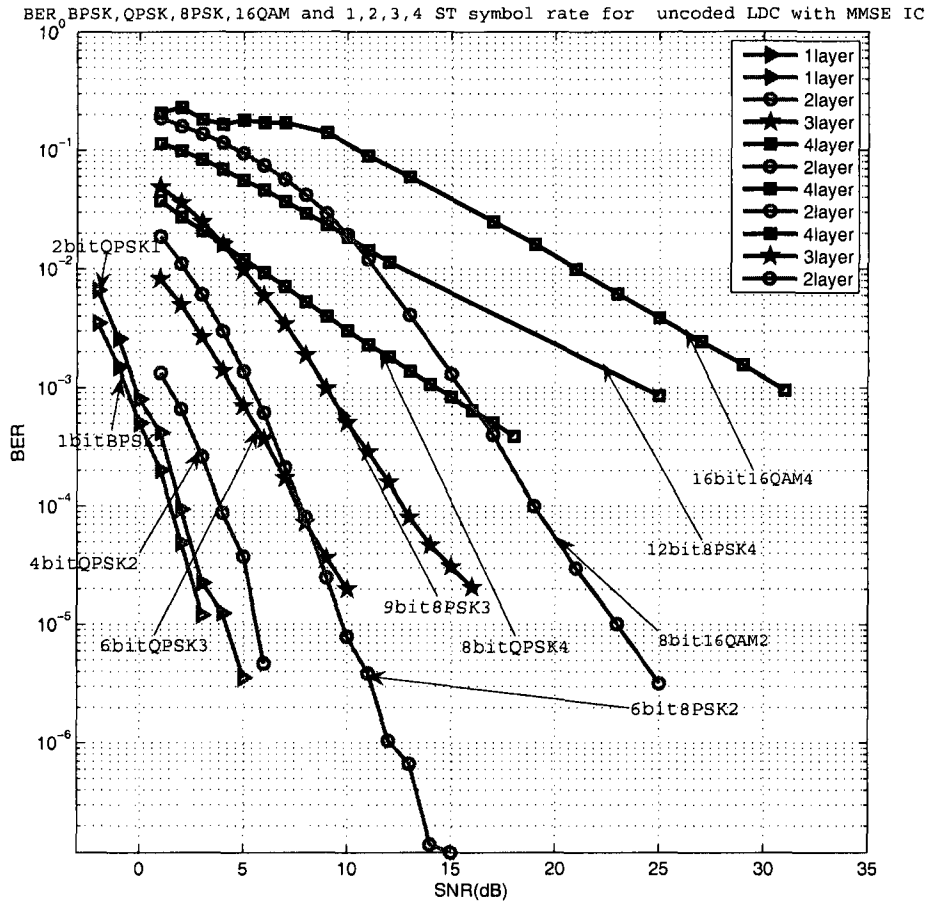

Figure 4.13: Joint adaptation of ST symbol rate and constellation size

We note from Figure 4.13 that we can reduce the gap between the selection modes further by adding more choices of the transmission rates. We conclude the result in Table 4.3, where $\gamma_\eta^{\frac{L}{T}}$ is the minimum SNR for the given transmission mode.

Table 4.3: Joint adaptation of ST symbol rate and constellation size

MODE	Constellation	L/T	R	$\gamma_\eta^{\frac{L}{T}}$
0	-	-	-	$\gamma < -0.6309$
1	BPSK	1	1	$-0.6309 \leq \gamma_1^1 < -0.1893$
2	QPSK	1	2	$-0.1893 \leq \gamma_1^2 < 1.4058$
3	QPSK	2	4	$1.4058 \leq \gamma_2^2 < 4.4833$
4	QPSK	3	6	$4.4833 \leq \gamma_3^2 < 8.9696$
5	8PSK	3	9	$8.9696 \leq \gamma_3^3 < 24.2533$
6	8PSK	4	12	$24.2533 \leq \gamma_4^3 < 30.8208$
7	16QAM	4	16	$\gamma_4^4 \geq 30.8208$

From the simulation results, we have the following observations:

- If the ST symbol rate is reduced, interference will be also reduced. As a result, the slope of the associated BER curve becomes steeper, which suggests a larger diversity;

- If the constellation size is reduced, the BER curve will shift to the left with a similar slope, which suggests that the diversity remains the same but the coding gain is improved.

There is a tradeoff between diversity gain and multiplexing gain [38]. However, this tradeoff cannot provide insight for an adaptive system with discrete constellations. From the above observations, we find that we can improve data rate by using the two adaptive parameters jointly. Specifically, in some cases, we can adjust the constellation size to improve rate and performance; while in the other cases, we will adjust the ST symbol rate, i.e., multiplexing gain, for adaptation. To proceed, we have the following proposition.

Proposition 1: The average transmission rate in the adaptive selection-mode system can be improved by adding more possible transmission modes, providing a

higher data rate than the corresponding original mode at the same SNR region.

Proof: Let us define the SNR regions of our adaptive system using one set of selection modes, as follows:

$$\Re_i \longrightarrow \gamma_i < \gamma < \gamma_{i+1} \qquad \text{associated} \quad \text{with} \longrightarrow R_i$$

If we add more possible selection modes, the SNR regions will be changed:

$$\aleph_i \longrightarrow \gamma_i < \gamma < \gamma_i^{'} \qquad \text{associated} \quad \text{with} \longrightarrow R_i$$

$$\aleph_i^{'} \longrightarrow \gamma_i^{'} < \gamma < \gamma_{i+1} \qquad \text{associated} \quad \text{with} \longrightarrow R_i^{'}$$

We assume $R_i^{'} > R_i$ for any i. The total average rate for an original scheme can be written as

$$\bar{R} = \sum_i R_i \int_{\gamma_i}^{\gamma_{i+1}} p_\Gamma(\gamma) d\gamma$$

The total average rate when for a scheme has more transmission modes can be written as

$$\bar{A} = \sum_i (R_i \int_{\gamma_i}^{\gamma_i^{'}} p_\Gamma(\gamma) d\gamma + R_i^{'} \int_{\gamma_i^{'}}^{\gamma_{i+1}} p_\Gamma(\gamma) d\gamma)$$

It is obvious that

$$\bar{A} > \bar{R}.$$

In Fig. 4.14, we compare the average spectral efficiency (ASE) for the three adaptive techniques. As can be seen from Fig. 4.14, the ASE of the joint adaptive scheme significantly outperforms the other two schemes from 0dB to 25dB. At high SNR (larger than 25 dB), the three schemes exhibit the same performance. As predicted by Proposition 1, if there are more modes available, the ASE can be improved further.

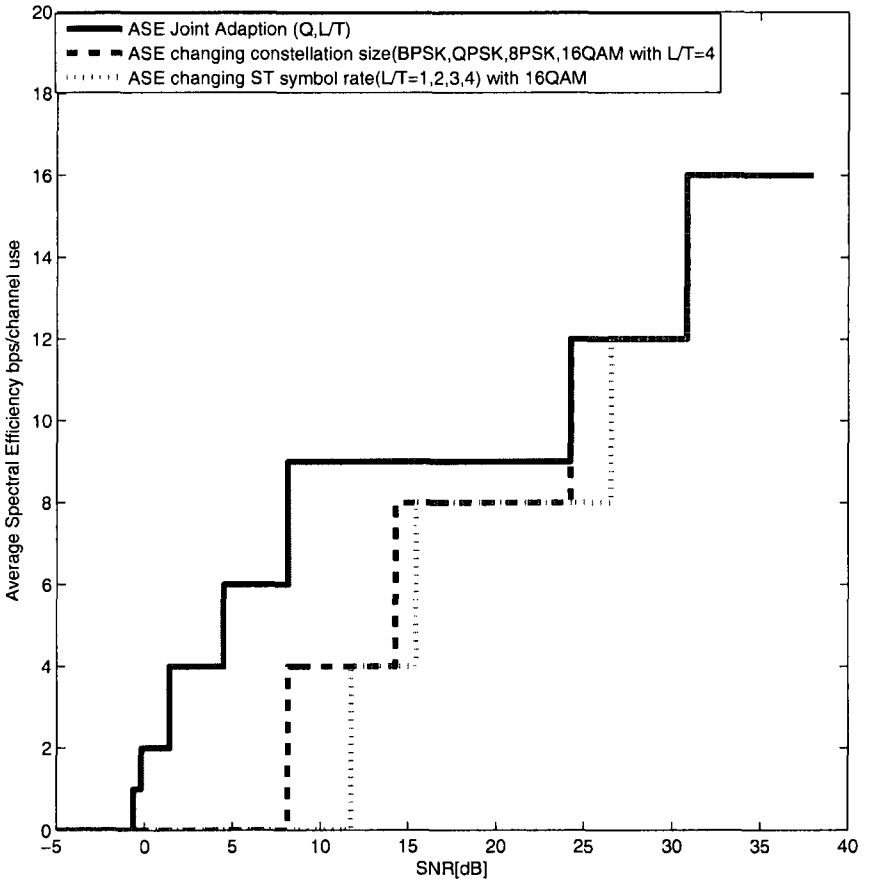

Figure 4.14: Average spectral efficiency comparison for the three adaptive schemes.

4.6 Conclusions

In this chapter, the statistics of the signal-to-interference-noise ratio were studied for linear dispersion codes with linear minimum-mean-square-error receivers. The associated probability density function of the signal-to-interference-noise was derived. The average bit-error rate for linear dispersion code with linear minimum-mean-square-error was found numerically. The simulation and numerical results are provided to verify our analysis. With these results as guidelines, we proposed a novel adaptive design with discrete selection modes, in which the linear dispersion code is applied. With application of the linear dispersion code the space-time symbol rate is available for adaptation. An adaptive algorithm is proposed for selection-mode adaptation. Based on the proposed algorithm, two adaptation techniques using constellation size and space-time symbol rate are studied, respectively. With joint adaptation of space-time symbol rate and constellation size, more transmission modes can be provided to reduce the rate gap among transmission modes. Theoretical analysis shows that the average transmission rate can be further improved with more available transmission modes. Additionally, by using the space-time symbol rate of the linear dispersion code, this adaptive design can be simplified and various levels of diversity and multiplexing gain can be provided. Simulation results were provided to demonstrate the merits of joint adaptation of constellation size and the space-time symbol rate.

Chapter 5

New Power Allocation Strategy among MIMO Spatial Subchannels - Beam-Nulling

5.1 Introduction

In the previous chapter, we presented and studied a new selection-mode adaptation scheme. When more feedback bandwidth is available, various beamforming schemes can be considered, as mentioned in Chapter 1. Based on the current beamforming schemes, we propose a new beamforming-like technique called minimum eigenvector "beam-nulling"(BN). This scheme uses the same feedback bandwidth as beamforming only one eigenvector is fed back to the transmitter. But, unlike beamforming, which uses the strongest spatial subchannel, the beam-nulling transmitter is informed which is the weakest subchannel and then sends signals over the spatial subspace orthogonal to the weakest subchannel. Note that the transmission power will be distributed equally among the other spatial subchannels except the weakest subchannel. Both transmitter and receiver should know how to generate spatial subspace by the same method. Hence, the loss of channel capacity associated with the optimal water-filling

scheme can be reduced. Although the transmitted symbols are "precoded" according to the feedback, beam-nulling is different from the other existing precoding schemes with limited feedback channel, which are independent of the instantaneous channel but the optimal precode depends on the instantaneous channel [54]-[56]. In this scheme, power is only allocated to the other good spatial subchannels, i.e., the orthogonal subspace. Compared to the beamforming scheme, this technique outperforms significantly in terms of channel capacity at medium and high SNR. Additionally, if more than one eigenvector, e.g. k eigenvectors, can be available at the transmitter, both the beamforming scheme and the proposed beam-nulling scheme can be further extended. The extended schemes will implement or discard k spatial subchannels and are referred to as "multi-dimensional" (MD) beamforming and MD beam-nulling, respectively.

5.2 Beam-Nulling

A new beamforming-like scheme called "beam-nulling" (BN) is proposed. This scheme uses the same feedback bandwidth as beamforming, so that only one eigenvector is fed back to the transmitter. Unlike the eigen-beamforming scheme in which only the best spatial subchannel is considered, in the beam-nulling scheme, only the worst spatial subchannel is discarded. Hence, the loss of channel capacity as compared to the optimal water-filling scheme can be reduced significantly. The beam-nulling scheme is shown in Figure 5.1.

We describe the beam-nulling scheme using the channel model in Chapter 2 as our base. In this scheme, the eigenvector associated with the minimum singular value from the transmitter side, i.e., $\mathbf{v}_{N_t}$ (refer to equation (2.1)), is fed back to the transmitter. By a certain rule, a subspace orthogonal to the weakest spatial channel

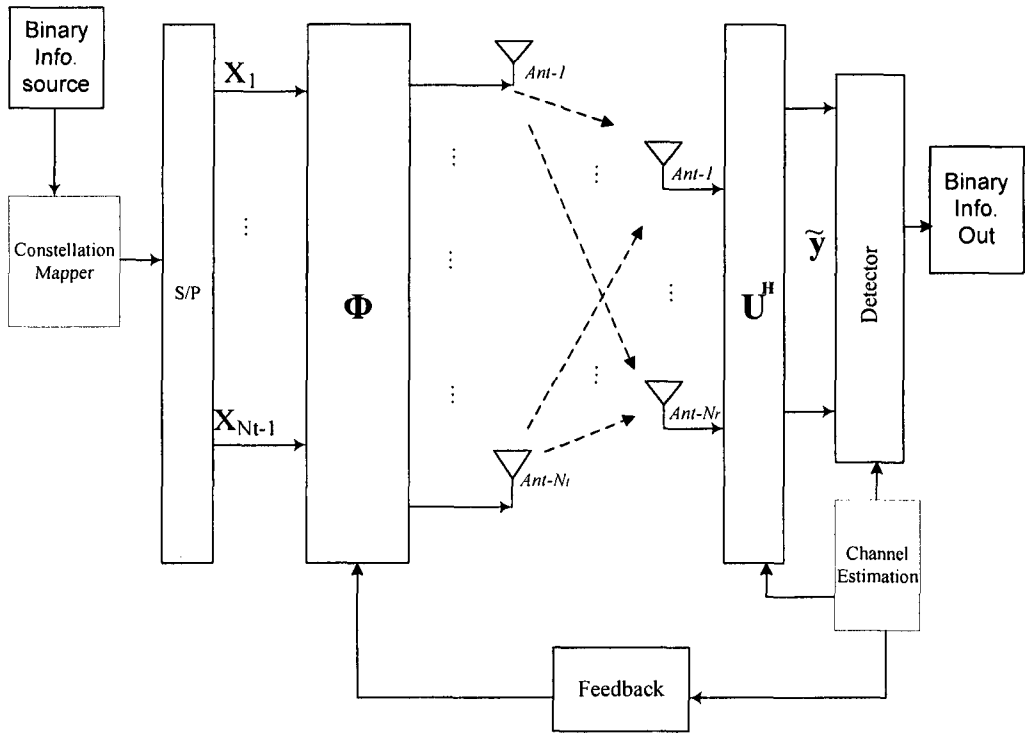

Figure 5.1: Beam-nulling scheme.

is constructed. The following condition must be satisfied:

$$\mathbf{\Phi}^H \cdot \mathbf{v}_{N_t} = \mathbf{0}_{(N_t-1)\times 1} \tag{5.1}$$

The $N_t \times (N_t - 1)$ matrix $\mathbf{\Phi} = [\mathbf{g}_1\ \mathbf{g}_2\ \ldots\ \mathbf{g}_{N_t-1}]$ spans the subspace. Note that the rule to construct the subspace $\mathbf{\Phi}$ should also be known to the receiver.

An example that shows how to construct the orthogonal subspace follows. We construct an $N_t \times N_t$ matrix

$$\mathbf{A} = [\mathbf{v}_{N_t}\ \ \mathbf{I}'] \tag{5.2}$$

where the column vectors of $\mathbf{I}'$ are independent of $\mathbf{v}_{N_t}$, and $\mathbf{I}'$ is known to both transmitter and receiver. In the next chapter, the design of the "seed" $\mathbf{I}'$ in terms of performance will be discussed. As can be seen in the following discussion, the selection of the seed $\mathbf{I}'$ does not affect the capacity. Here, as an example, we select $\mathbf{I}' = \left[\mathbf{I}_{(N_t-1)\times(N_t-1)}\ \ \mathbf{0}_{(N_t-1)\times 1}\right]^T$.

Applying QR decomposition to $\mathbf{A}$, we have

$$\mathbf{A} = \underbrace{[\mathbf{v}_{N_t} \quad \mathbf{\Phi}]}_{\equiv \mathbf{Q}} \cdot \mathbf{R} \tag{5.3}$$

where $\mathbf{Q}$ is a unitary matrix with the first column as $\mathbf{v}_{N_t}$, and $\mathbf{R}$ is an upper triangular matrix with the (1,1)-th entry equal to 1. $\mathbf{\Phi}$ is a subspace orthogonal to $\mathbf{v}_{N_t}$.

At the transmitter, $N_t - 1$ symbols denoted as $\mathbf{x}'$ are transmitted only over the orthogonal subspace $\mathbf{\Phi}$. The received signals at the receiver can be written as

$$\mathbf{y}' = \sqrt{\frac{P}{N_t - 1}} \mathbf{H} \mathbf{\Phi} \mathbf{x}' + \mathbf{z}' \tag{5.4}$$

where $\mathbf{z}'$ is an additive white Gaussian noise vector with *i.i.d.* symmetrical complex Gaussian elements of zero mean and variance σ_z^2.

Substituting (2.1) into (5.4) and multiplying $\mathbf{y}'$ by $\mathbf{U}^H$, we have

$$\tilde{\mathbf{y}} = \sqrt{\frac{P}{N_t - 1}} \mathbf{\Lambda} \begin{pmatrix} \mathbf{B} \\ \mathbf{0}^T \end{pmatrix} \mathbf{x}' + \tilde{\mathbf{z}} \tag{5.5}$$

where $\tilde{\mathbf{z}}$ is an additive white Gaussian noise vector with *i.i.d.* symmetrical complex Gaussian elements of zero mean and variance σ_z^2. With the condition in (5.1),

$$\mathbf{V}^H \mathbf{\Phi} = \begin{pmatrix} \mathbf{B} \\ \mathbf{0}^T \end{pmatrix} \tag{5.6}$$

where

$$\mathbf{B} = \begin{pmatrix} \mathbf{v}_1^H \mathbf{g}_1 & \mathbf{v}_1^H \mathbf{g}_2 & \cdots & \mathbf{v}_1^H \mathbf{g}_{N_t-1} \\ \mathbf{v}_2^H \mathbf{g}_1 & \ddots & \cdots & \vdots \\ \vdots & \vdots & \ddots & \vdots \\ \mathbf{v}_{N_t-1}^H \mathbf{g}_1 & \cdots & \cdots & \mathbf{v}_{N_t-1}^H \mathbf{g}_{N_t-1} \end{pmatrix} \tag{5.7}$$

in which $\mathbf{B}$ is an $(N_t - 1) \times (N_t - 1)$ unitary matrix. As can be seen from (5.5), the

available spatial channels are $N_t - 1$. Since the weakest spatial subchannel is "nulled" in this scheme, power can be allocated equally among the remaining "better" $N_t - 1$ subchannels. Equation (5.5) can be rewritten as

$$\tilde{\mathbf{y}}' = \sqrt{\frac{P}{N_t - 1}}\mathbf{\Lambda}'\mathbf{B}\mathbf{x}' + \tilde{\mathbf{z}}' \tag{5.8}$$

where $\tilde{\mathbf{y}}'$ and $\tilde{\mathbf{z}}'$ are column vectors with the first $(N_r - 1)$ elements of $\tilde{\mathbf{y}}$ and $\tilde{\mathbf{z}}$, respectively, and $\mathbf{\Lambda}' = \text{diag}[\lambda_1, \lambda_2, \ldots, \lambda_{(N_t-1)}]$. From (5.8), the associated instantaneous channel capacity with respect to $\mathbf{H}$ can be found as

$$C_{bn} = \sum_{i=1}^{N_t-1} \log\left(1 + \frac{P}{(N_t - 1)\sigma_z^2}\lambda_i^2\right) \tag{5.9}$$

The numerical results of ergodic (average) channel capacity for 2×2, 3×3 and 4×4 Rayleigh flat fading channels are shown in Figure 5.2.

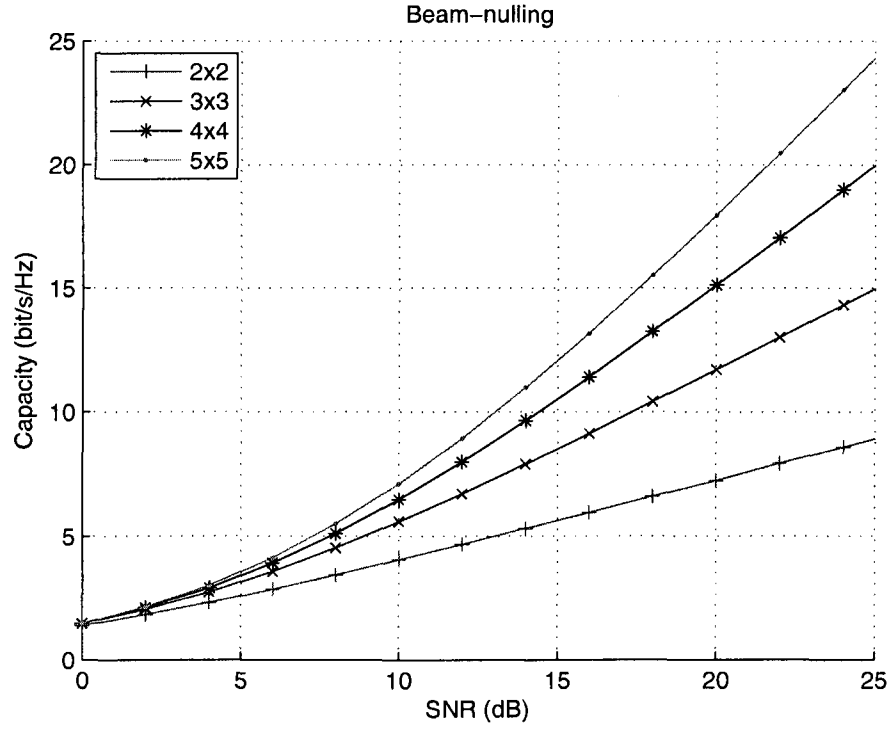

Figure 5.2: Capacity for beam-nulling.

The beam-nulling scheme only needs one eigenvector to be fed back. In addition, since only the worst spatial subchannel is discarded, this scheme can increase channel capacity significantly, compared to the conventional beamforming scheme.

5.3 Capacity Comparisons among Four Strategies

In this section, we compare the new proposed beam-nulling scheme with three other schemes and evaluate their respective capacities. Water-filling is the optimal solution among the four schemes for any SNR.

Let $\bar{C}_{eq}$, $\bar{C}_{bf}$, and $\bar{C}_{bn}$ denote the ergodic channel capacities of equal power, beamforming and beam-nulling, respectively. That is,

$$\bar{C}_{eq} = E(C_{eq}) \tag{5.10}$$

$$\bar{C}_{bf} = E(C_{bf}) \tag{5.11}$$

$$\bar{C}_{bn} = E(C_{bn}) \tag{5.12}$$

where $E()$ denotes the expectation with respect to $\mathbf{H}$. Let $\rho = P/\sigma_z^2$ denote the SNR. Differentiating the above ergodic capacities with respect to ρ, we have

$$\frac{\partial \bar{C}_{eq}}{\partial \rho} = E\left(\sum_{i=1}^{N_t} \frac{1}{\rho + \frac{N_t}{\lambda_i^2}}\right) \tag{5.13}$$

$$\frac{\partial \bar{C}_{bf}}{\partial \rho} = E\left(\frac{1}{\rho + \frac{1}{\lambda_1^2}}\right) \tag{5.14}$$

$$\frac{\partial \bar{C}_{bn}}{\partial \rho} = E\left(\sum_{i=1}^{N_t-1} \frac{1}{\rho + \frac{N_t-1}{\lambda_i^2}}\right) \tag{5.15}$$

The differential will also be referred to as "slope". The second order differentials are

listed as follows.

$$\frac{\partial^2 \bar{C}_{eq}}{\partial \rho^2} = E\left(\sum_{i=1}^{N_t} -\frac{1}{\left(\rho + \frac{N_t}{\lambda_i^2}\right)^2}\right) \tag{5.16}$$

$$\frac{\partial^2 \bar{C}_{bf}}{\partial \rho^2} = E\left(-\frac{1}{\left(\rho + \frac{1}{\lambda_1^2}\right)^2}\right) \tag{5.17}$$

$$\frac{\partial^2 \bar{C}_{bn}}{\partial \rho^2} = E\left(\sum_{i=1}^{N_t-1} -\frac{1}{\left(\rho + \frac{N_t-1}{\lambda_i^2}\right)^2}\right) \tag{5.18}$$

As can be seen, the above ergodic capacities are concave and monotonically increasing with respect to ρ. With the fact that $\lambda_1 \geq \lambda_2 \ldots \geq \lambda_{N_t}$, it can be readily verified that the slopes of the ergodic capacities associated with equal power and beam-nulling are bounded as follows:

$$E\left(\frac{N_t}{\rho + \frac{N_t}{\lambda_1}}\right) \geq \frac{\partial \bar{C}_{eq}}{\partial \rho} \geq E\left(\frac{N_t}{\rho + \frac{N_t}{\lambda_{N_t}}}\right) \tag{5.19}$$

$$E\left(\frac{N_t - 1}{\rho + \frac{N_t-1}{\lambda_1}}\right) \geq \frac{\partial \bar{C}_{bn}}{\partial \rho} \geq E\left(\frac{N_t - 1}{\rho + \frac{N_t-1}{\lambda_{(N_t-1)}}}\right) \tag{5.20}$$

For the case of $N_t = 2$, beamforming and beam-nulling have the same capacity for any SNR ρ, as can be seen from the equations of capacity and slope. If $\rho \to 0$, equivalently at low SNR, it can be easily found that

$$\frac{\partial \bar{C}_{bf}}{\partial \rho} \geq \frac{\partial \bar{C}_{bn}}{\partial \rho} \geq \frac{\partial \bar{C}_{eq}}{\partial \rho}, \rho \to 0 \tag{5.21}$$

And, if $\rho \to \infty$, equivalently at high SNR, it can be easily found that

$$\frac{\partial \bar{C}_{eq}}{\partial \rho} \geq \frac{\partial \bar{C}_{bn}}{\partial \rho} \geq \frac{\partial \bar{C}_{bf}}{\partial \rho}, \rho \to \infty \tag{5.22}$$

Note that $\bar{C}_{bf} = \bar{C}_{bn} = \bar{C}_{eq} = 0$ when $\rho = 0$ or minus infinity in dB. Hence, at medium SNR, the beam-nulling scheme has the largest value. In other words, among equal power, beamforming and beam-nulling, beamforming has the largest capacity at low SNR; for high SNR, equal power has the largest capacity; and for medium SNR, beam-nulling has the largest capacity. Numerical results will be provided to demonstrate our analysis.

The capacities of water-filling, beamforming, beam-nulling and equal power are compared over 2×2, 3×3, 4×4 and 5×5 Rayleigh fading channels, respectively, in Figures 5.3 to 5.6. Note that since SNR is measured in dB, the curves become convex. In these figures, "EQ" stands for equal power, "WF" represents water-filling, "BF" stands for beamforming and "BN" stands for beam-nulling. In the figures with subfigures, subfigure (a) is for all the SNR regions , subfigure (b) shows an SNR region from low to medium, and subfigure (c) refers to a region with medium to high SNR. Note that for a 2×2 channel, beamforming and beam-nulling have the same capacity.

As can be seen from these figures, water-filling has the best capacity at any SNR region. The other schemes perform differently at different SNR regions and these situations are discussed in the following subsections.

5.3.1 Capacity Comparisons at Low SNR

At low SNR, the beamforming technique is the closest to the optimal scheme, water-filling. A low SNR region is considered to be below 3 dB for a 3×3 fading channel, below 3.2 dB for a 4×4 fading channel, and the SNR region below 3.5 dB with a 5×5 fading channel. At low SNR, the water-filling scheme can only allocate power to one or two spatial subchannels. If only one spatial subchannel can be used, then beamforming is just as optimal as water-filling, which can be seen from the capacity of the 2×2 fading channel in Figure 5.3.

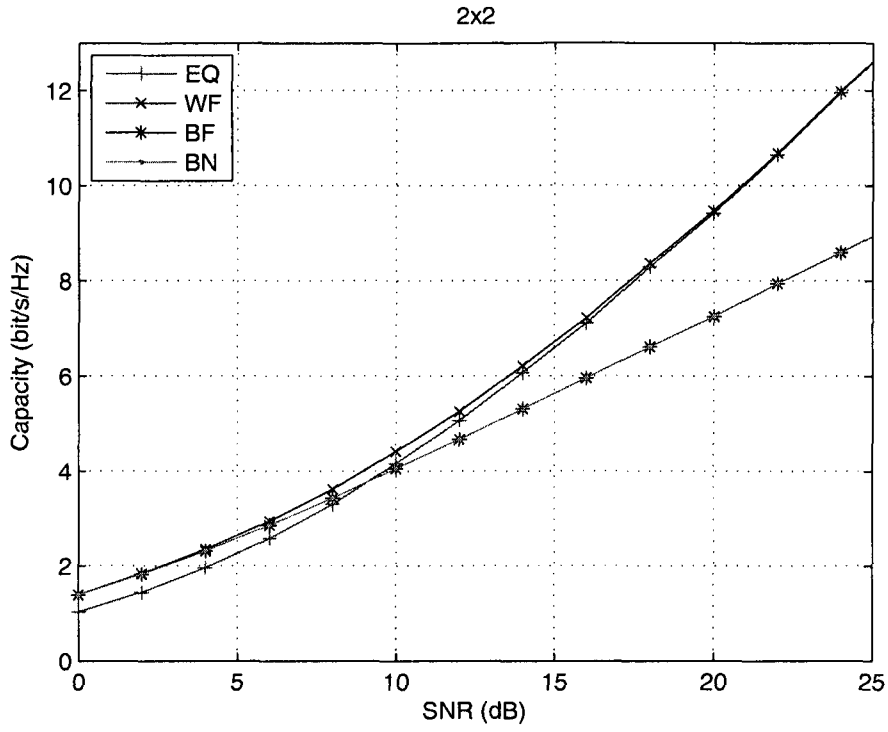

Figure 5.3: 2×2 Rayleigh fading channel.

5.3.2 Capacity Comparisons at Medium SNR

At medium SNR, the proposed beam-nulling scheme is the closest to the optimal water-filling scheme. Medium SNR regions have from 3 dB to 16 dB for 3×3 fading channels, from 3.2 dB to 20.5 dB for 4×4 fading channels, and from 3.5 dB to 23.5 dB for 5×5 fading channels. The beam-nulling scheme only discards the weakest spatial subchannel and allocates power to the other spatial subchannels. As can be seen from the numerical results, the beam-nulling scheme performs better than the other schemes in this case.

5.3.3 Capacity Comparisons at High SNR

At high SNR, the equal power scheme is the closest to the optimal water-filling scheme. High SNR regions are defined as over 16 dB for a 3×3 fading channel, over 20.5 dB for a 4×4 fading channel, and over 23.5 dB for 5×5 fading channel. As can be seen

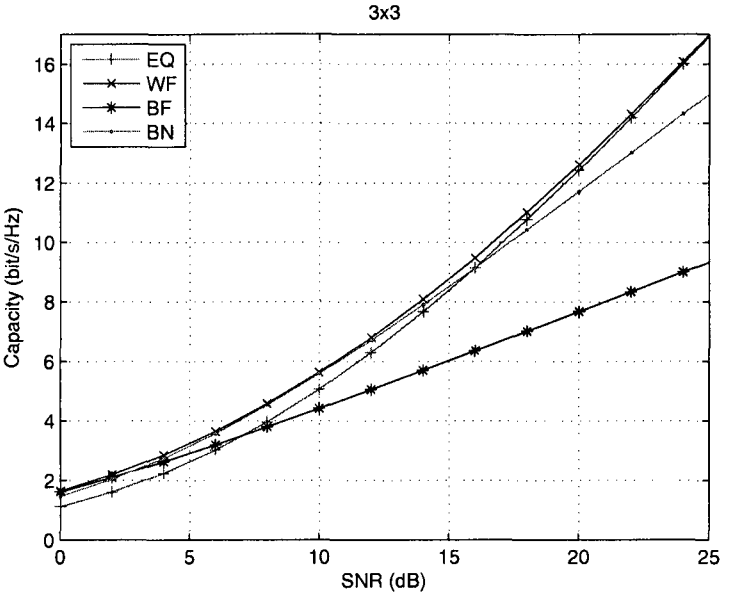

(a) 0 – 25 dB

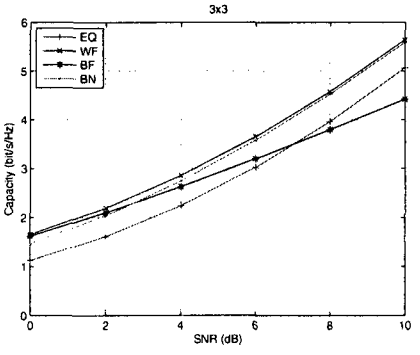

(b) 0 – 10 dB

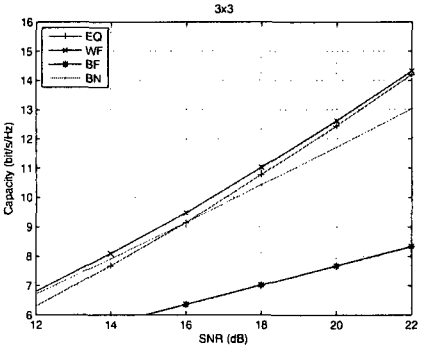

(c) 12 – 22 dB

Figure 5.4: 3×3 Rayleigh fading channel.

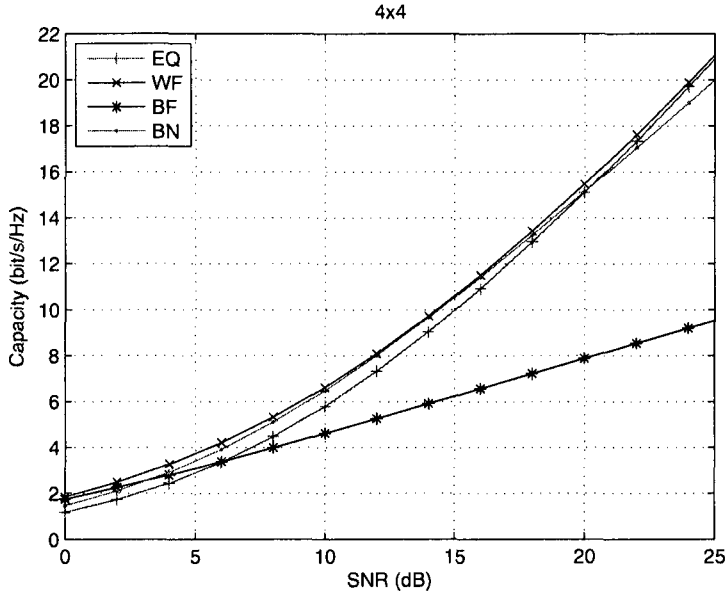

(a) $0 - 25$ dB

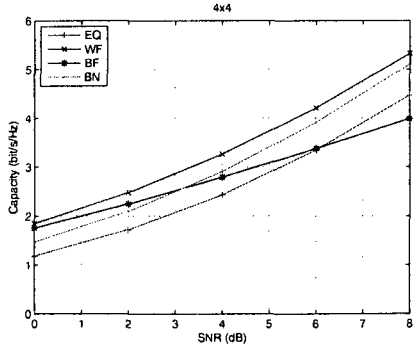

(b) $0 - 8$ dB

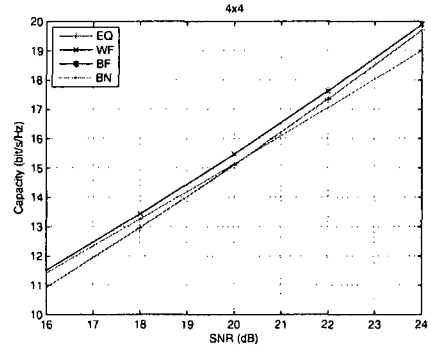

(c) $16 - 24$ dB

Figure 5.5: 4×4 Rayleigh fading channel.

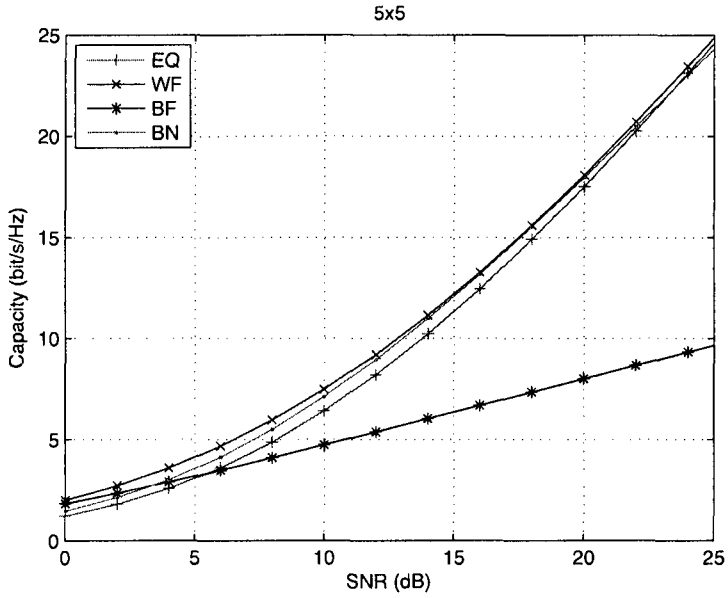

(a) 0 – 25 dB

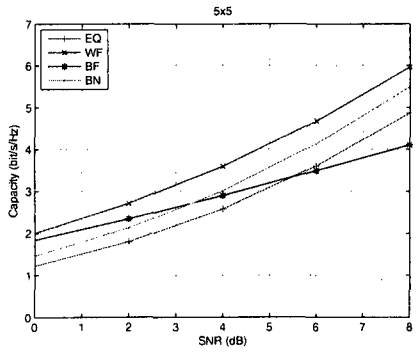

(b) 0 – 8 dB

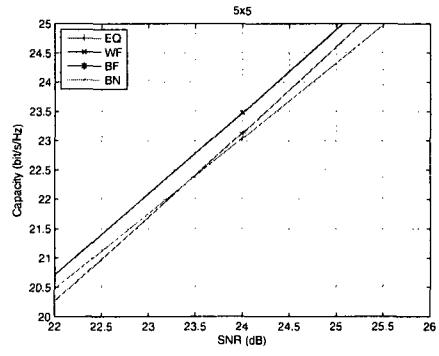

(c) 22 – 26 dB

Figure 5.6: 5×5 Rayleigh fading channel.

from the figures, at high SNR, the equal power scheme's will converge to that of the water-filling scheme.

In summary, the application of the above four schemes depends on the SNR region and the availability of CSI. At medium SNR, the proposed beam-nulling scheme can achieve larger capacity than a beamforming scheme with the same feedback bandwidth.

5.4 Extended Adaptive Frameworks

For the beamforming and beam-nulling schemes, only one eigenvector has been fed back to the transmitter. If more feedback bandwidth is available, e.g. k eigenvectors can be sent to the transmitter for adaptation, and we can extend our frameworks. The extended frameworks will be called multi-dimensional (MD) beamforming and MD beam-nulling. The original schemes can be referred to as 1D beamforming and 1D beam-nulling. To save bandwidth, $k \leq \lfloor \frac{N_t}{2} \rfloor$ should be satisfied, where $\lfloor \cdot \rfloor$ denotes rounding towards minus infinity. In other words, the extended frameworks determine whether the strongest or the weakest k spatial subchannels will be fed back according to the channel conditions. For example, at low SNRs, k strongest spatial subchannels will be fed back. At medium SNRs, k weakest spatial subchannels will be fed back.

5.4.1 MD Beamforming

For MD beamforming, we assume that k symbols, say $\mathbf{x}_k = [x_1, x_2, \ldots, x_k]^T$, are transmitted. At the receiver, the received vector can be written as

$$\mathbf{y}_k = \sqrt{\frac{P}{k}} \mathbf{H}[\mathbf{v}_1 \ldots \mathbf{v}_k]\mathbf{x}_k + \mathbf{z}_k \tag{5.23}$$

where $\mathbf{z}_k$ is the additive white Gaussian noise vector with *i.i.d.* symmetrical complex Gaussian elements of zero mean and variance σ_z^2.

The eigenvectors associated with the k maximum singular values from the receiver side, i.e., $[\mathbf{u}_1\mathbf{u}_2\ldots\mathbf{u}_k]^H$, are multiplied by the received vector $\mathbf{y}_k$;

$$\tilde{\mathbf{y}}_k = [\mathbf{u}_1\mathbf{u}_2\ldots\mathbf{u}_k]^H\mathbf{y}_k \tag{5.24}$$

If we assume $\tilde{\mathbf{y}}_k = [\tilde{y}_1, \tilde{y}_2, \ldots, \tilde{y}_k]^T$, we have

$$\tilde{y}_i = \sqrt{\frac{P}{k}}\lambda_i x_i + \tilde{z}_i, \forall i = 1, 2, \ldots, k \tag{5.25}$$

where $\tilde{z}_i$ is Gaussian with zero mean and variance σ_z^2. After the multiplication of $[\mathbf{u}_1\mathbf{u}_2\ldots\mathbf{u}_k]^H$ at the MD beamforming receiver, the original MIMO channels are converted to k parallel SISO subchannels.

Consequently, the associated instantaneous channel capacity with respect to $\mathbf{H}$ can be found as

$$C_{k,bf} = \sum_{i=1}^{k} \log\left(1 + \frac{P}{k\ \sigma_z^2}\lambda_i^2\right) \tag{5.26}$$

Let $\bar{C}_{k,bf}$ denote the ergodic channel capacity of k-D beamforming. That is,

$$\bar{C}_{k,bf} = E(C_{k,bf}) \tag{5.27}$$

where $E()$ denotes expectation with respect to $\mathbf{H}$. Let $\rho = P/\sigma_z^2$ denote the SNR. It can be readily verified that the capacity of MD beamforming is also concave and monotonically increasing with respect to the SNR ρ. Differentiating the above ergodic capacity with respect to ρ, we have

$$\frac{\partial \bar{C}_{k,bf}}{\partial \rho} = E\left(\sum_{i=1}^{k} \frac{1}{\rho + \frac{k}{\lambda_i^2}}\right) \tag{5.28}$$

If $\rho \rightarrow 0$, equivalently at low SNRs, it can be easily found that

$$\frac{\partial \bar{C}_{(k-1),bf}}{\partial \rho} > \frac{\partial \bar{C}_{k,bf}}{\partial \rho}, \rho \rightarrow 0 \tag{5.29}$$

If $\rho \rightarrow \infty$, equivalently at high SNRs, it can be easily found that

$$\frac{\partial \bar{C}_{k,bf}}{\partial \rho} > \frac{\partial \bar{C}_{(k-1),bf}}{\partial \rho}, \rho \rightarrow \infty \tag{5.30}$$

Note that $\bar{C}_{k,bf} = 0$ for any k when $\rho = 0$ or minus infinity in dB. Hence, at low SNRs, the capacity of the k-D beamforming scheme is worse than the $(k-1)$-D beamforming scheme, while at high SNRs, the capacity of the k-D beamforming scheme is better than the $(k-1)$-D beamforming scheme because of the cost in terms of feedback bandwidth.

For example, in Figure 5.7, the capacities of 1D beam-forming and 2D beam-forming schemes are compared with WF and equal power schemes over 5×5 Rayleigh fading channels at different SNR regions. It can be imagined that at very low SNRs, only one spatial subchannel can be allocated with power for a WF scheme. In this case, the 1D-beamforming scheme is equivalent to the WF scheme, which is optimal. As can be seen from the figure, at medium and high SNR, the 2D-beamforming scheme outperforms 1D-beamforming in terms of capacity with the expense of feedback bandwidth as predicted.

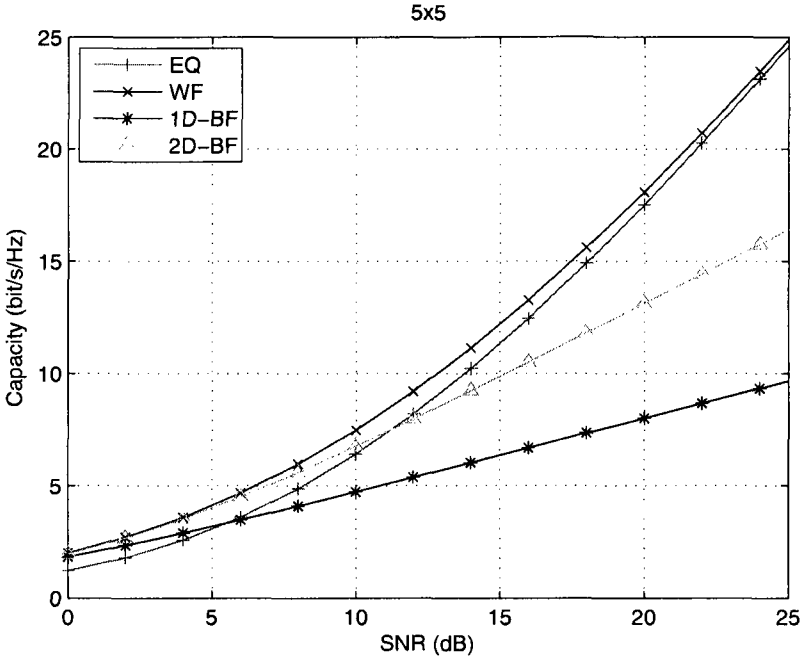

(a) 0 – 25 dB

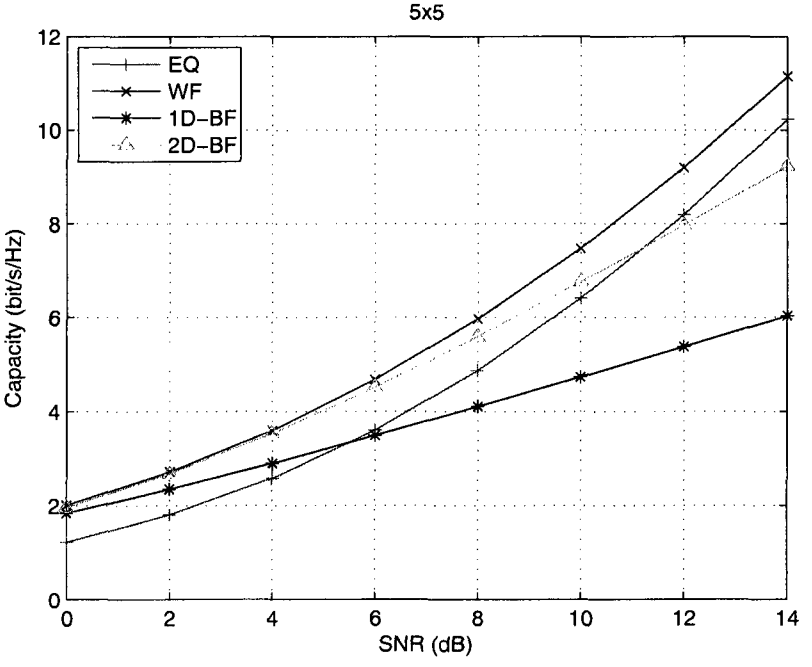

(b) 0 – 14 dB

Figure 5.7: MD beamforming over 5×5 Rayleigh fading channel.

5.4.2 MD Beam-nulling

For MD beam-nulling, similar to 1D-beam-nulling, by a certain rule, a subspace orthogonal to the k weakest spatial channel is constructed. That is, the following condition should be satisfied.

$$\mathbf{v}_n^H \mathbf{\Phi}^{(k)} = \mathbf{0}^T, \forall n = N_t - k + 1, \ldots, N_t. \tag{5.31}$$

The $N_t \times (N_t - k)$ matrix $\mathbf{\Phi}^{(k)} = [\mathbf{g}_1 \mathbf{g}_2 \ldots \mathbf{g}_{N_t-k}]$ spans the $(N_t - k)$-dimensional subspace.

At the transmitter, $N_t - k$ symbols denoted as $\mathbf{x}^{(k)}$ are transmitted only over the orthogonal subspace $\mathbf{\Phi}^{(k)}$. The received signals at the receiver can be written as

$$\mathbf{y}^{(k)} = \sqrt{\frac{P}{N_t - k}} \mathbf{H} \mathbf{\Phi}^{(k)} \mathbf{x}^{(k)} + \mathbf{z}^{(k)} \tag{5.32}$$

where $\mathbf{z}^{(k)}$ is an additive white Gaussian noise vector with *i.i.d.* symmetrical complex Gaussian elements of zero mean and variance σ_z^2. From (5.32), the associated instantaneous channel capacity with respect to $\mathbf{H}$ can be found as

$$C_{bn}^{(k)} = \sum_{i=1}^{N_t-k} \log \left(1 + \frac{P}{(N_t - k)\sigma_z^2} \lambda_i^2 \right) \tag{5.33}$$

Let $\bar{C}_{bn}^{(k)}$ denote the ergodic channel capacity of k-D beam-nulling. That is,

$$\bar{C}_{bn}^{(k)} = E(C_{bn}^{(k)}) \tag{5.34}$$

where $E()$ denotes expectation with respect to $\mathbf{H}$. It is easily verified that the capacity of MD beam-nulling is also concave and monotonically increasing with respect to SNR ρ. Let $\rho = P/\sigma_z^2$ denote the SNR. Differentiating the above ergodic capacity with

respect to ρ, we have

$$\frac{\partial \bar{C}_{bn}^{(k)}}{\partial \rho} = E\left(\sum_{i=1}^{N_t-k} \frac{1}{\rho + \frac{N_t-k}{\lambda_i^2}}\right) \tag{5.35}$$

If $\rho \to 0$, equivalently at low SNRs, it can be easily found that

$$\frac{\partial \bar{C}_{bn}^{(k)}}{\partial \rho} > \frac{\partial \bar{C}_{bn}^{(k-1)}}{\partial \rho}, \rho \to 0 \tag{5.36}$$

If $\rho \to \infty$, equivalently at a high SNR, it can be easily found that

$$\frac{\partial \bar{C}_{bn}^{(k-1)}}{\partial \rho} > \frac{\partial \bar{C}_{bn}^{(k)}}{\partial \rho}, \rho \to \infty \tag{5.37}$$

Note that $\bar{C}_{k,bn} = 0$ for any k when $\rho = 0$ or minus infinity in dB. Hence, at low SNRs, the capacity of the k-D beam-nulling scheme is better than the $(k-1)$-D beam-nulling scheme, at the cost of feedback bandwidth while at high SNRs, the capacity of the k-D beam-nulling scheme is worse than the $(k-1)$-D beam-nulling scheme.

For example, in Figure 5.8, capacities of 1D-beam-nulling and 2D-beam-nulling schemes are compared with WF and equal power schemes over 5×5 Rayleigh fading channels at different SNR regions. At relatively low SNRs, i.e., less than 13dB, the 2D-beam-nulling scheme outperforms the 1D-beam-nulling scheme in terms of capacity with a cost in feedback bandwidth. At relatively high SNRs, i.e., more than 13dB, the 1D-beam-nulling scheme, outperforms the 2D-beam-nulling scheme as predicted.

5.4.3 Capacity Comparison

Over 5×5 Rayleigh fading channels, the MD schemes are compared with WF and equal power schemes as shown in Figure 5.9. It can be readily verified that, at relatively low SNRs, MD beamforming schemes are better than MD beam-nulling schemes; while at relatively high SNRs, the opposite holds true. Specifically, at very low SNR, i.e. less than 0dB, the 1D beamforming scheme outperforms the other MD schemes as shown in Figure 5.9 (b). At the SNR region between 0dB and 5.5dB,

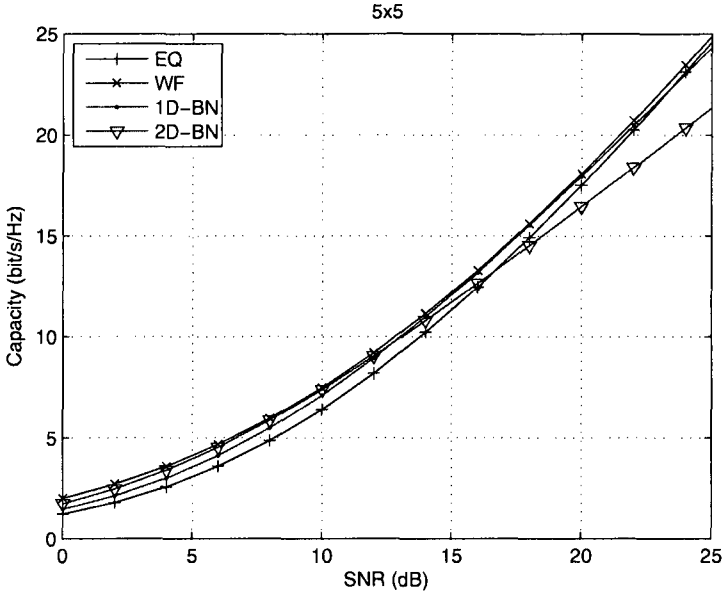

(a) $0 - 25$ dB

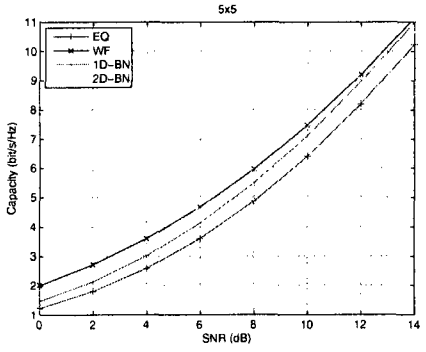

(b) $0 - 14$ dB

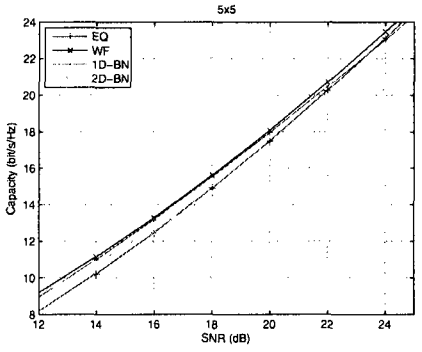

(c) $12 - 25$ dB

Figure 5.8: MD beam-nulling over 5×5 Rayleigh fading channel.

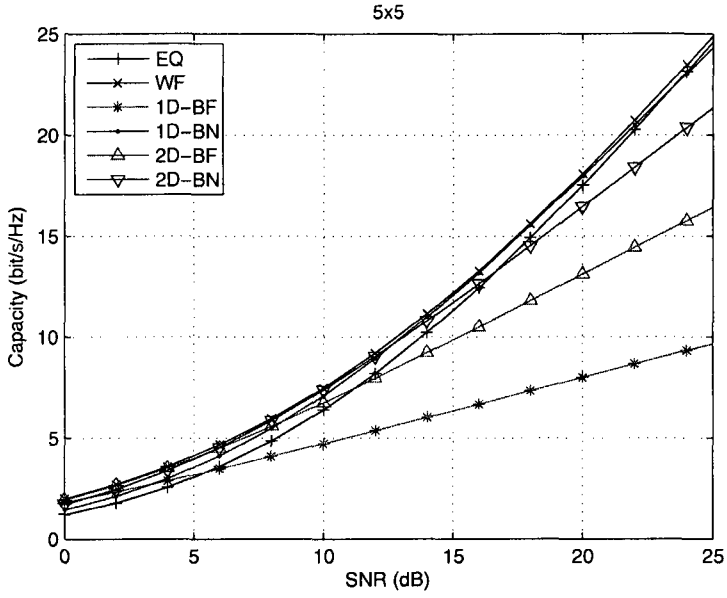

(a) 0 – 25 dB

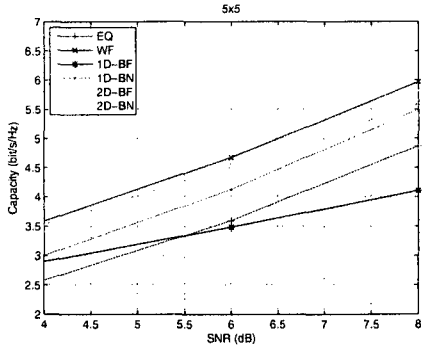

(b) 4 – 8 dB

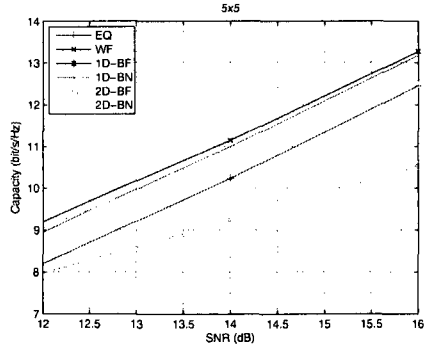

(c) 12 – 16 dB

Figure 5.9: Comparison over 5×5 Rayleigh fading channel.

the 2D beamforming scheme outperforms the other MD schemes. At the SNR region between 5.5dB and 12.7dB, the 2D beam-nulling scheme outperforms the other MD schemes. At the SNR region between 12.7dB and 23dB, the 1D beam-nulling scheme outperforms the other MD schemes. Again, when SNR is more than 23dB, the equal power scheme outperforms the other suboptimal schemes.

5.5 Conclusions

Via singular-value decomposition, the original MIMO channel is converted to uncorrelated spatial subchannels. Based on the concept of spatial subchannels, we studied various power allocation strategies for various channel state information scenarios, such as equal power, water-filling, and beamforming. Inspired by the beamforming scheme, we proposed a novel scheme called "beam-nulling". The new scheme exploits all spatial subchannels except the weakest one and thus achieves a significantly high capacity that is close to the optimal water-filling scheme at medium signal-to-noise ratio. Additionally, the capacities of equal power, beamforming and beam-nulling were compared via theoretical analysis, and then numerical results of these three schemes are also compared with the optimal water-filling scheme. The comparison showed that at low signal-to-noise ratio, beamforming is the closest to the optimal water-filling results, at medium signal-to-noise ratio, beam-nulling is the closest to the optimal solution, and at high signal-to-noise ratio, equal power is the closest to the optimal solution. If more than one eigenvector can be fed back to the transmitter, new extended schemes based on beamforming and the proposed beam-nulling are proposed. The new schemes are called multi-dimensional beamforming and multi-dimensional beam-nulling. The theoretical analysis and numeric results in terms of capacity are provided in order to evaluate the new extended schemes.

Chapter 6

Performance of New Power Allocation Scheme Beam-Nulling

6.1 Introduction

In the previous chapter, using the concept of spatial subchannels, we studied various power allocation strategies for certain CSI scenarios; equal power, water-filling, beamforming. Inspired by the beamforming scheme, a new scheme called beam-nulling is proposed. Unlike beamforming, which uses the strongest spatial subchannel, the beam-nulling transmitter is informed as to which is the weakest subchannel and then sends signals over the spatial subspace orthogonal to that the weakest subchannel. Both transmitter and receiver know how to generate the spatial subspace by the same method. In this scheme, power is only allocated to the other good spatial subchannels, i.e., the orthogonal subspace. The theoretical analysis and numeric results show that the beam-nulling scheme is the best suboptimal option at medium SNR. Beamforming and the new proposed beam-nulling schemes can be extended if more than one eigenvector is available at the transmitter. The new extended schemes are called multi-dimensional (MD) beamforming and MD beam-nulling. The existing beamforming and the proposed beam-nulling schemes will be referred to as 1D schemes.

In practice, the application of multi-dimensional schemes will depend on the SNR region and the availability of feedback bandwidth. The MD beamforming scheme can be viewed as a set of interference-free multiple subchannels, while the MD beam-nulling scheme can be viewed as a reduced "MIMO" channel without the weakest eigenvalues. In this chapter, we first study the performance of 1D schemes, i.e., 1D beamforming and 1D beam-nulling, when they are stand-alone. To achieve better performance, the proposed schemes, both MD beamforming and MD beam-nulling, can concatenate with the other schemes, such as STTC, STBC, LDC, etc. For simplicity and flexibility, linear structure of space-time coding is preferable, and so we propose to concatenate the MD schemes with LDC and STBC. The performances of MD schemes concatenated with LDC and with STBC are compared in terms of BER when the data rate is the same.

6.2 Performance of 1D Beamforming and 1D Beam-nulling

6.2.1 Performance of 1D Beamforming

We assume one symbol, say x_1, is transmitted. At the receiver, the received vector can be written as

$$\mathbf{y}_1 = \sqrt{P}\mathbf{H}\mathbf{v}_1 x_1 + \mathbf{z}_1 \tag{6.1}$$

where $\mathbf{z}_1$ is the additive white Gaussian noise vector with *i.i.d.* symmetrical complex Gaussian elements of zero mean and variance σ_z^2. The eigenvector associated with the maximum singular value from the receiver side, $\mathbf{u}_1$, is applied as the receiver beamformer. Then we have

$$\tilde{y}_1 = \mathbf{u}_1^H \mathbf{y}_1 = \sqrt{P}\lambda_1 x_1 + \tilde{z}_1 \tag{6.2}$$

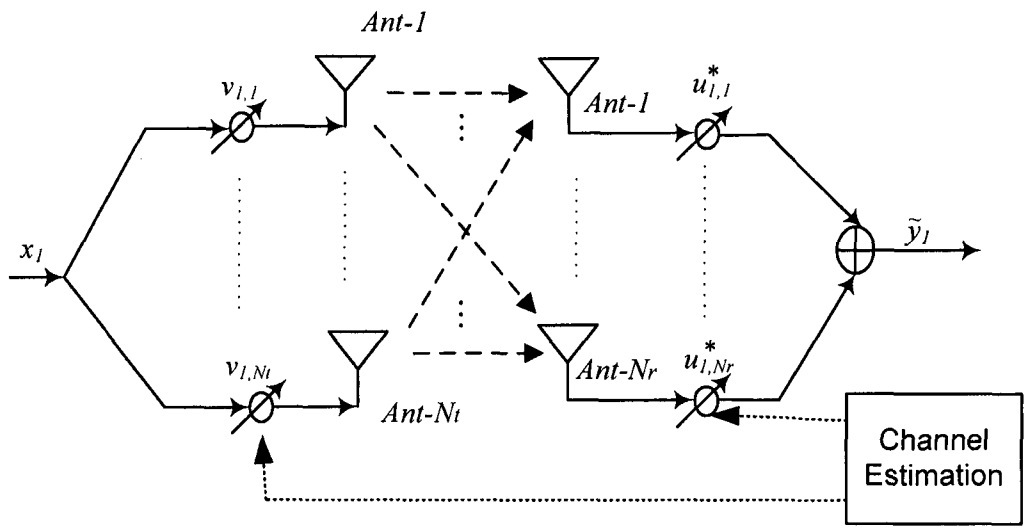

Figure 6.1: 1D beamforming scheme.

where $\tilde{z}_1$ is Gaussian with zero mean and variance σ_z^2.

For beamforming, the error probability can be found as follows. From equation (6.2), the SNR of the beamforming scheme for one channel realization is

$$\gamma_{bf} = \frac{P\lambda_{max}^2}{\sigma_z^2} \tag{6.3}$$

where $\lambda_{max} = \lambda_1$ is the maximum singular-value of channel matrix $\mathbf{H}$. The error probability for each constellation over a white Gaussian channel can be found in [52]. The average error probability over a fading channel can then be found by taking the expectation over λ_{max}. For example, if the constellation is BPSK, the average error probability can be written as

$$\begin{aligned} P_e &= E_{\lambda_{max}}\left(Q(\sqrt{\gamma_{bf}})\right) \\ &= \int Q(\sqrt{\frac{P}{\sigma_z^2}}\lambda_{max}) p_{\lambda_{max}}(\lambda_{max}) d\lambda_{max} \end{aligned} \tag{6.4}$$

where $p_{\lambda_{max}}()$ is the PDF of λ_{max}.

6.2.2 Performance of 1D Beam-nulling

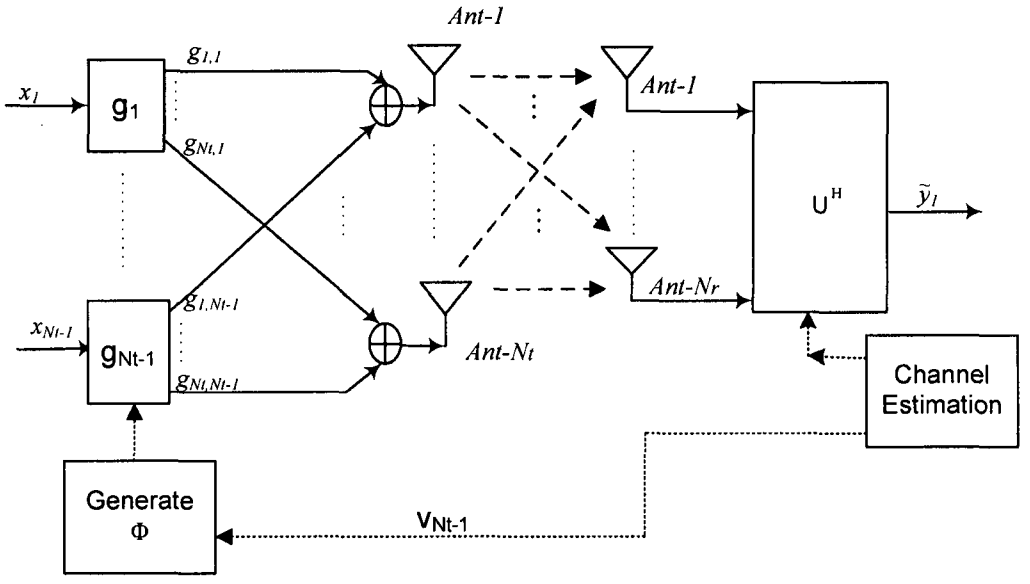

Figure 6.2: 1D beam-nulling scheme.

At the transmitter, $N_t - 1$ symbols denoted as $\mathbf{x}'$ are transmitted only over the orthogonal subspace $\mathbf{\Phi}$. The received signals at the receiver can be written as

$$\begin{aligned} \mathbf{y}' &= \sqrt{\frac{P}{N_t - 1}}\mathbf{H}\mathbf{\Phi}\mathbf{x}' + \mathbf{z}' \\ &= \widehat{\mathbf{H}}\mathbf{x}' + \mathbf{z}' \end{aligned} \tag{6.5}$$

where $\mathbf{z}'$ is an additive white Gaussian noise vector with *i.i.d.* symmetrical complex Gaussian elements of zero mean and variance σ_z^2 and $\widehat{\mathbf{H}} = \sqrt{\frac{P}{N_t-1}}\mathbf{H}\mathbf{\Phi}$.

For 1D beam-nulling, the error probability can be found as follows. From equation (6.5), the ML solution is

$$\hat{\mathbf{x}}_{ML} = \arg\min \|\mathbf{y}' - \widehat{\mathbf{H}}\mathbf{x}'\|^2 \tag{6.6}$$

The closed-form formula for error probability is clearly difficult to find. Other suboptimal receivers can also be implemented. The MMSE detector is especially popular

because of its low complexity and good performance. In the following context, the BER of the MMSE detector is analyzed for a 1D beam-nulling scheme.

Equation (6.5) can also be written as

$$\mathbf{y}' = \hat{\mathbf{h}}_i x_i + \sum_{j \neq i} \hat{\mathbf{h}}_j x_j + \mathbf{z}' \tag{6.7}$$

where x_i is the i-th element of $\mathbf{x}'$ and $\hat{\mathbf{h}}_i$ is the i-th column of $\widehat{\mathbf{H}}$.

Without loss of generality, we consider the detection of one symbol, say x_i. We collect the rest of the symbols into a column vector $\mathbf{x}_I$ and denote $\widehat{\mathbf{H}}_I = [\hat{\mathbf{h}}_1, .., \hat{\mathbf{h}}_{i-1}, \hat{\mathbf{h}}_{i+1}, ..., \hat{\mathbf{h}}_{N_t-1}]$ as the matrix obtained by removing the i-th column from $\widehat{\mathbf{H}}$.

A linear MMSE detector [48][49] is applied and the corresponding output is given by

$$\hat{x}_i = \mathbf{w}_i^H \mathbf{y} = x_i + \hat{z}_i. \tag{6.8}$$

where $\hat{z}_i$ is the zero mean noise, and can be approximated to be Gaussian [49]. The corresponding $\mathbf{w}_i$ can be found as

$$\mathbf{w}_i = \frac{\left(\hat{\mathbf{h}}_i \hat{\mathbf{h}}_i^H + \mathbf{R}_I\right)^{-1} \hat{\mathbf{h}}_i}{\hat{\mathbf{h}}_i^H \left(\hat{\mathbf{h}}_i \hat{\mathbf{h}}_i^H + \mathbf{R}_I\right)^{-1} \hat{\mathbf{h}}_i} \tag{6.9}$$

where $\mathbf{R}_I = \widehat{\mathbf{H}}_I \widehat{\mathbf{H}}_I^H + \sigma_z^2 \mathbf{I}$. Note that the scaling factor $\frac{1}{\hat{\mathbf{h}}_i^H \left(\hat{\mathbf{h}}_i \hat{\mathbf{h}}_i^H + \mathbf{R}_I\right)^{-1} \hat{\mathbf{h}}_i}$ in the coefficient vector of the MMSE detector $\mathbf{w}_i$ is added to ensure an unbiased detection as indicated by (6.8). The variance of the noise term $\hat{z}_i$ can be found from (6.8) and (6.9) as

$$\hat{\sigma}_i^2 = \mathbf{w}_i^H \mathbf{R}_I \mathbf{w}_i \tag{6.10}$$

Substituting the coefficient vector for the MMSE detector in (6.9) into (6.10), the

variance can be written as

$$\hat{\sigma}_i^2 = \frac{1}{\hat{\mathbf{h}}_i^H \mathbf{R}_I^{-1} \hat{\mathbf{h}}_i} \tag{6.11}$$

Then, the SINR of MMSE associated with x_i is $1/\hat{\sigma}_i^2$.

$$\gamma_i = \frac{1}{\hat{\sigma}_i^2} = \hat{\mathbf{h}}_i^H \mathbf{R}_I^{-1} \hat{\mathbf{h}}_i \tag{6.12}$$

Closed-form BER for a channel mode such as (6.8) can be found in [52]. The average BER over a MIMO fading channel for a given constellation can be found for 1D beam-nulling as follows:

$$BER_{av} = E_{\gamma_i}\left[\frac{1}{N_t - 1}\sum_i BER(\gamma_i)\right] \tag{6.13}$$

The closed-form formula for the average BER in (6.13) depends on the distribution of γ_i, which is difficult to find. Here, the above average BER is calculated numerically. For example, the average BER for 2^η-PSK is

$$BER_{av} = E_{\gamma_i}\left[\frac{1}{N_t - 1}\sum_i \frac{2}{\eta} Q\left(\sqrt{2\eta\ \gamma_i}\ \sin(\frac{\pi}{2^\eta})\right)\right] \tag{6.14}$$

and the average BER for rectangular 2^η-QAM is

$$BER_{av} = E_{\gamma_i}\left[\frac{1}{N_t - 1}\sum_i \frac{4}{\eta} Q\left(\sqrt{\frac{3\eta\ \gamma_i}{2^\eta - 1}}\right)\right] \tag{6.15}$$

where $Q(\cdot)$ denotes the Gaussian Q-function.

In Figure 6.3, numerical and simulation results are compared for 8PSK over a 3×3 fading channel and for QPSK over a 4×4 fading channel, respectively. As can be seen, the numerical and simulation results match very well.

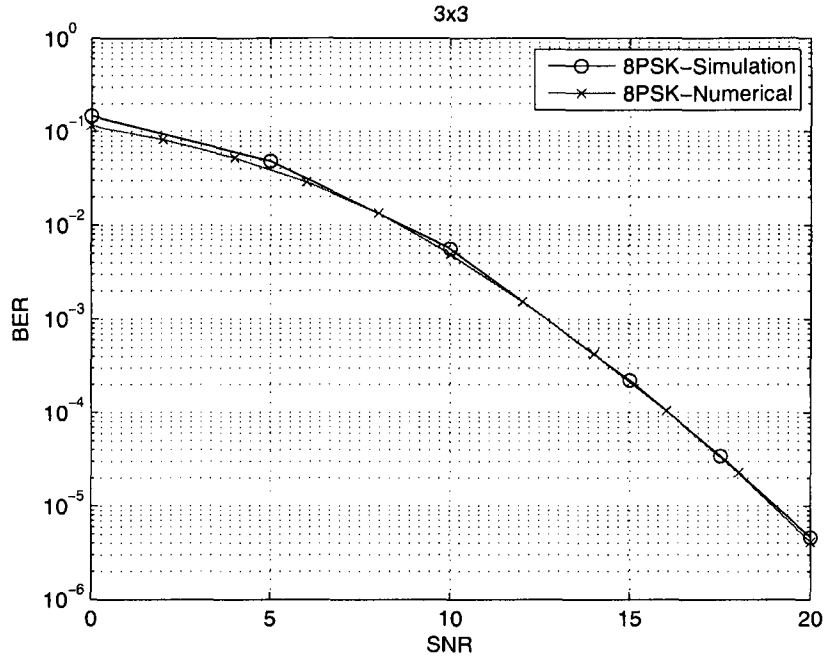

(a) 3×3, 8PSK

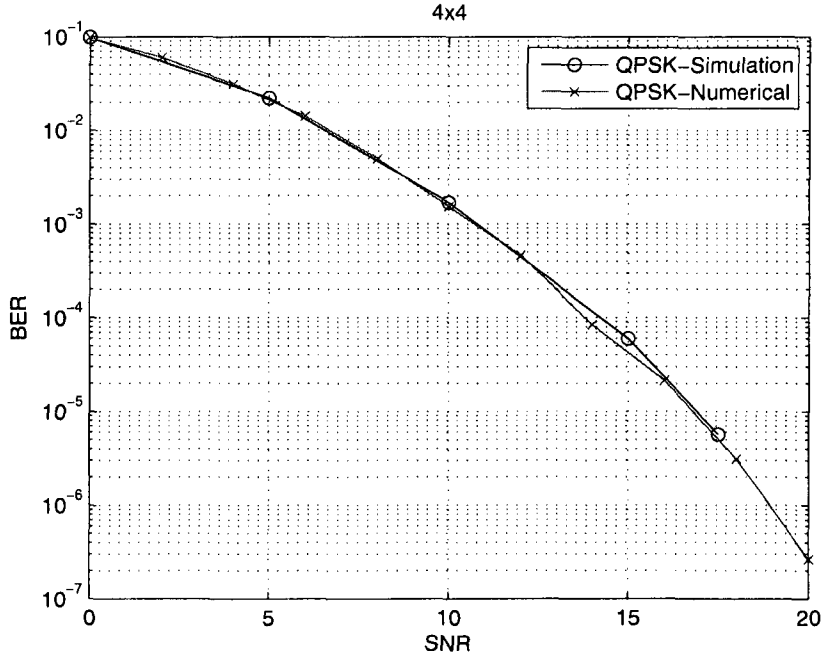

(b) 4×4, 4PSK

Figure 6.3: Numerical and simulation results for beam-nulling scheme.

6.2.3 Design of Subspaces Orthogonal to the Weakest Subchannel

The number of subspaces orthogonal to the weakest subchannel, i.e., satisfying $\mathbf{\Phi}^H \mathbf{v}_{N_t} = 0$, can be infinite. If QR decomposition is applied to find the optimal subspace, or $\mathbf{\Phi}$, the optimization problem is to find the optimal seed $\mathbf{I}'$ as defined in (5.2). After QR decomposition is applied to the matrix $[\mathbf{v}_{N_t} \ \mathbf{I}']$, as shown in (5.3), the orthogonal subspace $\mathbf{\Phi}$ will be the matrix containing all the column vectors of the unitary matrix $\mathbf{Q}$ except for the vector $\mathbf{v}_{N_t}$. Then, the optimization problem is given as:

$$\mathbf{I}'_{opt} = \arg \max_{\{\mathbf{I}'\}} \min_{\mathbf{x}_i \neq \mathbf{x}_j} \{(\mathbf{x}_i - \mathbf{x}_j)^H E_{\mathbf{H}} \left[\mathbf{\Phi}([\mathbf{v}_{N_t}(\mathbf{H}) \ \mathbf{I}'])^H \mathbf{H}^H \mathbf{H} \mathbf{\Phi}([\mathbf{v}_{N_t}(\mathbf{H}) \ \mathbf{I}']) \right] (\mathbf{x}_i - \mathbf{x}_j)\} \tag{6.16}$$

subject to power constraint

$$\mathrm{tr}(\mathbf{\Phi}([\mathbf{v}_{N_t}(\mathbf{H}) \ \mathbf{I}'])^H \mathbf{\Phi}([\mathbf{v}_{N_t}(\mathbf{H}) \ \mathbf{I}'])) \leq P.$$

Since the above minimum distance depends on the constellation as well as on the channel realization, it is difficult to derive a closed-form solution. Additionally, simulation results in Figure 6.4 show that even we use different ways to generate our orthogonal subspace, the performances of different schemes are not very significant.

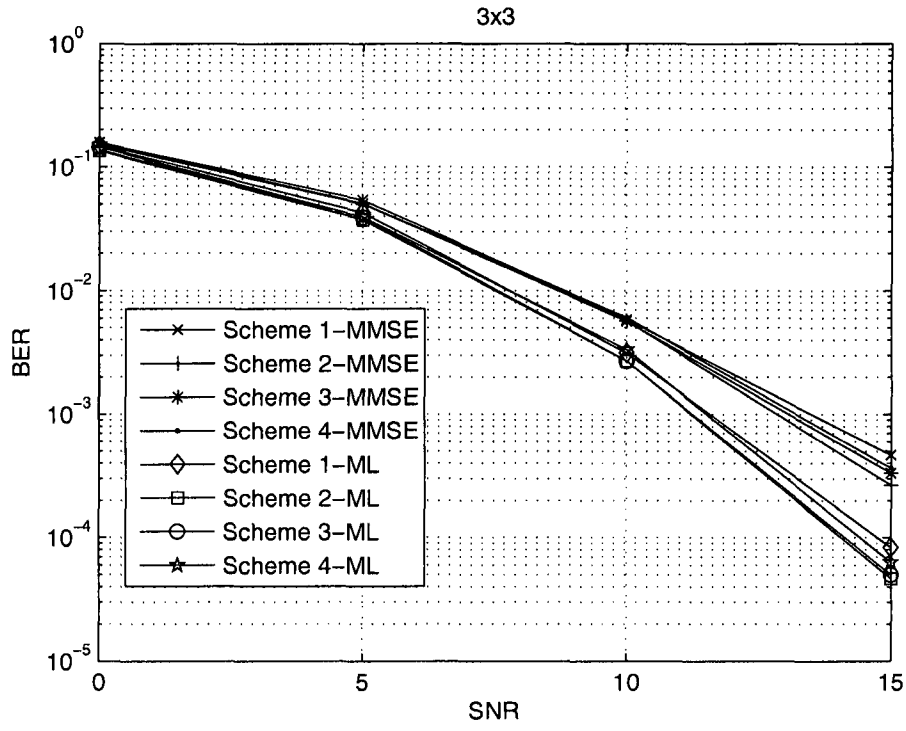

Figure 6.4: Different designs of $\mathbf{\Phi}$

6.2.4 Performance Comparison between 1D Beamforming and 1D Beam-nulling

In Figures 6.5 and 6.6, simulation results are compared for various data rates R over 3×3 and 4×4 fading channels, respectively. The 1D beamforming scheme is equivalent to an SISO channel using a maximum ratio combining (MRC) receiver [54]. For the 1D beam-nulling scheme, both the optimal ML receiver and the suboptimal MMSE receiver are used.

For a 3×3 fading channel with $R = 2$, the 1D beamforming scheme outperforms the 1D beam-nulling scheme significantly, for all SNR regions. The same observation can be noted for a 4×4 fading channel with $R = 3$. For 3×3 fading channels with $R = 4$ and $R = 6$, the 1D beam-nulling scheme outperforms the 1D beamforming scheme at low and medium SNR regions, even if the suboptimal MMSE is used. However, at high SNR, the 1D beamforming scheme begins to outperform the 1D beam-nulling

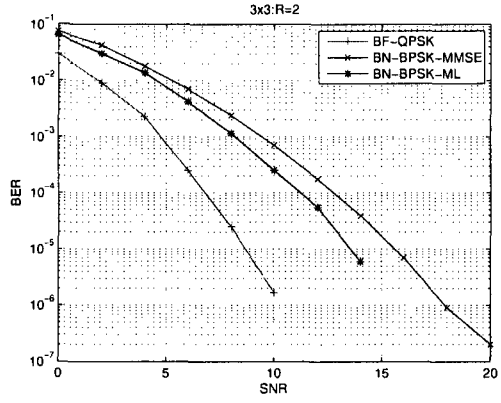

(a) R=2

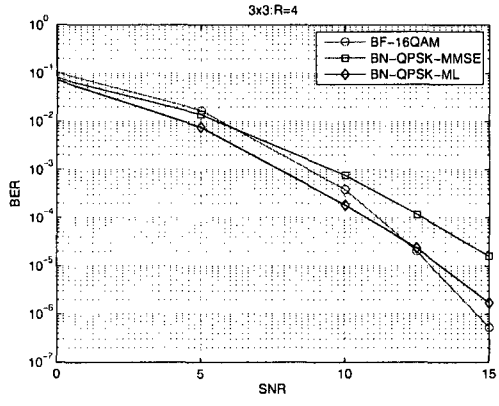

(b) R=4

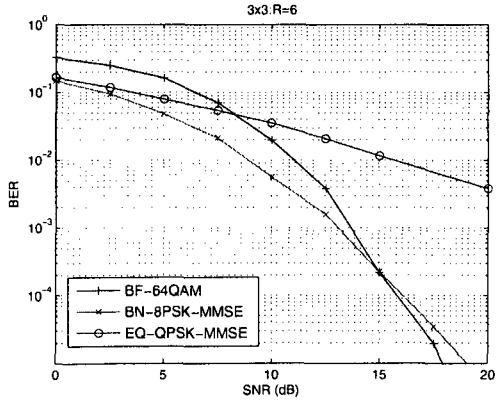

(c) R=6

Figure 6.5: Comparison over 3×3 Rayleigh fading channel.

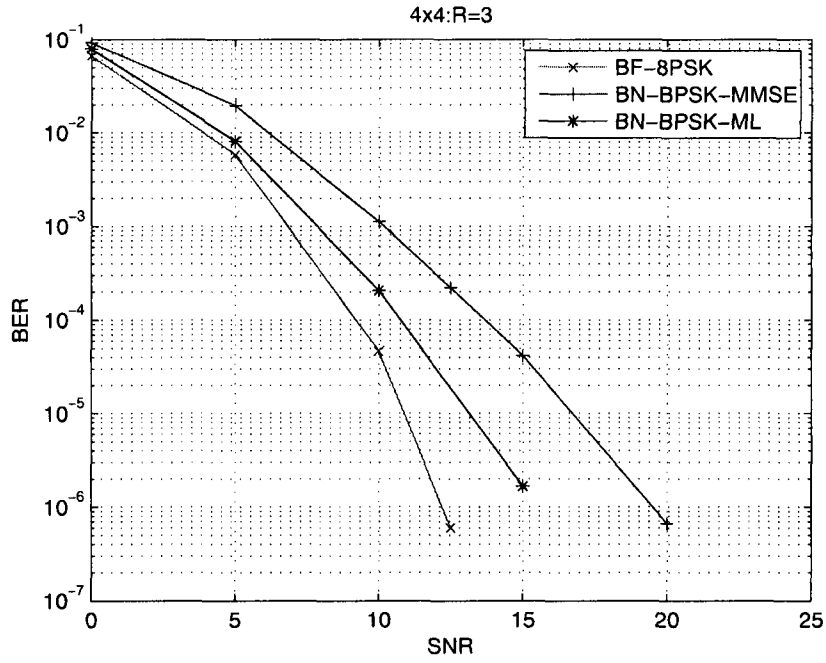

(a) R=3

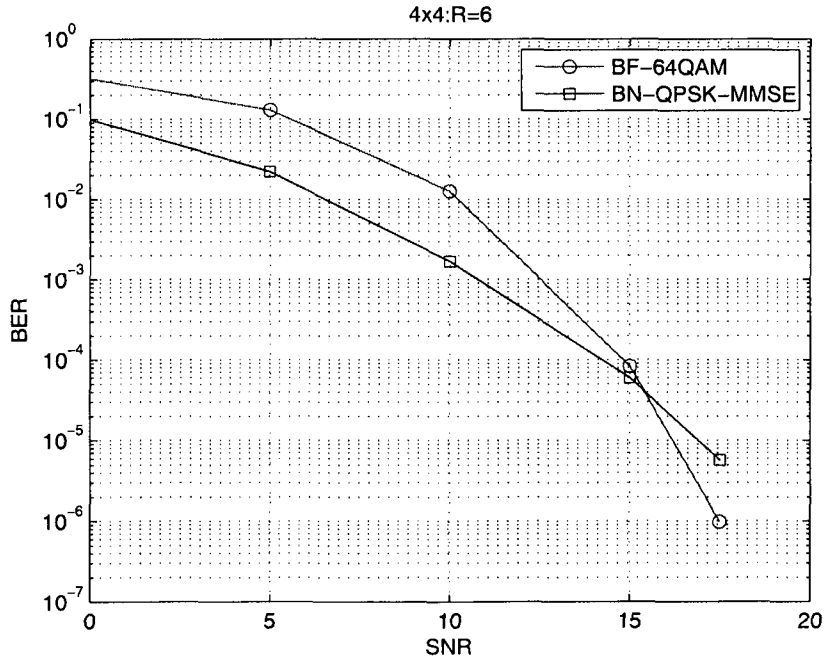

(b) R=6

Figure 6.6: Comparison over 4×4 Rayleigh fading channel.

scheme. The same observation can be noted for a 4×4 fading channel with $R = 6$. In Figure 6.5 (c), bit error rate of equal power (EQ) scheme is also presented. As can be seen, both beamforming and beam-nulling outperform equal power significantly. For example, at bit error rate of 10^{-3}, beam-nulling and beamforming outperform equal power about 13 dB and 12 dB, respectively.

In summary, with a low data rate is low, i.e., a small constellation size, 1D beamforming outperforms 1D beam-nulling. If the data rate is high, i.e., the constellation size is high, 1D beam-nulling outperforms 1D beamforming at low and medium SNR, but at high SNR the reverse holds true. Also, as can be seen in these figures, at a high data rate, the beam-nulling scheme outperforms the beamforming scheme, even with a suboptimal MMSE receiver.

6.2.5 Concatenation of 1D Beam-nulling and LDC

To further improve the performance of 1D beam-nulling with tractable complexity, we propose to concatenate 1D beam-nulling with a linear dispersion code. In order to meet error-rate requirements, multiple levels of error protection can be implemented. In this study, we focus on the space-time coding domain. The concatenated scheme is shown in figure 6.7,.

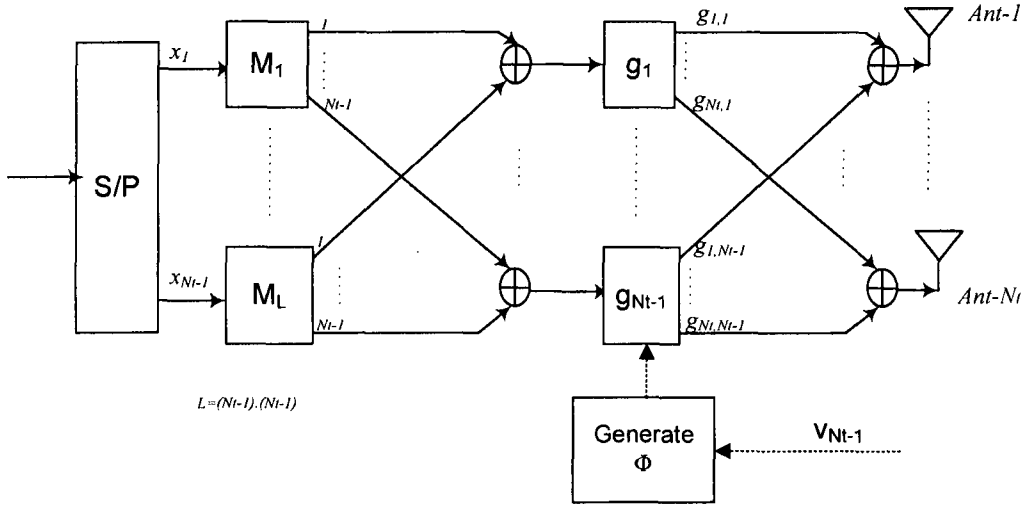

Figure 6.7: 1D beam-nulling concatenated with LDC scheme.

In this system, the information bits are first mapped into symbols. The symbol stream is then parsed into blocks of length $L = (N_t - 1)T$. The symbol vector associated with one modulation block is denoted by $\mathbf{x} = [x_1, x_2, \ldots, x_L]^T$ with $x_i \in \Omega \equiv \{\Omega_m | m = 0, 1, \ldots, 2^\eta - 1, \eta \geq 1\}$, i.e., a complex constellation of size 2^η, such as 2^η-QAM). The average symbol energy is assumed to be 1, so that $\frac{1}{2^\eta} \sum_{m=0}^{2^\eta - 1} |\Omega_m|^2 = 1$. Each symbol in a block will be mapped by the ST modulator to a dispersion matrix of size $N_t \times T$ (i.e., $\mathbf{M}_i$) and then combined linearly to form $(N_t - 1)$ data streams over T channel uses. The output $(N_t - 1)$ data streams are transmitted only over the subspace $\mathbf{\Phi}$ that is orthogonal to the weakest spatial channel. The generation of the orthogonal subspace $\mathbf{\Phi}$ is described in section 5.2. The received signals at the

receiver can be written as

$$\mathbf{y} = \sqrt{\frac{P}{N_t - 1}}\mathbf{H}\mathbf{\Phi}\sum_{i=1}^{L}\mathbf{M}_i x_i + \mathbf{z} \tag{6.17}$$

where $\mathbf{z}$ is an additive white Gaussian noise vector with *i.i.d.* symmetrical complex Gaussian elements of zero mean and variance σ_z^2.

Note that the traditional beamforming scheme cannot work with space-time coding since it can be viewed as an SISO channel. We will compare the concatenated scheme with the original 1D schemes at the same data rate.

6.2.6 Performance of 1D Beam-nulling with LDC

In Figure 6.8 and 6.9, simulation results are compared for various data rates R, over 3×3 and 4×4 fading channels, respectively. The optimal ML receiver and the suboptimal MMSE receiver are used for beam-nulling with and without LDC. In these figures, "BL" denotes 1D beam-nulling with LDC.

As can be seen, 1D beam-nulling with LDC outperforms 1D beam-nulling without LDC using the same receiver. The performance of 1D beam-nulling with LDC using an MMSE receiver is close to that of 1D beam-nulling without LDC using the optimal ML receiver.

For 3×3 fading channels with $R = 2$, 1D beamforming has the best performance, but at high SNR, the performance of 1D beam-nulling with LDC comes close to that of 1D beamforming. For 3×3 fading channels with $R = 4$ and $R = 6$, 1D beam-nulling with LDC outperforms 1D beamforming at low and medium SNR region, even when the suboptimal MMSE receiver is used. At high SNR, only 1D beam-nulling with LDC using the optimal ML receiver can outperform 1D beamforming.

For 4×4 fading channels with $R = 3$, 1D beam-nulling with LDC can outperform the 1D beamforming if the optimal ML receiver is used. For 4×4 fading channels with $R = 6$, 1D beam-nulling with LDC can outperform the 1D beamforming even

with the suboptimal MMSE receiver.

In summary, if the data rate is low, i.e., the constellation size is low, the performance of 1D beam-nulling with LDC can approach that of 1D beamforming at high SNR. If the data rate is high, i.e., the constellation size is high, 1D beam-nulling with LDC outperforms 1D beamforming at low and medium SNR, even when the suboptimal MMSE receiver is used.

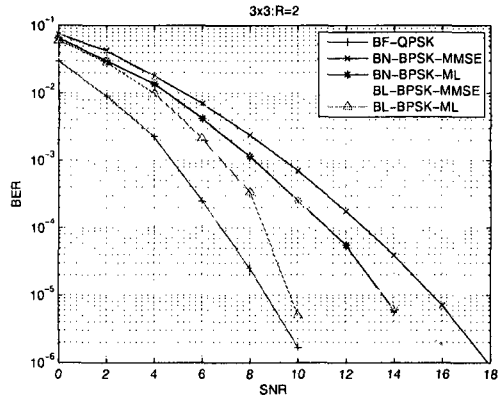

(a) $R = 2$

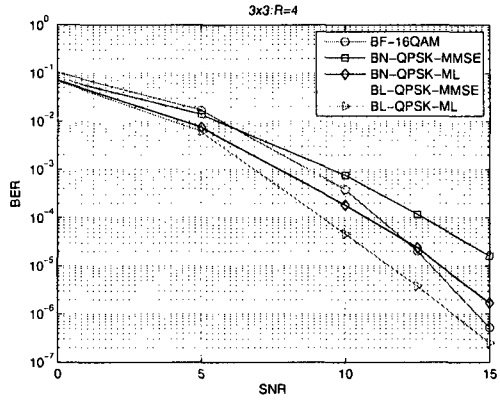

(b) $R = 4$

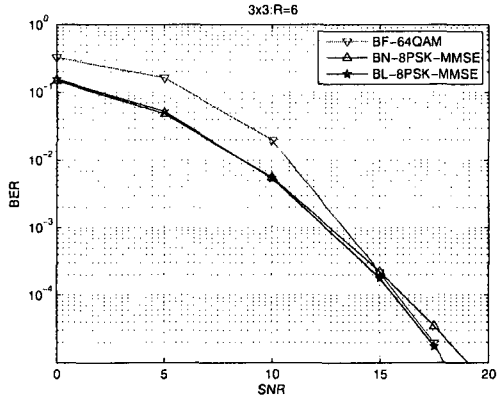

(c) $R = 6$

Figure 6.8: Comparison over 3×3 Rayleigh fading channel.

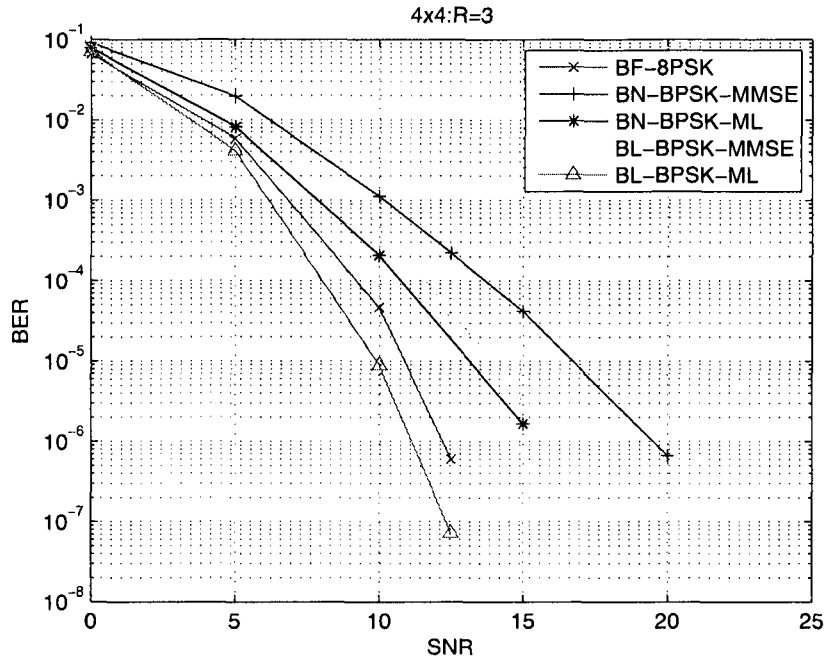

(a) $R = 3$

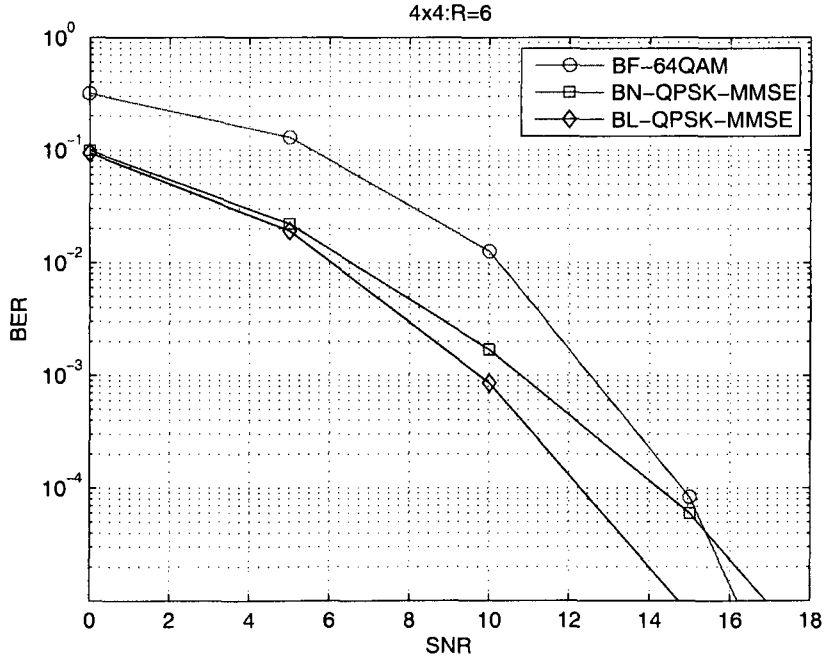

(b) $R = 6$

Figure 6.9: Comparison over 4×4 Rayleigh fading channel.

6.3 MD Schemes Concatenated with Linear Space-Time Code

As mentioned in the last chapter, if $k > 1$ eigenvectors can be sent to the transmitter for adaptation, multi-dimensional (MD) beamforming and MD beam-nulling can be applied. These MD schemes make k or $N_t - k$ spatial subchannels available. As a result, they can be concatenated with space-time schemes to improve performance. For the aforementioned reasons, space-time codes with linear structure, such as high-rate LDCs [34] and STBCs [5][30] (Orthogonal design), are preferable. It is worth of noting that the 2D beamforming scheme in [16] is simply a special case of MD beamforming. In this section, as shown in Figure 6.10 and in Figure 6.11, we propose to concatenate an MD scheme with an LDC or an STBC. Note that in these figures "OD" stands for orthogonal design, namely STBC.

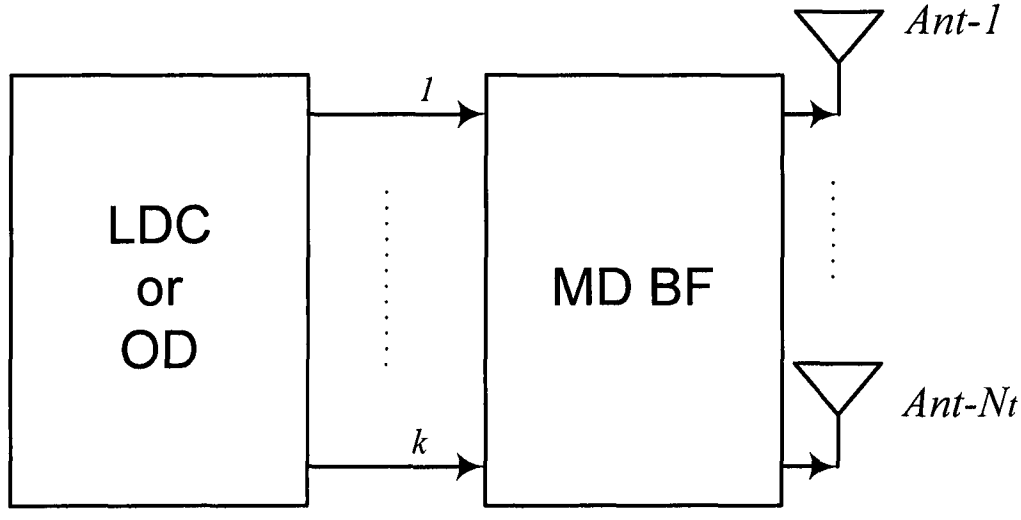

Figure 6.10: Concatenated MD beamforming scheme.

Over a 5×5 fading channel, concatenated MD schemes are compared at various data rates. In the simulation, two eigenvectors can be fed back to the transmitter. For an MD scheme with LDC, a suboptimal linear MMSE receiver is applied. Since MD schemes with STBC are orthogonal, a matched filter is applied, which is also

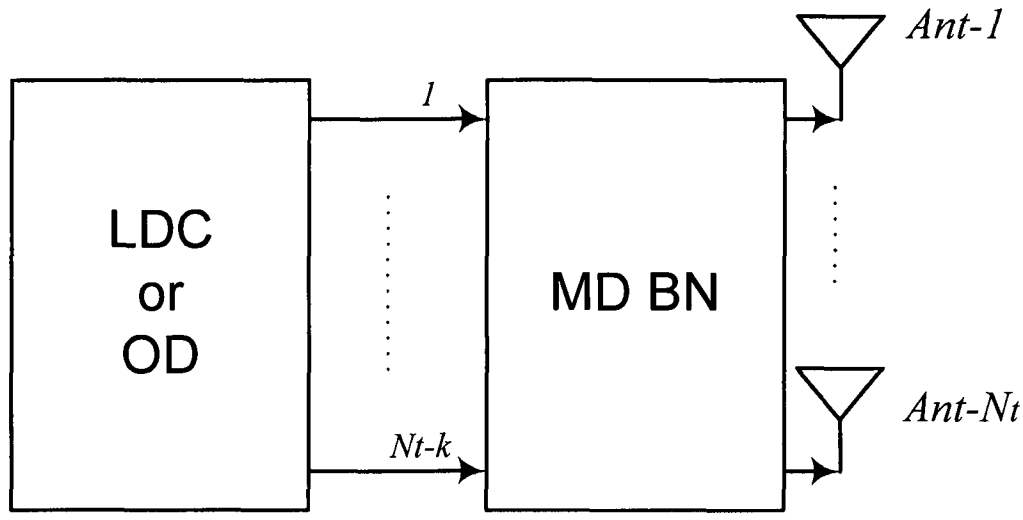

Figure 6.11: Concatenated MD beam-nulling scheme.

optimal.

In Figure 6.12 and Figure 6.14, MD beamforming schemes with STBC are compared with MD beamforming schemes with LDC in terms of BER when data rates are $R = 2$ and $R = 6$ per channel used. From these figures, it is clear that at high data rates, MD beamforming with LDC significantly outperforms MD beamforming with STBC even when a suboptimal MMSE receiver is applied. Specifically, when BER is 10^{-5}, the coding gain is 4dB. At a low data rate, MD beamforming with LDC performs slightly worse than MD beamforming with STBC, since the suboptimal receiver is applied. In this situation, when BER is 10^{-5}, the coding gain is approximately 1dB.

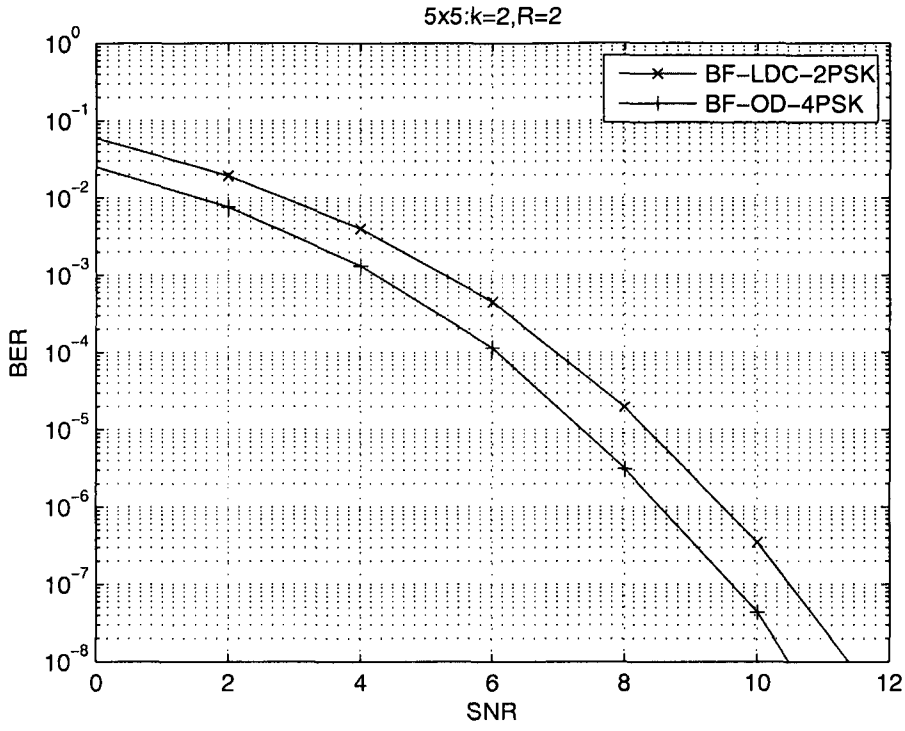

Figure 6.12: BER of concatenated MD beamforming when $R = 2$.

In Figure 6.13 and Figure 6.14, MD beam-nulling schemes with STBC are compared with MD beam-nulling schemes with LDC in terms of BER when the data rates are $R = 3$ and $R = 6$ per channel used. From these figures, it can be seen that at a high data rate, MD beam-nulling with LDC significantly outperforms MD beam-nulling with STBC even if a suboptimal MMSE receiver is applied. Specifically, when BER is 10^{-5}, the coding gain is about 6.8dB. At a low data rate, MD beam-nulling with LDC performs slightly worse than MD beam-nulling with STBC due to the suboptimal receiver. Specifically, when BER is 10^{-5}, the coding gain is approximately 1.5dB.

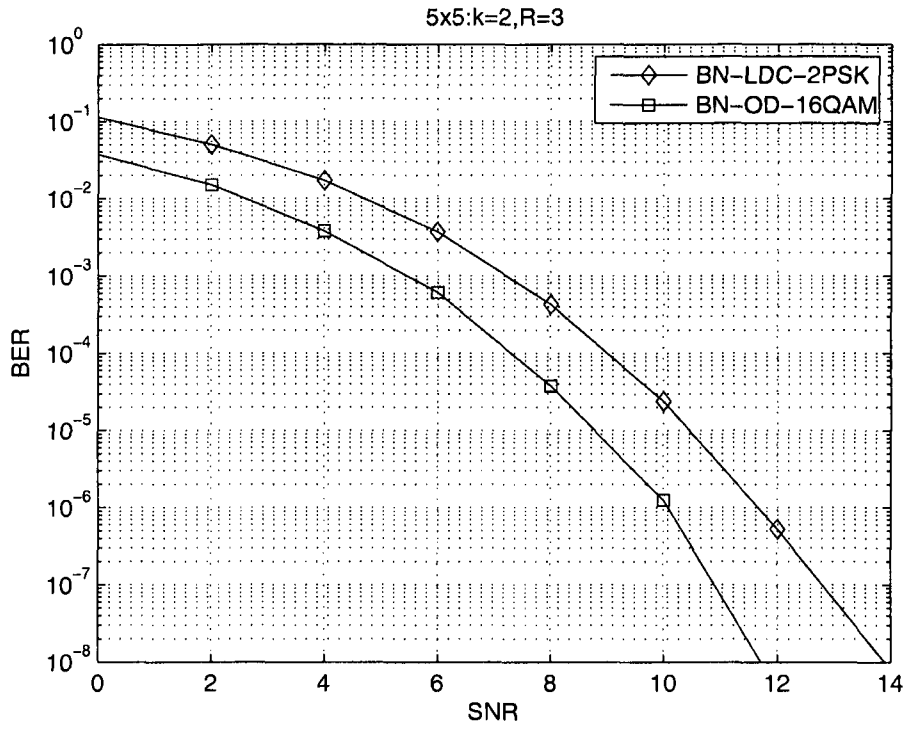

Figure 6.13: BER of concatenated MD beam-nulling when $R = 3$.

In Figure 6.14, four schemes are compared when the data rate is $R = 6$ per channel used. As shown in the figure, MD beam-nulling with LDC has the best BER performance even when a suboptimal MMSE receiver is used. In summary, an MD scheme with LDC outperforms an MD scheme with STBC, especially when the data rate is high. At low data rate, the performance will depend on the receiver. At high data rate, MD beam-nulling with LDC performs the best among the four schemes.

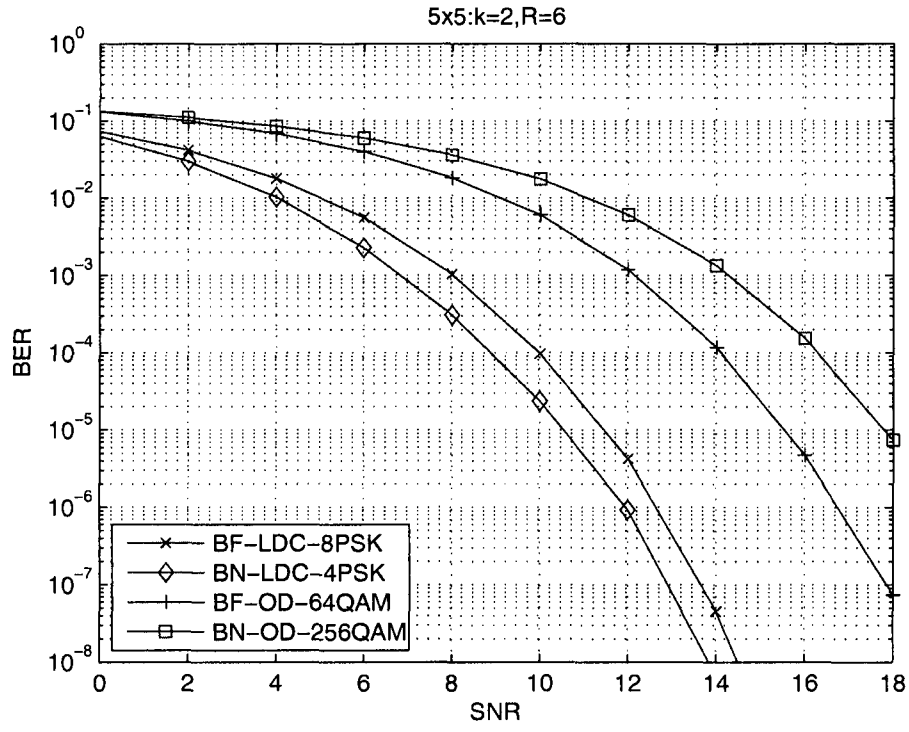

Figure 6.14: BER comparison of concatenated MD schemes when $R = 6$.

6.4 Conclusions

Average bit-error rates of stand-alone 1D beamforming and stand-alone 1D beam-nulling with MMSE receivers are given numerically and verified by simulation results. At the same data rate, 1D beamforming and 1D beam-nulling are compared in terms of bit-error rate. It is shown that at a low data rate, 1D beamforming outperforms 1D beam-nulling, while at a high rate, 1D beam-nulling outperforms 1D beamforming significantly, even when a suboptimal MMSE receiver is applied. To achieve better performance, 1D beam-nulling can be concatenated with a linear dispersion code. It is shown that even when a suboptimal MMSE receiver is applied, at low data rate, the performance of 1D beam-nulling can approach that of 1D beamforming at high SNR, while at a high data rate, 1D beam-nulling with linear dispersion code outperforms 1D beamforming at low and medium SNR. For simplicity and flexibility, both MD beamforming and MD beam-nulling can be concatenated with LDC and

STBC. Simulation results show that the MD scheme with LDC can significantly outperform the MD scheme with STBC when the data rate is high. Additionally, at a high data rate, MD beam-nulling with LDC outperforms MD beamforming with LDC, MD beamforming with STBC, and MD beam-nulling with STBC.

Chapter 7

Conclusions and Future Works

7.1 Conclusions

The accomplished work and the major contributions in this thesis are briefly summarized in the following subsections.

7.1.1 Theoretical Analysis of LDC

For simplicity, flexibility and performance, linear dispersion code is applied in the MIMO adaptation. To better analyze linear dispersion code, an ergodic capacity over Rayleigh fading channels was derived, as well as a tight upper bound of the pairwise error probability at high signal-to-noise ratio, in order to show the error probability versus the constellation size and the space-time symbol rate. Simulation results were provided to verify the theoretical results. These results will be aid in the design of linear dispersion code.

7.1.2 New Adaptive MIMO System

The statistics of the signal-to-interference-noise ratios were studied for the adaptive system with linear dispersion code and linear minimum-mean-square-error receiver.

The associated probability density function of the signal-to-interference-noise was derived. With these theoretical results as guidelines, an adaptive algorithm for the selection-mode adaptation was proposed. Based on the proposed algorithm, we have introduced three novel adaptation techniques for the adaptive system with linear dispersion code and linear minimum-mean-square-error receiver. The first technique is an extension of a commonly used adaptation technique based on linear dispersion code. We have identified the signal-to-noise ratio regions for which specific constellations can be applied. This technique is called as "adaptive constellation". The second new technique applies a new adaptive parameter, called the space-time symbol rate, which uses linear dispersion code. To further improve the average transmission rate, we introduced a novel adaptive procedure which takes advantage of both adaptive techniques. This third technique is called as "joint adaptation". In this design, more transmission rates can be selected and thus the average throughput can be improved. Theoretical analysis and simulation results are provided to show the advantages of our new design.

7.1.3 Capacity of Beam-Nulling and Extended Multi- Dimensional Frameworks

Inspired by various power allocation strategies over spatial subchannels, we proposed a novel scheme called "beam-nulling". Using the same feedback bandwidth as beamforming, the new scheme discards the worst spatial subchannel and then sends signals over a subspace orthogonal to that worst subchannel. The subspace can be generated by a certain rule known to both transmitter and receiver. Since only the weakest spatial subchannel is nulled, the proposed scheme can achieve significantly higher capacity. The capacity of existing schemes and this proposed scheme were compared through theoretical analysis and numerical results. The comparison showed that, among equal power, beamforming and beam-nulling, equal power has the largest

capacity at high SNR, beamforming has the largest capacity at low SNR, and beam-nulling has the largest capacity at medium SNR. If more than one eigenvector can be fed back to the transmitter, new extended schemes based on beamforming and the proposed beam-nulling were presented. The new schemes are called multi-dimensional beamforming and multi-dimensional beam-nulling, respectively. The theoretical analysis and numeric results in terms of capacity were also provided to evaluate the new extended schemes.

7.1.4 Performance of Beam-Nulling and Extended Multi- Dimensional Frameworks

Stand-alone 1D beamforming and stand-alone 1D beam-nulling systems with MMSE receivers were compared numerically in terms of bit-error rates. We show that at low data rate, 1D beamforming outperforms 1D beam-nulling while at a high data rate, 1D beam-nulling significantly outperforms 1D beamforming, even when a suboptimal MMSE receiver is applied. To further improve performance, 1D beam-nulling was concatenated with a linear dispersion code. It is shown that even when a suboptimal MMSE receiver is applied, at low data rate, the performance of 1D beam-nulling can be close to that of 1D beamforming at high SNR, while at a high data rate, 1D beam-nulling with linear dispersion code outperforms 1D beamforming at low and medium SNR. For performance and flexibility, both MD beamforming and MD beam-nulling were concatenated with LDC and with STBC, respectively. Simulation results show that the MD scheme with LDC can outperform the MD scheme with STBC significantly when the data rate is high. Moreover, it is shown that at high data rate, MD beam-nulling with LDC outperforms MD beamforming with LDC, MD beamforming with STBC and MD beam-nulling with STBC.

7.2 Future Works

Based on our study of MIMO adaptation, four research topics can be identified.

- Our results were developed on the assumption that the channel is spatially uncorrelated. However, in practice, that assumptions cannot be satisfied all the time. Future research could extend this study to spatially correlated channels.

- The feedback channel may introduce delays or errors to the CSI, and therefore an unreliable copy of the CSI maybe present at the transmitter. How to deal with unreliable CSI caused by delays or errors in the feedback channel is an interesting and important issue which should be investigated.

- In this thesis, we propose a scheme called "beam-nulling" for MIMO adaptation. In the beam-nulling scheme, the eigenvector of the weakest subchannel is fed back and then signals are sent over a generated subspace orthogonal to the weakest subchannel. The eigenvector of the weakest subchannel is often quantized. An interesting topic is then how to most efficiently quantize the feedback data, a problem related to vector quantization.

- In the practical system, the idea behind concatenated coding schemes has been applied to MIMO communications. By combining two or more relatively simple constituent codes, a concatenated coding scheme can achieve large coding gain with only moderately complex decoding. Optimization of an overall concatenated adaptive MIMO system would present clear advantages.

Bibliography

[1] I. E. Telatar, "Capacity of multi-antenna Gaussian channels," *Eur. Trans. Telecom.*, vol. 10, pp. 585-595, Nov. 1999.

[2] G. J. Foschini, M. J. Gans, "On limits of wireless communications in a fading environment when using multiple antennas," *Wireless Personal Communications*, vol. 6, no. 3, pp. 311-335, Mar. 1998.

[3] D. Gesbert, M. Shafi, D. S. Shiu, P. Smith and A. Naguib, "From theory to practice: An overview of MIMO space-time coded wireless systems," *IEEE J. Select. Areas Commun.*, vol. 21, pp. 281-302, Apr. 2003.

[4] V. Tarokh, N. Seshadri, and A. Calderbank, "Space-time codes for high data rate wireless communications: Performance criterion and code construction," *IEEE Trans. Inform. Theory*, vol. 44, pp. 744-765, Mar. 1998.

[5] S. Alamouti, "A simple transmitter diversity scheme for wireless communications," *IEEE J. Select. Areas Commun.*, vol. 16, pp. 1451-1458, Oct. 1998.

[6] J. K. Cavers, "Variable-rate transmission for Rayleigh fading channels," *IEEE Transactions on Communications*, vol. 20, no. 1, pp. 15-22, Feb. 1972.

[7] A. J. Goldsmith and S.-G. Chua, "Variable rate variable power MQAM for fading channels," *IEEE Trans. Commun.*, vol. 45, no. 10, pp. 1218-1230, Oct. 1997.

[8] S. T. Chung and A. J. Goldsmith, "Degrees of freedom in adaptive modulation: A unified view," *IEEE Trans. Commun.*, vol. 49, no. 9, pp. 1561-1571, Sep. 2001.

[9] A. J. Goldsmith and S.-G. Chua, "Adaptive coded modulation for fading channels," *IEEE Trans. Commun.*, vol. 46, no. 5, pp. 595-602, May 1998.

[10] S. Vishwanath and A. J. Goldsmith, "Adaptive turbo-coded modulation for flat-fading channels," *IEEE Trans. Commun.*, vol. 51, no. 6, pp. 964-972, Jun. 2003.

[11] D. Gesbert, R. W. Heath, S. Catreux, and V. Erceg, "Adaptive modulation and MIMO coding for broadband wireless data networks," *IEEE Communications Magazine*, vol. 40, pp. 108-115, June 2002.

[12] C. E. Shannon, "A mathematical theory of communication," *Bell Syst. Tech. J.*, vol. 27, pp. 379-423 (Part one), pp. 623-656 (Part two), Oct. 1948.

[13] S. Zhou and G. B. Giannakis, "Adaptive modulation for multiantenna transmissions with channel mean feedback," *IEEE Trans. Wireless Commun.*, vol. 3, no. 5, pp. 1626-1636, Sep. 2004.

[14] J. Mirkovic and B. Walke, "On performance of MIMO link adaptation in the presence of channel uncertainty," *IEEE International Conference on Wireless and Mobile Computing*, pp. 84-89, Oct. 2008.

[15] V. Lau and T. Wu, "On the encoding rate and discrete modulation adaptation design for MIMO links," *IEEE Trans. Wireless Commun.*, vol. 6, no. 1, pp. 50-54, Jan. 2007.

[16] S. Zhou and G. B. Giannakis, "Optimal transmitter eigen-beamforming and space-time block coding based on channel mean feedback," *IEEE Trans. on Signal Processing*, vol. 50, no. 10, pp. 2599-2613, Oct. 2002.

[17] J. Mitola, "The software radio architecture," *IEEE Communication Magazine*, vol. 33, no. 5, pp. 26-38, May 1995.

[18] L. Yang and L. Hanzo, "Software-defined-radio-assisted adaptive boardband frequency hopping multicarrier DS-CMDA," *IEEE Communication Magazine*, vol. 40, vol. 3, pp. 174-183, 2002.

[19] Z. Luo, H. Gao, Y. Liu and J. Gao, "Capacity limits of time-varying MIMO channels," *IEEE International Conference On Communications*, vol. 2, pp. 795-799, May 2005.

[20] Z. Shen, R. W. Heath, Jr., J. G. Andrews, and B. L. Evans, "Comparison of space-time water-filling and spatial water-filling for MIMO fading channels," *in Proc. IEEE Int Global Communications Conf.*, vol. 1, pp. 431-435, Nov. 2004, Dallas, TX, USA.

[21] Z. Zhou and B. Vucetic, "Design of adaptive modulation using imperfect CSI in MIMO systems," *Eelectronics Letters*, vol. 40, no. 17, Aug. 2004.

[22] X. Zhang and B. Ottersten, "Power allocation and bit loading for spatial multiplexing in MIMO systems," *IEEE Int. Conf.on Acoustics, Speech, and Signal Processing (ICASSP '03)*, vol. 5, pp. 54-56, Apr. 2003.

[23] J. K. Cavers, "Single-user and multiuser adaptive maximal ratio transmission for Rayleigh channels," *IEEE Trans. Veh. Technol.*, vol. 49, no. 6, pp. 2043-2050, Nov. 2000.

[24] P. Xia and G. B. Giannakis, "Multiantenna adaptive modulation with beamforming based on bandwidth-constrained feedback," *IEEE Transactions on Communications*, vol.53, no.3, pp. 526-536, Mar. 2005.

[25] B. Mondal and R. W. Heath, Jr., "Performance analysis of quantized beamforming MIMO systems," *IEEE Trans. on Signal Processing* , vol. 54, no. 12, pp. 4753-4766, Dec. 2006.

[26] S. Zhou and G. B. Giannakis, "How accurate channel prediction needs to be for transmit-beamforming with adaptive modulation over Rayleigh MIMO channels," *IEEE Trans. Wireless Comm.*, vol. 3, no. 4, pp. 1285-1294, July 2004.

[27] Y. Liu and M. Fitz, "Space-time turbo codes," *13th Annual Allerton Conf. on Commun. Control and Computing*, Sep. 1999.

[28] D. Cui and A. M. Haimovich, "Design and performance of turbo space-time coded modulation," *IEEE GLOBECOM'00*, vol. 3, pp. 1627-1631, Nov. 2000.

[29] D. Tujkovic, "Recursive space-time trellis codes for turbo coded modulation," *IEEE GLOBECOM'00* , vol. 2, pp. 1010-1015, Nov. 2000.

[30] V. Tarokh, H. Jafarkhani, and A. R. Calderbank, "Space-time block code from orthogonal designs," *IEEE Trans. Inform. Theory*, vol. 45, pp. 1456-1467, July 1999.

[31] G. J. Foschini, "Layered space-time architecture for wireless communication in fading environments when using multiple antennas," *Bell labs. Tech. J.*, vol. 1, no. 2, pp. 41-59, 1996.

[32] G. D. Golden, G. J. Foschini, R. A. Valenzuela, and P. W. Wolniansky, "Detection algorithm and initial laboratory results using V-BLAST space-time communication architecture," *Electron. Lett.*, vol. 35, pp. 14-16, Jan. 1999.

[33] H. El Gamal and A. R. Hammons Jr., "A new approach to layered space-time coding and signal processing," *IEEE Trans. Inf. Theory*, vol. 47, pp. 2321-2334. Sep. 2001.

[34] B. Hassibi and B. Hochwald, "High-rate codes that are linear in space and time," *IEEE Trans. Inform. Theory*, vol. 48, pp. 1804-1824, July 2002.

[35] R. W. Heath and A. Paulraj, "Linear dispersion codes for MIMO systems based on frame theory," *IEEE Trans. on Signal Processing*, vol. 50, no. 10, pp. 2429-2441, Oct. 2002.

[36] X. Ma and G. B. Giannakis, "Full-diversity full-rate complex-field space-time coding," *IEEE Trans. Signal Processing*, vol. 51, no. 11, pp. 2917-2930, July 2003.

[37] F. Behnamfar, F. Alajaji and T. Linder, "Exact pairwise error probability of space-time codes under MAP decoding with applications," *Fourty-Third Annual Allerton Conference on Communication, Control, and Computing*, Monticello, USA, Sep. 2005.

[38] L. Zheng and D. Tse, "Diversity and multiplexing: A fundamental tradeoff in multiple antenna channels," *IEEE Trans. Inform. Theory*, vol. 49, pp. 1073-96, May 2003.

[39] Y. Ko and C. Tepedelenlioglu, "Space-time block coded rate-adaptive modulation with uncertain SNR feedback," *IEEE Signals, Systems and Computers*, vol. 1, pp. 1032-1036, Nov. 2003.

[40] M. E. Bock, P. Diaconis, F. W. Huffer and M. D. Perlman, "Inequalities for linear combinations of Gamma random variables", *Canada J. Statistics*, vol. 15, pp. 387-395, 1987.

[41] A. Muller and J. Speidel,"Adaptive modulation for MIMO spatial multiplexing systems with zero-forcing receivers in semi-correlated Rayleigh fading channels," *International conference on Communications and mobile computing* , pp. 665-670, 2006.

[42] Z. Wu and X. F. Wang, "Design of coded space-time modulation," *IEEE International Conference on Wireless Networks, Communications and Mobile Computing*, vol. 2, pp. 1059-1064, Jun. 2005.

[43] R. J. Muirhead, *Aspects of Multivariate Statistical Theory*, New York: John Wiley and Sons Inc. 1982.

[44] T. W. Anderson, *An Introduction to Multivariate Statistical Analysis*, 2th ed. New York: John Wiley and Sons Inc., 1984.

[45] A. M. Kshirsagar, *Multivariate Analysis*, Volume 2. New York: Marcel Dekker Inc., 1972.

[46] I. S. Gradshteyn, I. M. Ryzhik, A. Jeffrey, and D. Zwillinger, *Table of Integrals, Series, and Products*, 6th ed. San Diego, Calif.: Academic Press, 2000.

[47] M. L. Mehta, *Random Matrices*, 2th ed. San Diego, Calif., Academic Press, 1991.

[48] R. Lupas and S. Verdu, "Linear multiuser detectors for synchronous code-division multiple-access channels," *IEEE Trans. inform. Theory*, vol. 35, pp. 123-136, Jan. 1989.

[49] H. V. Poor and S. Verdu,"Probability of error in MMSE multiuser detection," *IEEE Trans. inform. Theory*, vol. 43, pp. 858-871, May 1997.

[50] S. Verdu, *Multiuser Detection*, Cambridge University Press, 1998.

[51] G. E. Roberts and H. Kaufman, *Table of Laplace Transforms*, Volume 2. Philadelphia: W. B. Saunders Company, 1966.

[52] J. Proakis, *Digital Communications*, 4th ed. New York: McGraw-Hill, 2001.

[53] M. K. Simon and M.-S. Alouini, *Digital Communication over Fading Channels*, 2nd ed. John Wiley & Sons Ltd, Canada, 2005.

[54] D. J. Love, R. W. Heath Jr., and T. Strohmer, "Grassmannian beamforming for multiple-input multiple-output wireless systems," *IEEE Trans. on Information Theory*, vol. 49, pp. 2735-2747, Oct. 2003.

[55] H. R. Bahrami and T. Le-Ngoc, "Eigenstructures of MIMO fading channel correlation matrices and optimum linear precoding designs for maximum ergodic capacity," *EURASIP Journal on Advances in Signal Processing*, vol. 2007, Article ID 29749, 9 pages, 2007.

[56] J. Zheng and B. D. Rao, "Capacity analysis of MIMO systems using limited feedback transmit precoding schemes," *IEEE Trans. on Signal Processing*, vol. 56, no. 7, pp. 2886-2901, July 2008.

[57] T. Rapaport, *Wireless Communications: Principles and Practice*, 2nd ed. Prentice Hall, 2001

[58] M. Gheryani, Y. Shayan, Z. Wu, and X. Wang, "Error performance of linear dispersion codes," *IEEE Global Communication Conference (GLOBECOM 2008)*, New Orleans, USA, Nov. 2008.

[59] M. Gheryani, Y. Shayan, Z. Wu, and X. Wang, "Capacity and performance analysis of full rate rinear dispersion codes," *submitted to IEEE Transactions on Vehicular Technology* , Dec. 2008.

[60] M. Gheryani, Z. Wu, and Y. Shayan, "SINR analysis for full-rate linear dispersion code using linear MMSE," *IEEE International Symposium on Wireless Communication Systems (ISWCS 2007)*, pp 360-364, Trondheim, Norway, Oct. 2007.

[61] M. Gheryani, Z. Wu, and Y. Shayan, "Design of adaptive MIMO system using linear dispersion code," *IEEE Trans. Wireless Comm.*, vol.7, no.11, pp. 4739-4747, Nov. 2008.

[62] M. Gheryani, Z. Wu, and Y. Shayan, "Design of adaptive MIMO system using linear dispersion code," *IEEE 22nd Canadian Conference on Electrical and Com-*

puter Engineering (CCECE 2009), Newfoundland and Labrador, Canada, May 2009.

[63] M. Gheryani, Z. Wu, and Y. Shayan, "Capacity and performance of adaptive MIMO system based on beam-nulling," *IEEE International Conference on Communications (ICC 2009)*, Dresden, Germany, June 2009.

[64] M. Gheryani, Z. Wu, and Y. Shayan, "Power allocation strategy for MIMO system based on beam-nulling," *IEEE 22nd Canadian Conference on Electrical and Computer Engineering (CCECE 2009)*, Newfoundland and Labrador, Canada, May 2009.

[65] M. Gheryani, Z. Wu, and Y. Shayan, "Multi-Dimensional beamforming for adaptive MIMO systems," *IEEE International Symposium on Wireless and Pervasive Computing (ISWPC 2009)*, Melbourne, Australia, Feb. 2009.

[66] M. Gheryani, Z. Wu, and Y. Shayan, "Performance of adaptive MIMO system based on beam-nulling," *IEEE International Symposium on Wireless and Pervasive Computing (ISWPC 2009)*, Melbourne, Australia, Feb. 2009.

[67] M. Gheryani, Z. Wu, and Y. Shayan, "Capacity and performance of adaptive MIMO system based on beam-nulling," *submitted to IEEE Trans. on Information Theory*, July 2008.